Thesis for the degree of Doctor of Philosophy

Nonlinear Propagation Property and Its Mitigation of Digital Coherent Optical Signal through Single-Mode Optical Fiber for Advanced Fiber-Optic Communication Systems

光ファイバ通信の高性能化に向けたディジタルコヒーレント光信号の単一モード光ファイバ非線形伝送特性とその抑制に関する研究

XIN ZHANG

Saitama Institute of Technology

February, 2019

要旨

近年、より大容量なネットワークの実現に向けて、コヒーレント光通信技術とデジタル信号処理技術を融合させたデジタルコヒーレント光伝送方式の実用化研究が急速に進展している。本研究では、この次世代システムの伝送容量および伝送距離の主要な制限要因となる光ファイバの非線形光学効果の影響とその回避策について検討した。特に、コア拡大単一モード光ファイバを伝送路とする無中継光伝送システムでの最大送信パワーを制限する非線形光学現象を数値解析により分析し、自己位相変調・相互位相変調を起源とする非線形位相雑音として現れることを解明し、多値変調方式、ビットレート（変調速度）、波長多重チャネル数依存性などを初めて定量化した。また、従来、大洋横断光増幅中継伝送システムのような超長距離相互作用システムのみに適用可能とされていた非線形位相雑音のガウス雑音（ＧＮ）モデルを、新たなパラメータを導入することにより無中継システムの性能予測へ応用できることを初めて示した。また、非線形位相雑音を抑制する手段について、受信側デジタルバックプロパゲーション(DBP)、コンスタレーションシェーピングならびに光ファイバラマン増幅などの研究を行った。すなわち、DBP による非線形補償では、送信側に負分散値を有する光学的な分散補償ファイバと併用することにより、単独の場合に比べて補償量が改善できることを初めて明らかにした。また、光ファイバラマン増幅により、最大送信パワー限界値を非ラマン増幅時と比べて 8.0dB 程度まで緩和できることを示した。

学位論文は、全 8 章で構成されている。第 1 章では、本研究の背景と目的などを述べた。第 2 章では、デジタルコヒーレント技術の基本的な定義から始めて、種々の変調方式および信号検出方式について述べた。第 3 章では、単一モード光ファイバの光伝送特性を取り扱う非線形シュレディンガー方程式および種々の非線形光学効果について記述し、光伝送システムの計算例として、10Gbps 信号の分散シフト光ファイバ光伝送特性を解明した結果について述べた。

第 4 章では、伝送速度 100Gbps およびそれ以上の変調速度を有する無中継光伝送システムの性能解析結果について述べ、非線形劣化要因の分析および最大送信パワーの多値変調方式、ビットレート（変調速度）、波長多重チャネル数依存性などを初めて定量化した結果について述べた。第 5 章では、第 4 章の数値計算結果が、新たに調整パラメータを導入した変形ガウス雑音モデルによって記述でき、無中継システムの性能予測へ応用できることを初めて示した。第 6 章では、非線形位相雑音を抑制する手段として、それぞれ受信側デジタルバックプロパゲーション(DBP)およびコンスタレーションシェーピングの研究結果につ

いて述べた。さらに、第 7 章では、光ファイバラマン増幅の適用により、最大送信パワー限界値を緩和できることを示し、定量的に議論した。最後に、第 8 章では、本研究の総括として、各章から得られた結論をまとめた。

Abstract

With the increase of bandwidth consuming applications, worldwide communication capacity demand has increased rapidly over the past a few decades. While fiber optic communication systems have already being served as infrastructures for such global and core networks, much efforts are continuously being paid to develop higher capacity and longer systems by adopting the state-of-the-art technologies. Because optical signal is transmitted through optical fiber, transmission performance impairments caused by optical fibers nonlinearity are one of the most important factors that limit the capacity of the next generation Wavelength Division Multiplexing (WDM) systems. In this paper, the nonlinear transmission property of optical signal in optical fiber for next generation optical communication systems is studied.

The thesis consists of 8 chapters. The second chapter is devoted to the modulation formats and detection schemes. The coherent detection technology based on Digital Signal Processing (DSP) technology combined with advanced modulation formats, can significantly improve the transmission capacity of the system, and simplify the complexity of the system if the polarization multiplexing technology is recombined. Polarization multiplexing (PM) can double the spectral efficiency of the system. In this chapter, we summarize the modulation format and Forward Error Correction (FEC) of optical coherent link, and describe some important aspects of DSP and coherence detection.

Chapter 3 focuses on fiber dispersion and nonlinearity, which are extremely important to consider for the high-capacity systems. Starting with introducing the fundamental nonlinear Schrodinger equation, such as attenuation, chromatic dispersion, polarization model dispersion (PMD), nonlinear interference noise. Then, we have comprehensively investigated transmission property of single-channel 10 Gbps signal in dispersion shifted fiber (DSF). Quite different feature of signal degradation in positive and negative dispersion regimes is clarified in terms of signal operation wavelength as well as transmission distance. Intrinsic nonlinear degradation near zero dispersion is found to be symmetric in terms of wavelength despite that modulation instability gain should vanish in normal dispersion with deviation from zero dispersion.

Chapter 4 investigates the non-repeatered systems performance using numerical method for 100Gbps and beyond 100Gbps systems. We have numerically evaluated very high power transmission property and BER performance of 120Gbps digital coherent signals. If the maximum transmitter powers are defined as the powers at which BER floor levels are 1.0×10^{-2} without error correction, those are found to be approximately +20.4

dBm, +14.8 dBm and +10.6 dBm, respectively, for single-channel 120Gbps DP-QPSK, DP-16QAM and DP-64QAM formats in large-core and low-loss single-mode silica fibers. We also show that the maximum transmitter powers gradually decrease in logarithmic feature with the increase of the number of DWDM channels. The channel number dependence is newly shown to be almost independent on the modulation format.

Chapter 5 investigated that the modified GN-model with adjustment parameters, can be an accurate way to describe the nonlinearity impairments in non-repeatered transmission system. In this chapter we have introduced theoretically the GN model and bibliographical background, and introduced the model formulas, also the main derivation steps are given. Then we directly discuss the subject of GN model accuracy with adjustment parameters. The calculation results using extended Gaussian-Noise (GN) model with adjustment parameters have been compared with the numerical simulation results, not only to confirm the validity of the results but to explore possible new analytical modeling for non-repeatered systems.

Chapter 6 is devoted to nonlinear mitigation techniques, digital back propagation to compensate nonlinearity impairments in non-repeatered systems. With nonlinear compensation by using digital back propagation (DBP) at receiver side, we have found that 2 dB improvement is achievable compared with the performance without DBP. However, the performance is affected by nonlinear channel interference in DWDM non-repeatered systems, the improvement has been reduced to 0.6dB due to disturbance from neighboring DWDM channels. Furthermore we newly confirmed that the negative dispersion which change the optical pulse waveform at transmitter side increase the maximum input power by 0.2dB in single channel.

In chapter 7, Raman amplifier is studied to improve the maximum transmitter power in non-repeatered systems. We investigated the implementation of up to third-order Raman amplification as well as conventional (first order) Raman amplification. Then, a comparison of the resulting performances are made for first-order through third-order pumpings. For third-order Raman amplification, the equivalent Tx power is enhanced +24.0dBm, about 8dB increase compared with that without Raman Amplifier.

Finally, chapter 8 gives a conclusion of this paper.

Acknowledgements

I would like to express the deepest appreciation to my mentor Professor Aoki, who has the attitude and the substance of a genius: he continually and convincingly conveyed a spirit of adventure in regard to research and scholarship, and an excitement in regard to teaching. Without his guidance and persistent help this dissertation would not have been possible.

Also, I would like to thank all the members of my Dissertation Committee, Professor D. Y. JU, Professor J. T. Cao, Professor S. Sato, Professor S. Furuya, who has provided me extensive personal and professional guidance and taught me a great deal about both scientific research and life in general. Especially, I would like to thank Professor D. Y. JU, as my teacher and mentor, he has taught me more than I could ever give him credit here.

I am grateful to all of those with whom I have had the pleasure to work during this research work. Team work is so important during the research.

Also, I would like to express my sincere thanks to all my friend, who take good care of my life during these years.

Most importantly, I wish to thank my loving and supportive parents, relatives, whose love and guidance are with me in whatever I pursue.

Table of contents

List of figures and tables

List of acronyms and abbreviations

ADC	Analog to digital converter
AGN	Additive Gaussian noise
ASE	Amplified Spontaneous Emission
AWGN	Additive White Gaussian Noise
BER	Bit Error Rate
BPSK	Binary Phase-Shift Keying
CD	Chromatic Dispersion
CW	Continuous Wave
DAC	Digital to Analog Converter
DBP	Digital Back Propagation
DCF	Dispersion Compensating Fiber
DM	Dispersion Managed
DSP	Digital Signal Processing
DWDM	Dense Wavelength Division Multiplexing
EDFA	Erbium-Doped Fiber Amplifier
FEC	Forward Error-Correcting Code
FWM	Four-Wave-Mixing
GN	Gaussian Noise
GNRF	GN model reference formula
ITU	International Telecommunication Union
LO	Local Oscillator
MIMO	Multiple-Input Multiple-Output
MZ	Mach-Zehnder Modulator
NLIN	Non-Linear Interference Noise
NLSE	Non-Linear Schrödinger Equation
NRZ	Non-Return to zero
OFDM	Orthogonal Frequency Division Multiplexing
OPT MUX	Optical Multiplexer
OPT DEMUX	Optical Demultiplexer
OSNR	Optical Signal to Noise Ratio
PBS	Polarization Beam Splitter
PBC	Polarization Beam Combiner

PM	Polarization Multiplexed
PD	Photodiode
PSCF	Pure Silica Core Fiber
PSK	Phase-Shift Keying
PTP	Point To Point Links
QAM	Quadrature Amplitude Modulation
QPSK	Quadrature Phase-Shift Keying
SE	Spectral Efficiency
SNR	Signal To Noise Ratio
SMF	Single-to-Noise Ratio
SPM	Self-Phase-Modulation
SBS	Stimulated Brillouin Scattering
SRS	Stimulated Raman Scattering
WDM	Wavelength Division Multiplexing
XPM	Cross-Phase-Modulation
XPolM	Cross-Polarization Modulation

Chapter 1 Introduction

1.1 Background

With the increase of bandwidth consuming applications, worldwide communication capacity demand has increased rapidly over the past a few decades. While fiber optic communication systems have already being served as infrastructures for such global and core networks, much efforts are continuously being paid to develop higher capacity and longer systems by adopting the state-of-the-art technologies. Because optical signal is transmitted through optical fiber, transmission performance impairments caused by optical fibers nonlinearity are one of the most important factors that limit the capacity of the next generation Wavelength Division Multiplexing (WDM) systems. In this paper, the nonlinear transmission property of optical signal in optical fiber for next generation optical communication systems is studied.

With the development of high-speed digital signal processing technology (DSP) and analog-to-digital conversion technology, coherent optical transmission technology has been a hot issue in the optical communication field. Using the combination of coherent detection and digital signal processing (DSP), long-haul optical transmission [1-3] can be realized without optical dispersion compensation. This enables us to configure 100Gbps-based DWDM subsea and transcontinental trunk practical systems by utilizing ultra-low loss and large effective area (A_{eff}) single-mode silicon fiber (SMFs) for transmission lines [4-5].

For non-repeatered system application, several reports have been published on both high-capacity and long-reach transmission [6]. And single-span transmission exceeding 400 km and/or a capacity-reach product of over 5 Pbps-km have been demonstrated by adoption of optimized Raman/Remote Optically Pumped Amplifier (ROPA) as well as high power booster amplifiers[7-11]. In those systems, the maximum transmission powers are considered to be limited by optical fiber nonlinearity, but, to the best of our knowledge, neither quantitative simulation studies nor experimental investigations have so far been reported on this topic.

It should be stressed here that although long-length fiber transmission with dispersion-uncompensated SMF have already been clarified by the Gaussian-Noise (GN) model [12, 13] for long-haul repeatered system application, the results cannot be directly extended to the non-repeatered system, because it inevitably handles very high power transmission with localized nonlinearity (i.e., nonlinear interaction is less than the effective fiber length) while long-haul repeatered systems are configured with low signal powers,

resulted in relatively mild nonlinearity over the entire system length. The establishment of high power transmission technology is particularly beneficial for non-repeatered application because it surely offers a greater power budget.

It is expected that the next generation WDM communication system operate at 400Gbps or 1Tbps rate. Meanwhile, in optical fibers transmission nonlinear impairments are regarded as the most remarkable factor which limits the capacity of the next generation WDM systems set by the nonlinear Shannon capacity. Digital back propagation (DBP) could be a general technique to compensate both linear and nonlinear impairments.

Further, fiber loss is one of important factor of limiting the optical fiber transmission length. With the coming forth and commercial using of erbium-doped fiber amplifiers (EDFA) and the Raman amplification, it made the development of expanding span distance and capacity.

1.2 Objective of this project

In this paper, the nonlinear transmission property of optical signal in optical fiber for next generation optical communication systems is studied. We have comprehensively evaluated by numerical simulation very high power transmission property and bit error rate (BER) performance of 120Gbps Dual-Polarization Quadrature Phase Shift Keying (DP-QPSK), DP-16QAM (Quadrature Amplitude Modulation) and DP-64QAM modulation formats in large effective area and low-loss SMFs without and with nonlinear compensation. We limit our discussion in C-band transmission because channel interaction due to stimulated Raman scattering (SRS) effect is not considered.

We have clarified for the first time how and at what powers the BER deteriorates with transmitter power increase. Based on BER characteristics, we have quantitatively discussed the maximum transmitter powers set by fiber nonlinearity, and we have shown that the maximum transmitter (Tx) powers gradually decrease in logarithmic feature with the increase of the number of DWDM channels. The channel number dependence has newly been shown to be almost independent on the modulation format. Furthermore, the simulated results have been compared with extended GN model with introducing adjustment parameters to explore possible new analytical model for non-repeatered system.

We have evaluate the performance of digital coherent non-repeatered systems by utilizing higher-order modulation based on 120Gbps DP-16QAM, nonlinearity compensation by digital back propagation (DBP), larger effective area ultra-low loss fibers, and broaden bandwidth EDFAs. We have studied the maximum Tx power increase by using digital back propagation method for nonlinear compensation for non-repeatered

systems. Also, we have explored mitigation techniques of nonlinear impairment by higher order Raman amplifier scheme and constellation shaping.

1.3 Outline of the dissertation

The thesis consists of 8 chapters. The second chapter is devoted to the modulation formats and detection schemes. The coherent detection technology based on Digital Signal Processing (DSP) technology combined with advanced modulation formats, can significantly improve the transmission capacity of the system, and simplify the complexity of the system if the polarization multiplexing technology is recombined. Polarization multiplexing (PM) can double the spectral efficiency of the system. In this chapter, we summarize the modulation format and Forward Error Correction (FEC) of optical coherent link, and describe some important aspects of DSP and coherence detection.

Chapter 3 focuses on fiber dispersion and nonlinearity, which are extremely important to consider for the high-capacity systems. Starting with introducing the fundamental nonlinear Schrodinger equation, such as attenuation, chromatic dispersion, polarization model dispersion (PMD), nonlinear interference noise. Then, we have comprehensively investigated transmission property of single-channel 10 Gbps signal in dispersion shifted fiber (DSF). Quite different feature of signal degradation in positive and negative dispersion regimes is clarified in terms of signal operation wavelength as well as transmission distance. Intrinsic nonlinear degradation near zero dispersion is found to be symmetric in terms of wavelength despite that modulation instability gain should vanish in normal dispersion with deviation from zero dispersion.

Chapter 4 investigates the non-repeatered systems performance using numerical method for 100Gbps and beyond 100Gbps systems. We have numerically evaluated very high power transmission property and BER performance of 120Gbps digital coherent signals. If the maximum transmitter powers are defined as the powers at which BER floor levels are 1.0×10^{-2} without error correction, those are found to be approximately +20.4 dBm, +14.8 dBm and +10.6 dBm, respectively, for single-channel 120Gbps DP-QPSK, DP-16QAM and DP-64QAM formats in large-core and low-loss single-mode silica fibers. We also show that the maximum transmitter powers gradually decrease in logarithmic feature with the increase of the number of DWDM channels. The channel number dependence is newly shown to be almost independent on the modulation format.

Chapter 5 investigated that the modified GN-model with adjustment parameters, can be an accurate way to describe the nonlinearity impairments in non-repeatered transmission system. In this chapter we have introduced theoretically the GN model and

bibliographical background, and introduced the model formulas, also the main derivation steps are given. Then we directly discuss the subject of GN model accuracy with adjustment parameters. The calculation results using extended Gaussian-Noise (GN) model with adjustment parameters have been compared with the numerical simulation results, not only to confirm the validity of the results but to explore possible new analytical modeling for non-repeatered systems.

Chapter 6 is devoted to nonlinear mitigation techniques, digital back propagation to compensate nonlinearity impairments in non-repeatered systems. With nonlinear compensation by using digital back propagation (DBP) at receiver side, we have found that 2 dB improvement is achievable compared with the performance without DBP. However, the performance is affected by nonlinear channel interference in DWDM non-repeatered systems, the improvement has been reduced to 0.6dB due to disturbance from neighboring DWDM channels. Furthermore we newly confirmed that the negative dispersion which change the optical pulse waveform at transmitter side increase the maximum input power by 0.2dB in single channel.

In chapter 7, Raman amplifier is studied to improve the maximum transmitter power in non-repeatered systems. We investigated the implementation of up to third-order Raman amplification as well as conventional (first order) Raman amplification. Then, a comparison of the resulting performances are made for first-order through third-order pumpings. For third-order Raman amplification, the equivalent Tx power is enhanced +24.0dBm, about 8dB increase compared with that without Raman Amplifier.

Finally, chapter 8 gives a conclusion of this paper.

References

[1] Z. Xiang, and, C. J. Xie, “Chapter 1 Introduction and references therein” in Enabling Technology for High-Efficiency Optical Communication Networks, ed. Z. Xiang and C. J. Xie, pp. 1-11, John Wiley & Sons, Inc., 2016.

[2] K. Kikuchi, “Fundamentals of Coherent Optical Fiber Communications,” Journal of Lightwave Technology, vol. 34, no. 1, pp. 157-179, 2016.

[3] M. Nakazawa, K. Kikuchi, and T. Miyazaki, ed., High Spectral Density Optical Communication Technologies, Springer, 2010.

[4] Y. Aoki, Y. Inada, T. Ogata, L. Xu, S. L. Zhang, F. Yaman, and E. Mateo, “Next-generation 100 Gb/s undersea optical communications,” IEEE Communications Magazine, vol. 50 , no. 2, pp. 50-57, 2012.

[5] “FASTER cable system ready for service,”

http://www.capacitymedia.com/Article/3565973/FASTER-cable-system-ready-for-service. Jun. 2016.
[6] H. Fevrier, B. Clesca, P. Perrier, D. Chang and W. S. Pelouch, “Chapter7 Unrepeatered Transmission and references therein” in Undersea Fiber Communication Systems, 2nd ed., ed. J. Chesnoy, pp. 261-300, Academic Press, 2016.
[7] V. Gainov, N. Gurkin, S. Lukinih, S. Makovejs, S. Akopov, S. Ten, O. Nanii, V. Treshchikov, and M. Sleptsov, “Record 500 km unrepeatered 1 Tbits/s (10×100G) transmission over an ultra-low loss fiber,” Optics Express, vol. 22, no. 19, pp. 22308-22313, 2014.
[8] H. Bissessur, C. Bastide, S. Dubost, and S. Etienne, “80 × 200 Gb/s 16-QAM unrepeatered transmission over 321 km with third order Raman amplification,” Optical Fiber Communication Conference 2015 (OFC2015), paper W4E.2, 2015.
[9] D. Chang, W. Pelouch, P. Perrier, H. Fevrier, S. Ten, C. Towery, and S. Makovejs, “150 × 120 Gb/s unrepeatered transmission over 409.6 km of large effective area fiber with commercial Raman DWDM system,” Optics Express, vol. 22, no. 25, pp. 31057-31062, 2014.
[10] D. Chang, P. Perrier, H. Fevrier, S. Makovejs, C. Towery, X. T. Jia, L. Deng, and B. Z. Li, “Ultra-long unrepeatered transmission over 607 km at 100G and 632 km at 10G,” Optics Express, vol. 23, no. 19, pp. 25028-25033, 2015.
[11] T. J. Xia, D. L. Peterson, G. A. Wellbrock, D. Chang, P. Perrier, H. Fevrier, S. Ten, C. Tower, and G. Mills, “557-km Unrepeatered 100G Transmission with Commercial Raman DWDM System, Enhanced ROPA, and Cabled Large A_{eff} Ultra-Low Loss Fiber in OSP Environment,” Optical Fiber Communication Conference 2014 (OFC2014), no. Th5A.7, 2014.
[12] P. Poggiolini, “The GN Model of Non-Linear Propagation in Uncompensated Coherent Optical Systems,” Journal of Lightwave Technology, vol. 30, no. 24, pp. 3857-3879, 2012.
[13] D. Semrau, R. I. Killey, and P. Bayvel, “The Gaussian Noise Model in the Presence of Inter-Channel Stimulated Raman Scattering,” Journal of Lightwave Technology, vol. 36, no. 14, pp. 3046-3055, 2018.

Chapter 2 Modulation and detection schemes

2.1 Introduction

Optical fiber communication systems traditionally uses basic modulation, such as on-off-keying (OOK) and differential phase shift keying (DPSK) [1]. Coherent receiver technology promotes the emergence of advanced modulation formats, and the simplest form is the binary phase shift keying (BPSK) in all four quadrature parallels and polarization multiplexed quadrature shift keying (PM-QPSK) [2-3]. The choice of modulation formats in optical fiber communication system is very important for it determines the upper limit of spectrum efficiency. Furthermore, it measures the degree of channel space utilization (bandwidth and signal dimension). In addition, increasing FEC can improve the noise tolerance, as a result of reducing the spectral efficiency.

The combination of coherent detection and DSP technology makes it possible to recover carrier phase in electric field, and the matching of polarization state of signal with local oscillator light becomes possible, which eliminates two main technical obstacles of traditional coherent optical communication system. The coherent receiver based on DSP technology has simple structure and transparent hardware. It can compensate linear and non-linear transmission impairment in the electric field, simplify transmission link, reduce transmission cost, support multi-level modulation format and polarization state multiplexing, and easily realize high spectral efficiency optical fiber transmission. Many advantages make coherent optical transmission system based on DSP technology an important choice for the next generation optical communication system, and the research on its transmission characteristics and receiving algorithms has been developed rapidly.

The framework of this chapter is organized as follows. In the next section, the basic definitions and performance advantages of traditional modulation formats are introduced. In section 2.3, the main coherent modulation formats and their performance characteristics are shown. In section 2.4, we introduce digital coherent detection technology, including coherent detection technology and digital signal processing. In Section 2.5, some basic parameters for evaluating the system performance are introduced. In section 2.6, we test the simulation results of different modulation formats, which are basically consistent with the predicted theoretical values. Finally, we summarize in section 2.7.

2.2 IM-DD (Intensity modulation / direct detection)

2.2.1 NRZ modulated signal

Non-return-to-zero (NRZ) modulation format is used to denote "0" when there is no voltage (or current). When the positive voltage is constant, it means "1". This simple waveform can be represented by the following rectangular profile:

$$\mathrm{a(t)} = \begin{cases} 1 & for\ 0 < t < T \\ 0 & elsewhere \end{cases}$$

Each bit encoding takes up the width of all the symbols. In this way, there is no gap between a bit and its next bit, and it is not easy to distinguish.

The low spectrum spread of NRZ coding makes it less sensitive to dispersion. However, due to continuous waveform overlap and inter symbol interference, it is vulnerable to system damage. A long sequence of identical symbols will lead to the loss information of digital period and phase, which makes the synchronization in the receiver very difficult.

2.2.2 RZ modulated signal

In return-to-zero (RZ) coding, positive level represents logic 1, and negative level represents logic 0, and the signal returns to zero level after every bit transmitted. The duration of the light pulse εT is much shorter than the bit period. The rectangular waveform function of RZ is shown below:

$$\mathrm{a(t)} = \begin{cases} 1 & for\ 0 < t < \varepsilon T \\ 0 & elsewhere \end{cases}$$

The parameter $\varepsilon < 1$ is called the duty of the modulation. For the pulse duration is very short, RZ coding can be used in optical time division multiplexing (OTDM). RZ coding also has some resistance to optical fiber nonlinearity. Therefore, it can effectively reduce its bandwidth requirements in practical applications.

2.3 Modulation scheme for coherent detection

The process of mapping data to waveforms and vice versa is called digital modulation. The mapping process is divided into three steps. Firstly, additional bits are added to the payload. Secondly, m-bits are mapped to a symbol as a vector in n-dimensional space. Thirdly, the sequence of symbol of the symbols is mapped to the waveforms. At the receiver side, a coherent receiver is used to perform the opposite operation, thus getting the original data.

First, blind estimation or pilot-aided estimation algorithm [4-6] is used to recover carrier phase, symbol clock and polarization. Second, the waveform is filtered and sampled. The third and last procedure receives a sequence of bits by connecting the bits corresponding to each symbol. Then the digital overhead was removed, including FEC decoding and frame synchronization. When choosing the modulation format, the spectral efficiency, noise tolerance and modulation complexity should be considered.

In this section, modulation and coding are discussed. We represent digital modulation symbols as sequence of complex numbers and then use it to generate actual waveforms. We introduce the basic modulation principles of QPSK and QAM, and their constellation diagram. Finally, the basic principles of FEC.

2.3.1 QPSK

Phase shift keying (PSK) represents 1 and 0 by changing the phase of the carrier signal. In a bit period, the peak amplitude and frequency remain constant. The function expression is as follows:

$$\mathrm{s(t)} = \begin{cases} Acos(2\pi f_c t), & binary\ 1 \\ Acos(2\pi f_c t + \pi), & binary\ 0 \end{cases}$$

A: amplitude. f_c: frequency of carrier signal.

Phase shift keying is less error-prone than amplitude shift keying and requires the same bandwidth as amplitude shift keying. However, the process of signal detection and recovery is more complex than ASK and frequency shifter keying (FSK).

Quadrature shift keying (QPSK): equals to 4-PSK, and the phase shifts of π/2 rad, generated 4 different signals of each representing 2 bits. The function expression is as follows:

$$\mathrm{s(t)} = \begin{cases} Acos(2\pi f_c t), & binary\ 00 \\ Acos\left(2\pi f_c t + \frac{\pi}{2}\right), & binary\ 01 \\ Acos(2\pi f_c t + \pi), & binary\ 10 \\ Acos\left(2\pi f_c t + \frac{3\pi}{2}\right), & binary\ 11 \end{cases}$$

A: amplitude. f_c: frequency of carrier signal.

QPSK carriers more data rate than PSK at the same bandwidth. However, higher rate PSK schemes are limited by the ability of equipment to distinguish small differences in phase.

2.3.2 QAM

For quadrature amplitude modulation (QAM), two 90-degree phase-shifted carriers are modulated, which results in the amplitude and phase changes of the generated signal [7]. At the receiver, the phase and amplitude, or the two quadrature of the field, must be clearly measured. The arrangement of points in the constellation gives it the maximum possible distance so that they can be more easily distinguished after channel demage. However, in order to make modulation more convenient, these points are arranged on square grids with the same vertical and horizontal spacing. Although square QAM does not fully maximize the Euclidean distance between constellation points, it is widely used because it is easy to implement.

As we can see from the Fig. 2.1, QAM uses two-dimensional signals. The original information flow is divided into two sequences, which are composed of odd symbols and even symbols. For example, x (t) and y (t). x (t) sequence is modulated by$cos(2\pi f_c t)$. y (t) sequence is modulated by $sin(2\pi f_c t)$. Composite signal x(t)$cos(2\pi f_c t) + y(t)sin(2\pi f_c t)$ is sent through the channel.

QAM demodulation by multiplying x(t)$cos(2\pi f_c t) + y(t)sin(2\pi f_c t)$ by $cos(2\pi f_c t)$ and then low-pass filtering the resultant signal, sequence x (t) is obtained. And by multiplying x(t)$cos(2\pi f_c t) + y(t)sin(2\pi f_c t)$ by $sin(2\pi f_c t)$ and then low-pass filtering the resultant signal, sequence y (t) is obtained. In QAM, the combination of various amplitudes and phases can achieve a higher data rate. The variations of amplitude are susceptible to noise. In QAM system, the number of phase shifts is larger than the number of amplitude shifts.

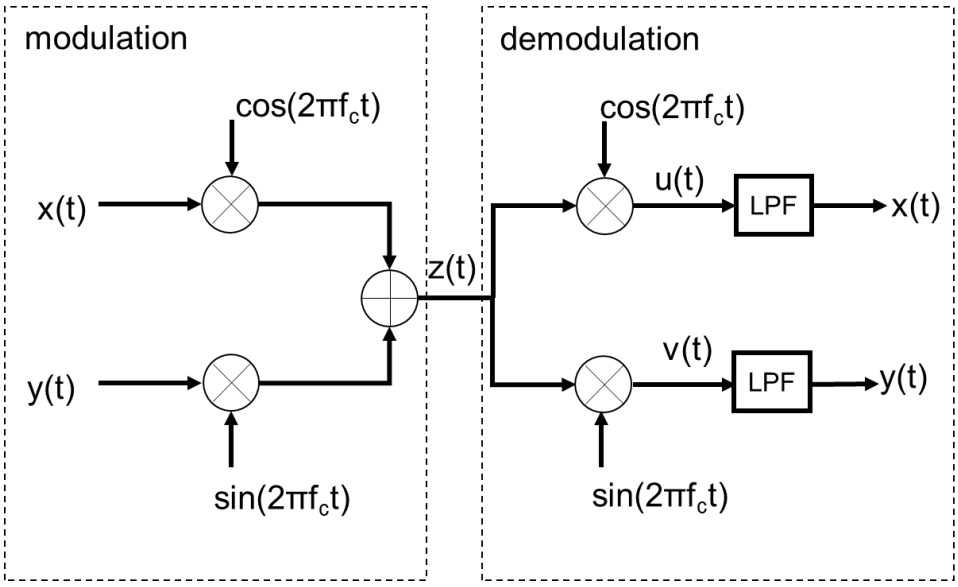

Figure 2.1 Modulation of Digital Data: QAM.

2.3.3 Constellation diagram

Constellation diagram is used to represent a possible symbol of the selected modulation scheme, as shown in Figure 2.2.

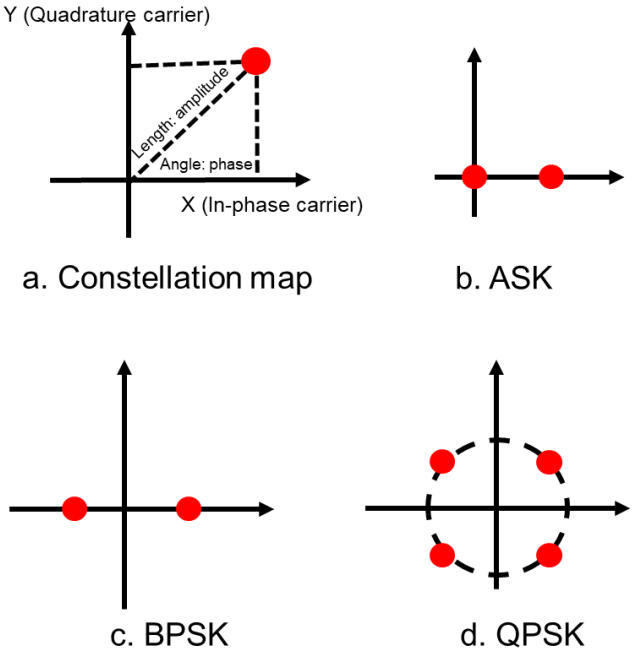

Figure 2.2 a. Constellation Diagram for b. ASK (OOK), c. BPSK and d. QPSK.

The X-axis represents the in-phase carrier, and the projection of the in-phase carrier on the X-axis defines the peak amplitude of the in-phase component. The Y-axis represents the quadrature component, and the projection of the quadrature carrier on the Y-axis defines the peak amplitude of the quadrature component. The linear length from the connection point to the origin is the peak amplitude of the signal. The angle between the line and the X-axis is the phase of the signal element.

2.4 Digital coherent detection technology

2.4.1 Coherent detection

During 2004-2005, several research groups proposed the concept of digital coherent communication [8-11]. After that, this technology was considered to be the best technology for 40 Gb/s, 100Gb/s and beyond WDM transmission systems. The main reasons are as follows: (i) coherence technology retains amplitude and phase information, allowing all four dimensional light fields (each of the two orthogonal polarizations of in phase and orthogonal components) to be used for information coding, thus providing more spectral efficiency than intensity modulation direct detection (IMDD) systems; (ii) Coherence technology, including powerful DSP, helps to solve the problem suffered by

IMDD system at 10Gb/s, as a result of providing significantly increased capacity; (iii) Coherent detection provides better sensitivity than IMDD systems; (iv)Digital coherence detection has dramatically changed the way to manage nonlinear impairments in optical communication systems. Many nonlinear mitigation techniques developed for direct detection systems such as dispersion management are not effective and become unsatisfactory in coherent detection systems [12-13]. PMD helps to reduce fiber nonlinearity [14-15], and fiber nonlinearity can be mitigated through DSP in transmitters and receivers [16].

2.4.2 DSP

The development of advanced digital signal processing (DSP) has led to the paradigm shift of coherent optical receivers in optical communications. Figure 2.3 shows the functional block diagram of a typical DSP enabled coherent transmitter and receiver.

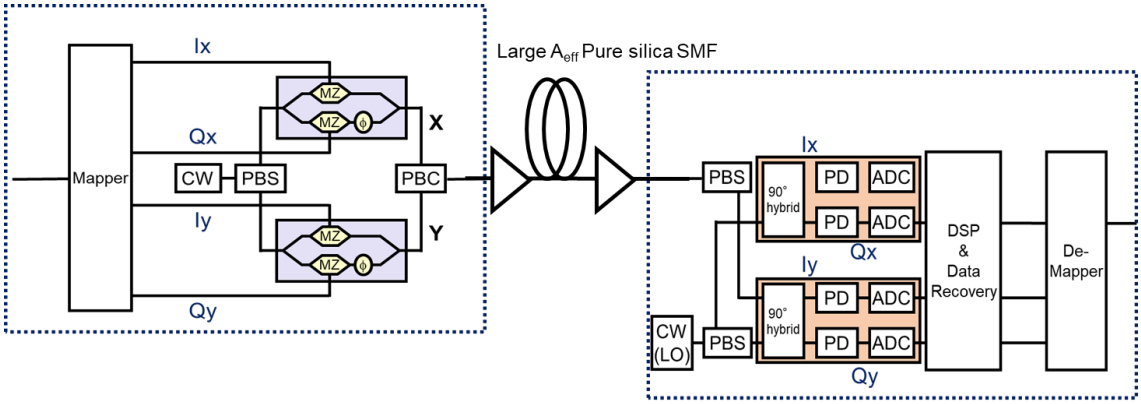

Figure 2.3 Functional block diagrams for coherent transmitter and receiver.

For the transmitter shown in the left figure, a continuous wave (CW) from a low linewidth laser is divided into two parts, one for each polarization, and each part is modulated by an in-phase/quadrature (I/Q) modulator by electrical signals from digital-to-analog converter (DACs).

The binary client signals are first encoded by FEC encoders, and then the FEC coded binary signals are mapped into the required multi-level modulation symbols, such as common quadrature amplitude modulation (QAM) symbols. After that, various digital spectrum shaping techniques can be applied to QAM mapping signals to improve transmission performance or to reduce transmission impairments. For example, the Nyquist pulse shaping technology can be an effective method to improve the spectrum efficiency of WDM without resorting to higher-order modulation formats. After digital spectral shaping, the in-phase and quadrature components of the digital QAM signal are

converted into two analog signals, which are used to drive the I/Q modulator to up-convert the baseband electrical signal into optical signal for transmission. During the propagation of the optical fiber, the signal polarization is not maintained, but rotated randomly.

With the development of high-speed electronic technology, signals are first mixed with local oscillator (LO) in photoelectric detector of coherent receiver by analog-to-digital converters (ADCs), then converted into digital format. The signal is recovered by digital signal processing (DSP), for example carrier phase recovery and polarization alignment and separation are the main obstacles to early coherent receiver simulation, which can be realized by complex DSP in the electrical field.

The post-transmission DSP includes the main functional blocks shown in Figure 2.4: (i) filter and resampling, (ii) dispersion compensation, (iii) nonlinearity compensation, (iv) adaptive equalizer, and (v) frequency offset estimation and carrier phase offset estimation. The Digital Square and filter algorithm [17] is used for timing recovery scheme. Then, the adaptive equalizer by two-stage constant modulus algorithm-radius directed (CMA-RD) algorithm [18, 19] is used to compensate for residual chromatic dispersion, polarization mode dispersion (PMD) and to reduce inter- symbol interference. In the equalizer, the butterfly structure is applied for polarization demultiplex. After that, frequency offset estimation (FOE) and carrier phase offset estimation (CPE), by the blind phase search (BPS) algorithm [20], are performed to regenerate the I/Q signal.

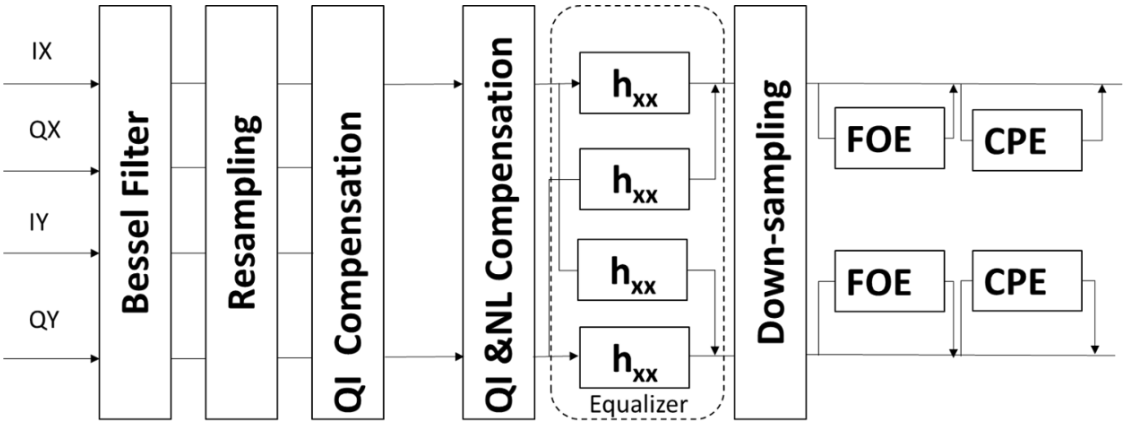

Figure 2.4 Universal DSP algorithm design. FOE: frequency offset estimation. CPE: carrier phase offset estimation.

2.5 BER, SNR and Q Value

Optical Signal-to-Noise Ratio (OSNR): Used to quantify the degree of interference of optical noise with optical signals. It is the ratio of signal power to noise power within effective bandwidth [21].

Bit Error Rate (BER): The ultimate indicator of transmission quality. Due to noise, nonlinear effects, and chromatic dispersion, polarization mode dispersion, the waveform of the optical signals coupled into the fiber will be distorted when transmitted to the terminal. So when the receiver converts the optical signal into electrical signals, bit error will occur.

The optical signal-to-noise ratio can indirectly reflect the bit error rate and can provide an early warning of BER degradation.

Q value: The Q value and the bit error rate have a one to one mapping. A smaller BER value represents a larger Q value and better link performance. Gray coding is assumed for all formats. The BER for each modulation format is given by the following formula.

$$\mathrm{BER} = C_1 \mathrm{erfc}\sqrt{C_2 SNR}$$

$$\mathrm{OSNR} = \mathrm{SNR}(R_s/B_{ref})$$

$$\mathrm{erfc(x)} = 1 - \mathrm{erf(x)} = \frac{2}{\sqrt{\pi}}\int_x^{\infty} e^{-t^2}\,dt = e^{-x^2} erfcx(x);$$

Where C_1 and C_2 can be found in the following Table 2.1. And in Figure 2.5, shows the relationship between BER and SNR.

Table 2.1 C_1 and C_2 for different modulation formats

Modulation Format	Symbol Rate	C_1	C_2
DP-BPSK	60	1/2	1
DP-QPSK	30	1/2	1/2
DP-16QAM	15	3/8	1/10
DP-64QAM	7.5	7/24	1/28

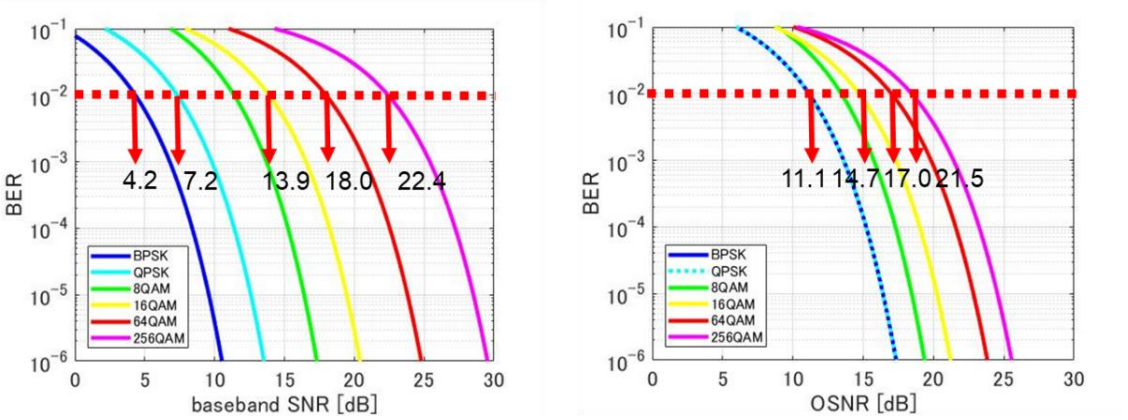

Figure 2.5 Relationship between BER and SNR (baseband SNR and OSNR).

2.6 Simulations for different modulation format

Figure 2.6 shows the simulation examples for different modulation format, the constellation map and spectrum. Figure 2.7 shows the back to back receiver sensitivity. The OSNR at BER=1.0×10^{-2} are 11dB, 12dB, 15dB, 16dB, 20dB and 21dB for BPSK, QPSK, 8QAM, 16QAM, 32QAM and 64QAM, respectively, which is in accordance with the theoretical results in Figure 2.5.

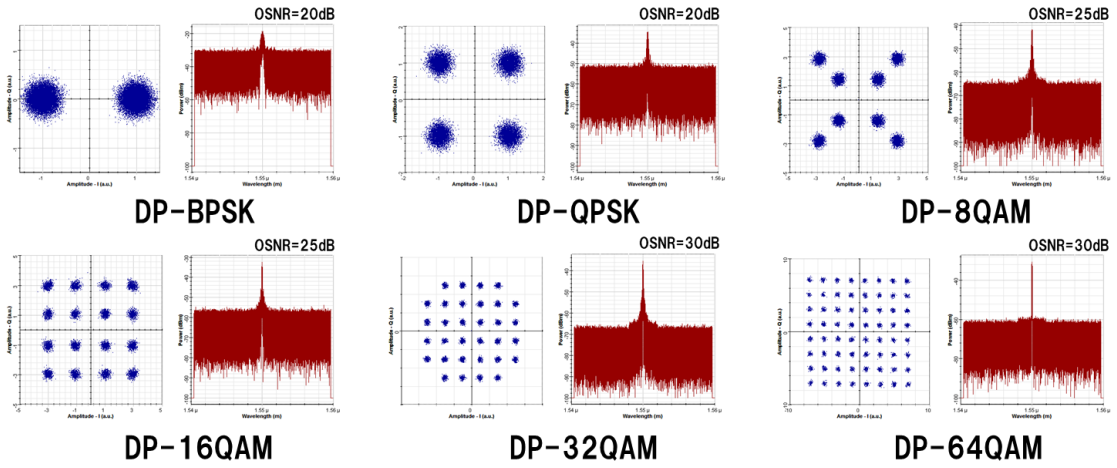

Figure 2.6 the constellation map and spectrum for different modulation format.

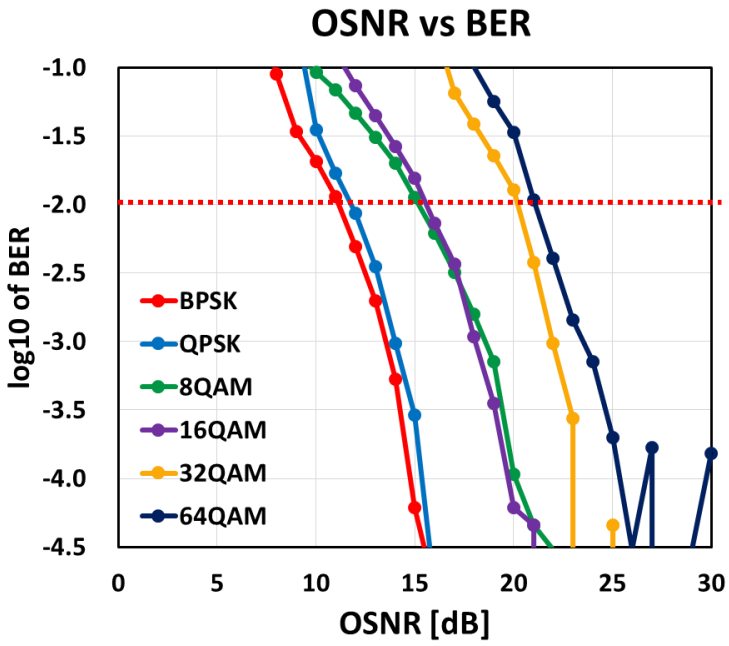

Figure 2.7 the back to back receiver sensitivity for modulation formats.

2.7 Concluding remarks

The coherent detection technology based on DSP technology combined with advanced modulation formats, such as quadrature phase shift keying (QPSK) and quadrature amplitude modulation (QAM), can greatly improve the transmission capacity of the system, and simplify the complexity of the system if the polarization multiplexing technology is recombined. Polarization multiplexing (PM) can double the spectral efficiency of the system.

In this chapter, we summarize the basic definitions and performance advantages of traditional modulation formats, the main coherent modulation formats and their performance characteristics. We introduce digital coherent detection technology, including coherent detection technology and digital signal processing. Some basic parameters for evaluating the system performance are introduced. Finally we test the simulation results of different modulation formats, which are basically consistent with the predicted theoretical values.

References

[1] A. H. Gnauck, and P. J. Winzer, “Optical phase-shift-keyed transmission,” Journal of Lightwave Technology, vol. 23, no. 1, pp. 115-130, 2005.

[2] G. Charlet, M. Salsi, J. Renaudier, O. B. Pardo, H. Mardoyan, S. Bigo, “Performance comparison of singly-polarised and polarisation-multiplexed coherent transmission at 10 Gbauds under linear impairments”, Electron Letter, vol. 43, no. 20, pp. 1109-1111, 2007.
[3] H. Sun, K. T. Wu, and K. Roberts, “Real-time measurements of a 40 Gb/s coherent system,” Optics Express, vol. 16, no. 2, pp. 873-879, 2008.
[4] S. J. Savory, “Digital coherent optical receivers: algorithms and subsystems,” IEEE Journal of Selected Topics in Quantum Electronics, vol. 16, no. 5, pp. 1164-1179, 2010.
[5] X. Zhou, “Efficient clock and carrier recovery algorithms for single-carrier coherent optical systems,” IEEE Signal Process Magazine, vol. 31, no.2, pp. 35-45, 2014.
[6] A. P. T. Lau, et al., “Advanced DSP techniques enabling high spectral efficiency and flexible transmissions,” IEEE Signal Process Magazine, vol. 31, no. 2, pp. 82-92, 2014.
[7] J. G. Proakis, Digital communications, 3rd ed., New York, McGraw-Hill Inc., 1995.
[8] M. G. Taylor, “Coherent detection method using DSP for demodulation of signal and subsequent equalization of propagation impairments,” IEEE Photon Technology Letter, vol. 16, no.2, pp. 674-676, 2004.
[9] R. Noe, “PLL-free synchronous QPSK polarization multiplex/diversity receiver concept with digital I&Q baseband processing,” IEEE Photon Technology Letter, vol. 17, pp. 887-889, 2005.
[10] K. Kikuchi, “Phase-diversity homodyne detection of multilevel optical modulation with digital carrier phase estimation,” IEEE Journal of Selected Topics in Quantum Electronics, vol. 12, no. 4, pp. 563-570, 2006.
[11] Y. Han, and G. Li, “Coherent optical communication using polarization multiple-input multiple-output,” Optics Express, vol. 13, pp. 7527-7534, 2005.
[12] V. Curri, P. Poggiolini, A. Carena, and F. Forghieri, “Dispersion compensation and mitigation of nonlinear effects in 111-Gb/s WDM coherent PM-QPSK systems,” IEEE Photonics Technology Letters, vol. 20, pp. 1473-1475, 2008.
[13] A. Bononi, N. Rossi, and P. Serena, “Transmission limitations due to fiber nonlinearity,” Proceedings of OFC/NFOEC’2011, paper OWO7, 2011.
[14] G. Charlet, J. Renaudier, M. Salsi, H. Mardoyan, P. Tran, and S. Bigo, “Efficient mitigation of fiber impairments in an ultra-long haul transmission of 40Gbit/s polarization-multiplexed data by digital processing in a coherent receiver,” Proceedings of OFC/NFOEC’2007, paper PDP17, 2007.
[15] N. Kaneda, and A. Leven, “Coherent polarization-division-multiplexed QPSK receiver with fractionally spaced CMA for PMD compensation,” IEEE Photonics Technology Letters, vol. 21, pp. 203-205, 2009.

[16] L. Li, Z. Tao, L. Dou, W. Yan, S. Oda, T. Tanimura, T. Hoshida, and J. C. Rasmussen, “Implementation efficient nonlinear equalizer based on correlated digital backpropagation,” Proceedings of OFC/NFOEC’2011, paper OWW3, 2011.
[17] M. Oerder, and H. Meyr, “Digital Filter and Square Timing Recovery”, IEEE transactions on communications, vol. 36, no. 5, pp. 605-612, 1988.
[18] D. N. Godard, “Self-Recovering Equalization and Carrier Tracking in Two-Dimensional Data Communication Systems”, IEEE Transactions on Communications, vol. COM-28, no. 11, pp. 1867-1875, 1980.
[19] W. A. Sethares, G. A. Rey, and C. R. Johnson, “Approaches to blind equalization of signals with multiple modulus,” Proc. Int. Conf. Acoustics, Speech, Signal Process, vol. 2, pp. 972-975, 1989.
[20] T. Pfau, S. Hoffmann, and R. Noe, “Hardware-Efficient Coherent Digital Receiver Concept With Feed-forward Carrier Recovery for M-QAM Constellations”, Journal of Lightwave Technology, vol. 27, no. 8, pp. 989-999, 2009.
[21]http://support.huawei.com/onlinetoolsweb/resources/en/16_osnr.html

Chapter 3 Fundamentals of optical fiber propagation

3.1 Introduction

The combination of advanced modulation formats such as DP-QPSK, DP-16QAM and DP-64QAM with coherent detection technology has become the preferred scheme for realizing 40/100G optical network. The scheme can compensate for the linear impairments introduced by the optical signal in the transmission process at the receiver. Therefore, the important factors that limit the communication performance of this scheme are the nonlinear impairment caused by optical signals in the transmission process, including self-phase modulation (SPM), cross-phase modulation (XPM), four-wave mixing (FWM) and nonlinear phase noise and so on. For the common multichannel wavelength division multiplexing (WDM) systems, the XPM effect between channels is particularly serious for polarization multiplexing systems. It not only disturbs the phase of the signal, but also causes another serious nonlinear damage, called cross-polarization modulation between channels.

In this chapter, nonlinear Schrodinger equation in optical communication systems are mainly discussed in section 3.2, including attenuation, chromatic dispersion, polarization mode dispersion and nonlinear interference noise (SPM, XPM, FWM). Then in section 3.3 nonlinear propagation characteristics of 10Gbps signal in DSF was investigated by simulation methods. Finally, we make a conclusion in section 3.4.

3.2 Non-linear Schrödinger equation

Like any other physical propagation, an optical communication channel is called a waveform channel, which communicates a time-varying voltage from one point to another. A complication for optical links is that the fiber propagation of the signal waveform is conventionally modeled with a nonlinear partial differential equation, the nonlinear Schrödinger equation (NLSE), where fiber dispersion, nonlinearities, and amplifier noise distort the signal:

$$\frac{\partial E(z,t)}{\partial z} = j\frac{\beta_2}{2}\frac{\partial^2}{\partial t^2}E(z,t) - \alpha E(z,t) - j\gamma|E(z,t)|^2 E(z,t)$$

E is the electric field, α is the attenuation coefficient, β_2 is the dispersion parameter, γ is the nonlinear coefficient, z and t are the propagation direction and time, respectively.

An even more effective one is the Manakov equation which accounts for both polarizations:

$$\frac{\partial E_x(z,t)}{\partial z} = j\frac{\beta_2}{2}\frac{\partial^2}{\partial t^2}E_x(z,t) - \alpha E_x(z,t) - j\gamma\frac{8}{9}[|E_x(z,t)|^2 + |E_y(z,t)|^2]E_x(z,t)$$

$$\frac{\partial E_y(z,t)}{\partial z} = j\frac{\beta_2}{2}\frac{\partial^2}{\partial t^2}E_y(z,t) - \alpha E_y(z,t) - j\gamma\frac{8}{9}\left[|E_x(z,t)|^2 + |E_y(z,t)|^2\right]E_y(z,t)$$

3.2.1 Attenuation

The attenuation of an optical fiber measures the amount of light lost between input and output. Optical losses of a fiber are usually expressed in decibels per kilometer (dB/km). The expression in called the fiber attenuation coefficient a and the expression is

$$\alpha = -\frac{10}{z[km]}\log(\frac{P(z)}{P(0)})$$

where $P(z)$ is the optical power at a position z from the origin, $P(0)$ is the power at the origin.

For a given fiber, these losses are wavelength-dependent which is shown in the figure below. The value of the attenuation factor depends greatly on the fiber material and the manufacturing tolerances. It can be divided in three window shown in Figure 3.1:

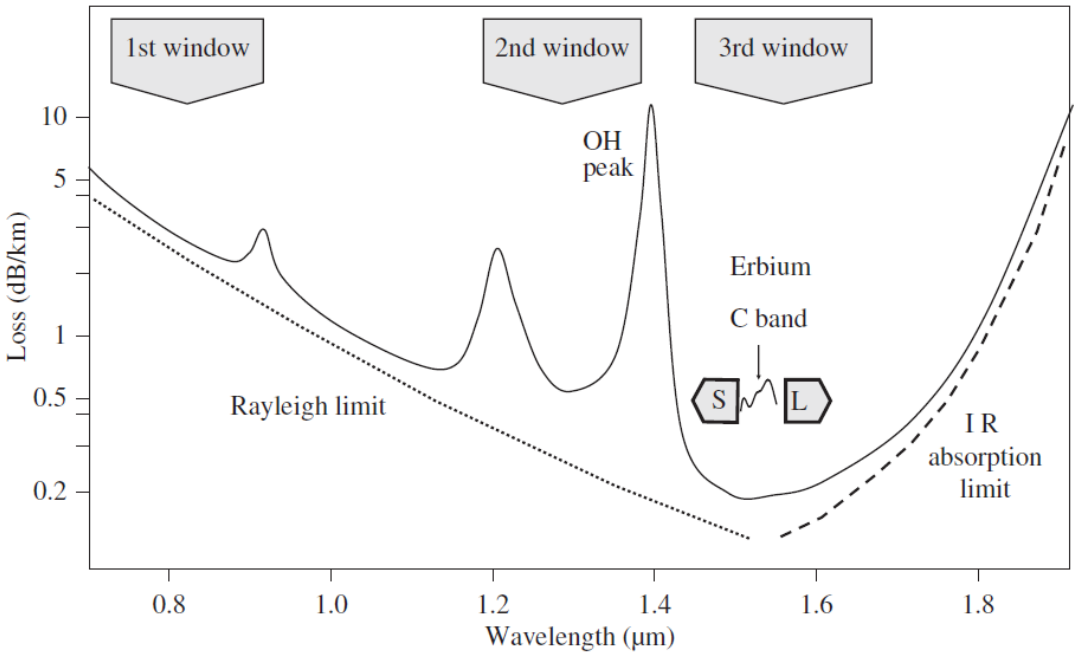

Figure 3.1 Attenuation Spectrum of optical fiber. (After reference Chesnoy, José Undersea Fiber Communication Systems, Second Edition-Academic Press (2015) chapter 1)

First window centered around 850nm with typical value of attenuation of 2 to 3dB/km.

Second window centered around 1300nm with typical value of attenuation of 0.4 to 0.5 dB/km.

Third window centered around 1550nm with value of attenuation of 0.2 to 0.25 dB/km.

3.2.2 Chromatic dispersion and Polarization model dispersion

Chromatic dispersion (CD) is an important factor in fiber optic communications. It is the result of the different wavelengths, in a light beam arriving at their destination at slightly different times. It can be seen that in the frequency domain the chromatic dispersion introduces a distortion on the phase of the signal spectrum without changing the spectral power distribution and at the end of the propagation the pulse result broadened.

The group velocity dispersion (GVD) parameter β_2 gives the time delay between two different spectral component separated by a certain frequency interval. Usually the dispersion is measured with the dispersion coefficient D defined as:

$$\mathrm{D} = -\frac{2\pi c}{\lambda^2}\beta_2$$

where $\lambda = -2\pi c/\omega$ is the carrier wavelength and c is the speed of light. D gives the time delay between two different spectral component separated by a certain wavelength interval.

Polarization is the property of waves, which can oscillate with more than one orientation. Until recently, with the emergence of digital coherent detection, polarization division multiplexing (PDM) of transmitted signals on two orthogonal states of polarization of the same wavelength has been widely used in optical communication systems [1-4]. Since all optical field information can be retained and accessed after coherent detection, optical phase and polarization can be used to encode data, which significantly improves the spectral efficiency and capacity of optical communication systems. In details, signals are first mixed with local oscillator (LO) in photoelectric detector of coherent receiver by analog-to-digital converter (ADC), then converted to digital format, and digital signal processing (DSP) is used to recover signals.

3.2.3 Nonlinear interference noise

In addition to linear impairments, nonlinear effects have become a serious performance limitation at high input power and high bit rate transmission systems. Nonlinear interference caused by Kerr effect in optical fibers can be divided into three types. (i) signal-signal interference caused by the non-linear interaction involving one or more optical signals; (ii) signal-noise interference caused by the nonlinear interaction between

signal and co-propagating optical amplifier noise; (iii) noise-noise contributions caused by the nonlinear interaction between amplifier noise and its own [5]. In practical related WDM systems, the transmitted signals are obviously stronger than the co-propagating noise, so the signal-signal contribution constitutes the main nonlinear impairments [6-7].

Nonlinear effects can also be caused by inelastic scattering, such as simulated Brillouin scattering (SBS) and stimulated Raman scattering (SRS). SBS and SRS are inelastic processes in which part of the optical wave power is absorbed by the optical medium. These effects can be neglected because channel interaction due to stimulated Raman scattering (SRS) effect is not considered in C-band [8].

In general, the nonlinearity of optical fibers can be divided into intra-channel and inter-channel nonlinearities. Intra-channel nonlinearity can be further divided into SPM, intra-channel FWM (IFWM) and intra-channel XPM (IXPM) [9,10]. Inter-channel nonlinearity includes FWM, XPM and XPolM. According to the system parameters such as CD value, bit rate and modulation formats, one or more non-linear effects are more dominant than other effects. For example, in systems with low bit rate and CD value, FWM is the main nonlinear effect [11, 12], and XPolM may be the most disadvantageous nonlinear effect [13] in similar WDM PDM-QPSK systems with dispersion management.

Regardless of direct detection or coherent detection, the nonlinearity of optical fibers propagating in optical fibers is the same, but the difference lies in the transmission mode of information. In coherent detection system, besides amplitude, information is also carried by phase, and PDM is usually used to double the spectral efficiency. As a result, the phase and polarization distortion caused by XPM and XPolM, which are neglected in direct detection system, may cause serious damage in coherent detection system.

In coherent systems without any optical dispersion compensator, the signals spread rapidly in time due to large cumulative CD. The main nonlinear effects are intra-channel nonlinearity, such as IFWM and IXPM. For dispersion compensated coherent optical communication systems with inline optical dispersion compensators, the main non-linearity effect is inter-channel nonlinearity, including inter-channel XPolM and inter-channel XPM. Whether XPolM or XPM is dominant depends on the actual system configurations.

3.3 Nonlinear Propagation Characteristics of 10 Gbps Signal in DSF

3.3.1 10Gbps optical signal at and near zero dispersion of DSF

The modulation instability (MI) can be interpreted in terms of four-wave-mixing (FWM) process that is phase-matched by self-phase modulation (SPM), and this requires anomalous (positive) dispersion to occur for single wavelength input [14]. If the signal wavelength is set at or near zero dispersion region of transmission fiber in long-haul optical amplifier repeatered system, severe SNR degradation is known to be induced due to parametric amplification (MI gain) of ASE noise on each side of the signal [15]. In order to mitigate the degradation, non-zero dispersion shifted fiber, dispersion management fiber, and etc. are applied in most of optical amplifier repeatered systems [16]. Probably due to the effectiveness of such a dispersion management, nonlinear propagation at and near zero dispersion has so far attracted little attention.

In this section, we have comprehensively investigated transmission property of single-channel 10 Gbps signal in DSF at and near zero dispersion in terms of signal power and wavelength as well as transmission distance. We consider typical optical amplifier repeatered system as shown in Figure 3.2.

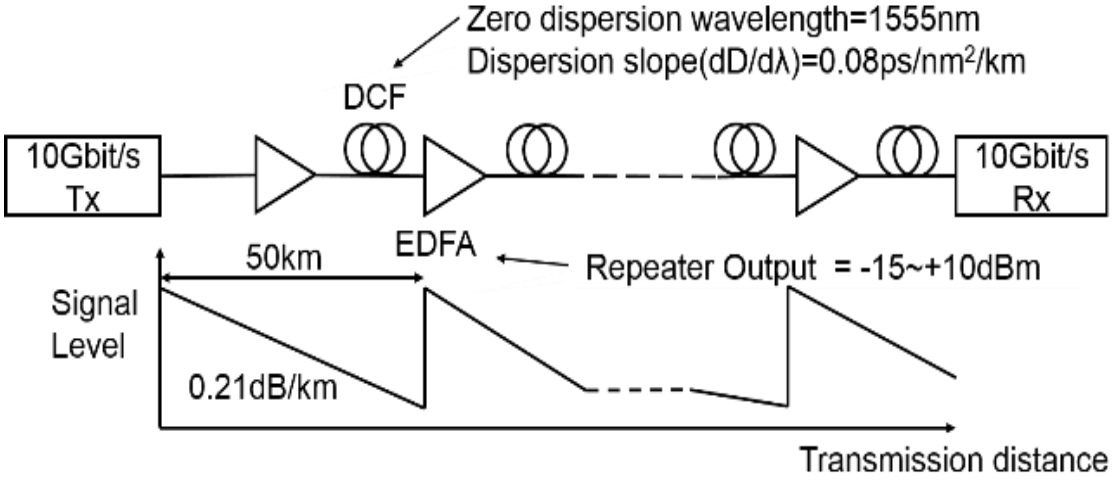

Figure 3.2 Simulated system model.

3.3.2 Results and discussions

Figures 3.3 and 3.4 show evolution of Q values and examples of received signal waveforms without dispersion compensation, respectively, as a function of transmission distance, at a wavelength of 1552 nm, 1555 nm and 1558 nm. Here, transmitter power and repeaters' output power are set at +3dBm. It can be seen from Fig.3.3 that, in all cases, Q values decreases with distance that is due to combined effect of noise accumulation, dispersion and fiber nonlinearity.

Figure 3.4 reveals, however, that the Q degradations are induced in difference ways, depending on operating signal wavelength. In case of negative dispersion (-0.24

ps/nm/km) at 1552 nm wavelength, signal waveforms broadened with distance and severe inter-symbol-interference (ISI) occurs for distances exceeding approximately 1000 km transmission distance. This is a typical appearance of self-phase-modulation. By contrast, at 1555 nm and 1558nm of zero and positive dispersion (+0.24 ps/nm/km), large noise-like fluctuations are seen to impose on "mark" symbols. This enhancement of fluctuations is presumably due to nonlinear parametric interaction between signal and ASE noise, which excessively amplifies the noise on each side of the signal wavelength.

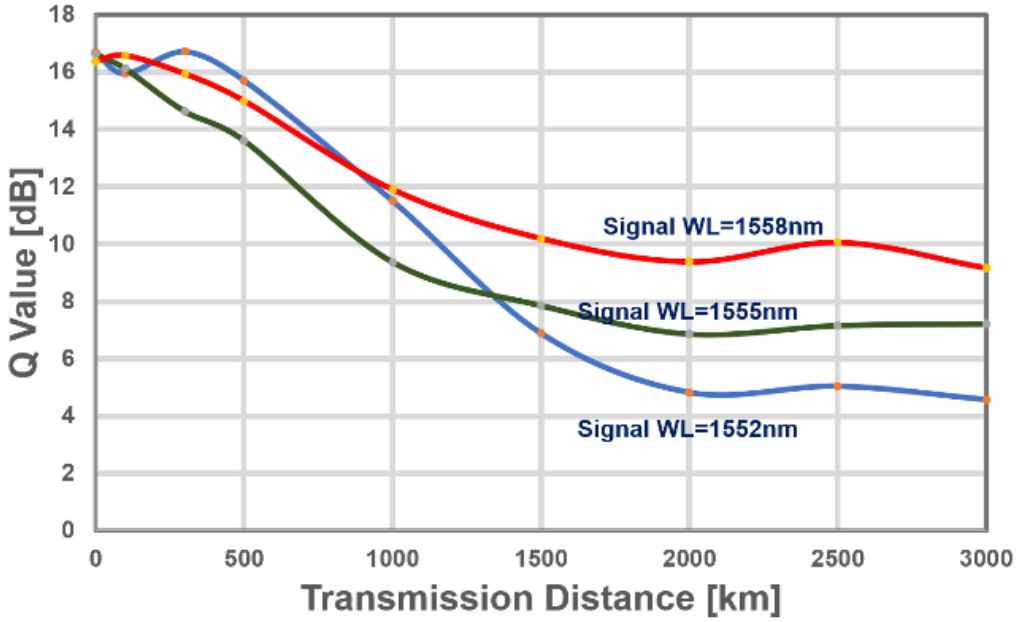

Figure 3.3 Q value evolution with transmission distance.

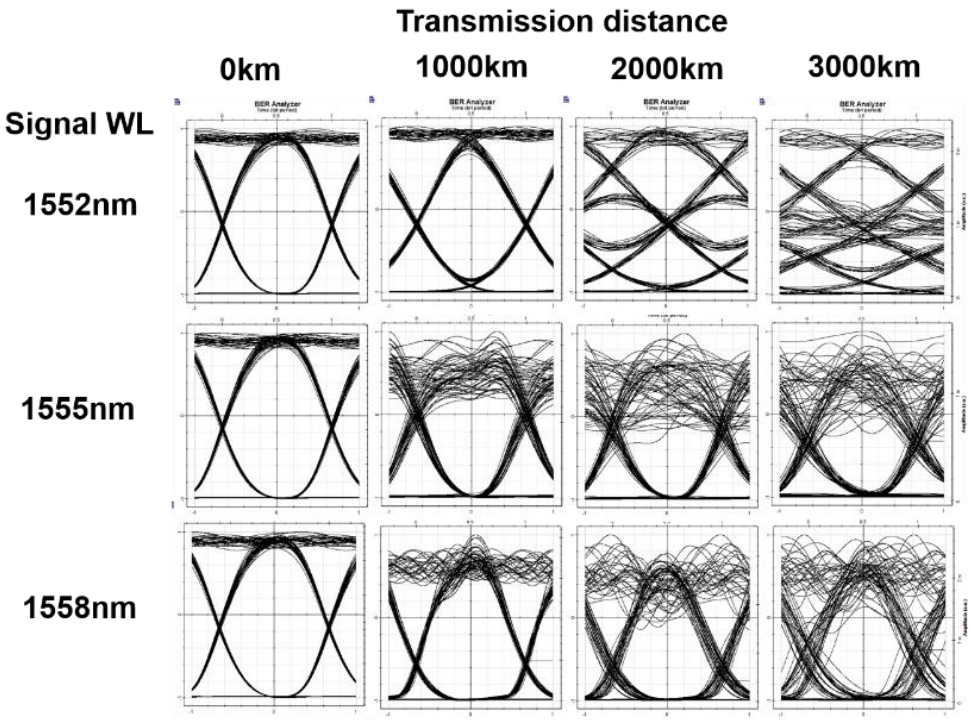

Figure 3.4 Examples of received waveforms.

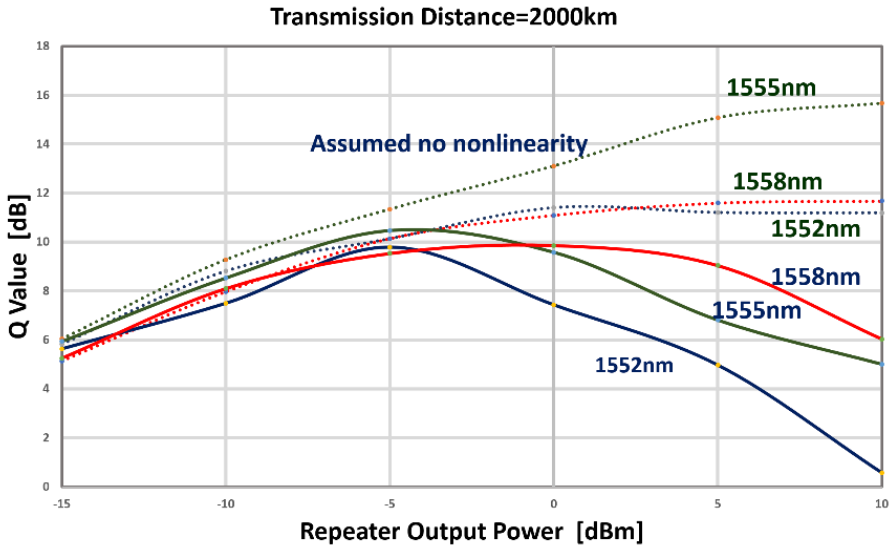

Figure 3.5 Q value dependence on repeater output power.

Figure 3.5 indicates Q value dependence on repeater output power at 2,000 km transmission for the three wavelengths. Dispersion compensation is not applied in this calculation. For reference purpose, hypothetical calculation results by setting nonlinear coefficient of DSF to zero are also plotted with dotted curves. In this case, the Q performances are dominated only by linear effect with loss and dispersion.

As is seen in this figure that for lower signal powers, Q value increases with power in linear fashion, while with power increase, it saturated and then started to decrease. So there is the optimum power that maximize the transmission performance, which is dependent on signal wavelength or dispersion.

We have further investigated the Q value dependence on the operation wavelength with and without dispersion compensation. The results of Q values are shown in Fig.3.6. Here, in Fig.3.6, dotted and dashed-dotted lines are for hypothetical cases of being free from dispersion & nonlinearity and nonlinearity, respectively, to analyze the contribution of each effect on Q degradation. In this simulation, the dispersion compensation is applied at receiver side only and tuned to the optimum, at which the Q value is maximized. In addition, the compensation period is tested at both 200 km and 500 km and the results are also compared in the figure.

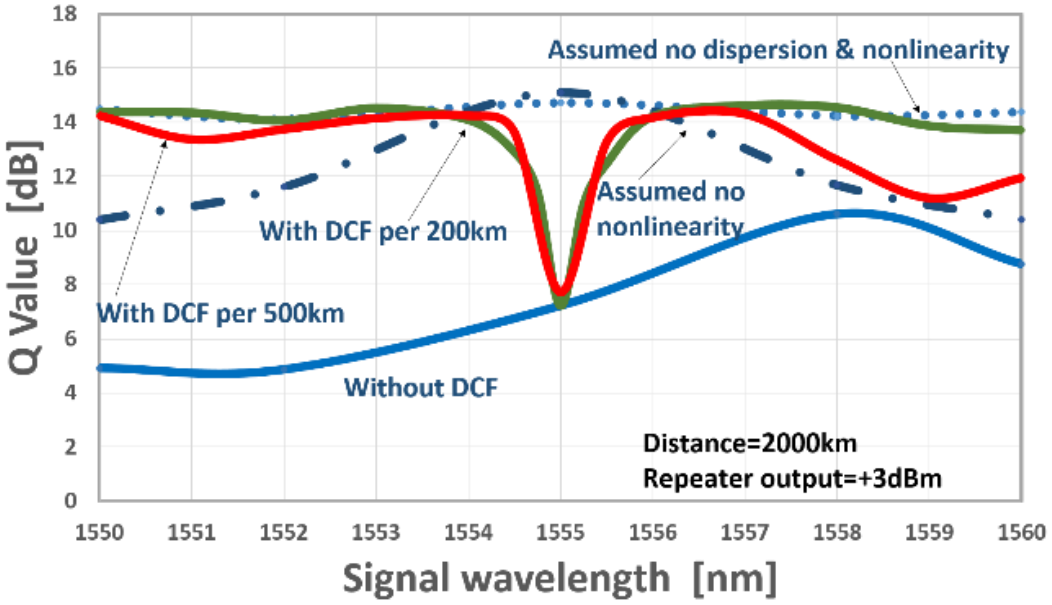

Figure 3.6 Q performance with and without dispersion compensation at 2000km transmission.

It can be seen from Fig.3.6 that, in case of without dispersion compensation, the Q value maximized at a wavelength of 1558 nm, which is due to soliton effect or balance between linear pulse broadening and nonlinear pulse compression. It is also clearly seen in this figure that, even with dispersion compensation, the Q value degradations were unable to be alleviated for $\lambda_0 \pm 1$ nm wavelength region, while, outside this wavelength band, the degradation was effectively cancelled out by dispersion compensation.

This implies that the degradation of $\lambda_0 \pm 1$ nm is not by inter-symbol-interference, but by ASE noise increase. It was also found that, by shortening the dispersion compensation period to 200 km, the transmission degradation could be reduced to about 1 dB or less in

a wide signal wavelength range of 10 nm or more, excluding the wavelength range of $\lambda_0 \pm 1$ nm. It should be worthy to note that inherent nonlinear degradation near zero dispersion appears to be symmetric in terms of wavelength despite that MI gain should vanish in normal dispersion with deviation from zero dispersion.

3.4 Concluding remarks

Nonlinear effects have increasingly become an important factor limiting the transmission capacity of optical fiber communication system. In this chapter, nonlinear Schrodinger equation in optical communication systems are mainly discussed in section 3.2, including attenuation, chromatic dispersion, polarization mode dispersion and nonlinear interference noise (SPM, XPM, FWM). Then in section 3.3, we have comprehensively investigated transmission property of single-channel 10 Gbps signal in DSF. Quite different feature of signal degradation in positive and negative dispersion regimes is clarified in terms of signal operation wavelength as well as transmission distance. Further, intrinsic nonlinear degradation near zero dispersion is found to be symmetric in terms of wavelength despite that MI gain should vanish in normal dispersion with deviation from zero dispersion.

References

[1] S. J. Savory, et al., "Digital equalization of 40 Gbit/s per wavelength transmission over 2480 km of standard fiber without optical dispersion compensation," Proceedings of ECOC'2006, paper Th2.5.5, 2006.

[2] H. Sun, K. T. Wu and K. Roberts, "Real-time measurements of a 40 Gb/s coherent systems," Optics Express, vol.16, no. 2, pp. 873-879, 2008.

[3] W. Shieh, H. Bao, and Y. Tang, "Coherent optical OFDM: theory and design," Optics Express, vol. 16, no. 2, pp. 841-859, 2008.

[4] A. H. Gnauck, et al., "Generation and transmission of 21.4-Gbaud PDM 64-QAM using a novel high-power DAC driving a single I/Q modulator, " Journal of Lightwave Technology, vol. 30, no. 4, pp. 532-536, 2012.

[5] A. Amari, D. Octavia, Venkatesan R, Kumar O. S. Sunish, C. Philippe, and J. Yves, "A survey on fiber nonlinearity compensation for 400Gbps and beyond optical communication systems", IEEE Communications Surveys & Tutorials, pp. 1-40, 2017.

[6] R. J. Essiambre, G. Kramer, P. J. Winzer, G. J. Foschini, and B. Goebel, "Capacity limits of optical fiber networks," Journal of Lightwave Technology, vol. 28, no. 4, pp. 662-701, 2010.

[7] P. Serena, “Nonlinear signal noise interaction in optical links with nonlinear equalization,” Journal of Lightwave Technology, vol. 34, no.6, pp. 1476-1483, 2016.
[8] D. Semrau, R. I. Killey, and P. Bayvel, “The Gaussian Noise Model in the Presence of Inter-Channel Stimulated Raman Scattering,” Journal of Lightwave Technology, vol. 36, no. 14, pp.3046-3055, July 15, 2018.
[9] R. J. Essiambre, B. Mikkelsen, and G. Raybon, “Intra-channel cross-phase modulation and four-wave mixing in high-speed TDM systems” Electronics Letters, vol. 35, no.18, pp. 1576-1578, 1999.
[10] P. V. Mamyshev, and N. A. Mamysheva, “Pulse-overlapped dispersion-managed data transmission and intra-channel four-wave mixing,” Optics Letters, vol. 24, no. 21, pp. 1454-1456, 1999.
[11] R. W. Tkach, A. R. Chraplyvy, F. Forghieri, and A. H. Gnauck, “Four-photon mixing and high-speed WDM systems,” Journal of Lightwave Technology, vol. 13, no. 5, pp. 841-849, 1995.
[12] P. J. Winzer and R. J. Essiambre, “Advanced modulation formats for high-capacity optical transport networks,” Journal of Lightwave Technology, vol.24, no. 12, pp. 4711-4728, 2006.
[13] C. Xie, “Inter-channel nonlinearities in coherent polarization-division-multiplexed quadrature-phase-shift-keying systems,” IEEE Photonics Technology Letters, vol. 21, pp. 274-276, 2009.
[14] G. P. Agrawal, Nonlinear Fiber Optics, Academic Press, fifth ed., Chapter5, 2013.
[15] N. Henmi, Y. Aoki, T. Ogata, T. Saito, and S. Nakaya, “A new design arrangement of transmission fiber dispersion for suppressing nonlinear degradation in long-distance optical transmission systems with optical repeater amplifiers,” Journal of Lightwave Technology, vol. 11, no. 10, pp. 1615-1621, 1993.
[16] G. P. Agrawal, Fiber Optic Communication Systems, John Wiley & Sons, Inc. fourth ed., Chapter8, 2010.

Chapter 4 Non-repeatered system and simulation results

4.1 Introduction

In recent years, with the progress of high speed digital signal processing technology (DSP) and analog to digital conversion technology, coherent optical transmission technology has become a hot topic in the field of optical communication. With the combined technologies of coherent detection and digital signal processing (DSP), long-haul optical transmissions have become possible without optical dispersion compensation [1-3]. This enabled us to configure 100Gbps-based dense wavelength division multiplexed (DWDM) undersea and transcontinental trunk practical systems by utilizing ultra-low-loss and large effective area (Aeff) single-mode silica fibers (SMFs) for transmission line [4-5].

For non-repeatered system application, several reports have been published on both high-capacity and long-reach transmission [6]. And single-span transmission exceeding 400 km and/or a capacity-reach product of over 5 Pbps-km have been demonstrated by adoption of optimized Raman/Remote Optically Pumped Amplifier (ROPA) as well as high power booster amplifiers[7-11]. In those systems, the maximum transmission powers are considered to be limited by optical fiber nonlinearity, but, to the best of our knowledge, neither quantitative simulation studies nor experimental investigations have so far been reported on this topic.

4.2 BER characteristic on modulation formats

4.2.1 System configuration and simulation method

We consider simplest non-repeatered system without any Raman/ROPA as shown in Fig.4.1. For comparison purpose, we have tested three kinds of modulation/detection schemes, those are, 120 Gbps, Gray-coded DP-QPSK (NRZ), DP-16 QAM (NRZ) and DP-64 QAM (NRZ) with up to 80 channels, while keeping channel spacing at 50 GHz. The 120 Gbps corresponds to a net throughput of 100 Gbps plus 20 % of overhead/redundant bits for forward error correction (FEC) [4]. The laser linewidth assumed is 100 kHz (FWHM, Gaussian) by considering laser phase noise. Optical bandwidths for both OPT MUX and OPT DEMUX are assumed 45 GHz with 5th Bessel filtering for DP-QPSK, while those are 30 GHz with the same filter shapes for both DP-

16QAM and DP-64QAM. The transmission fiber assumed is a typical advanced silica SMF with a loss coefficient of 0.16 dB/km, effective core area of 130 μm^2, chromatic dispersion of 20.5 ps/nm/km, and the nonlinear refractive index n2 of 2.2 $\times 10^{-20}$ m^2/W. The PMD is assumed 0.05 $ps/km^{1/2}$. Each of the coherent receiver is set to receive -10 dBm/ch signal power through optical pre-amplifier with a noise figure of 4 dB, while the local oscillator power in the receiver is set at +10 dBm, so that shot noise limited receiver sensitivity can be achieved. The frequency response of electrical circuits are assumed to be ideally flat in both Tx and Rx. In the receiver, 4th order Bessel filter with bandwidth of 0.75 ×0.5 ×symbol rate is applied, in view of the pulse format of NRZ.

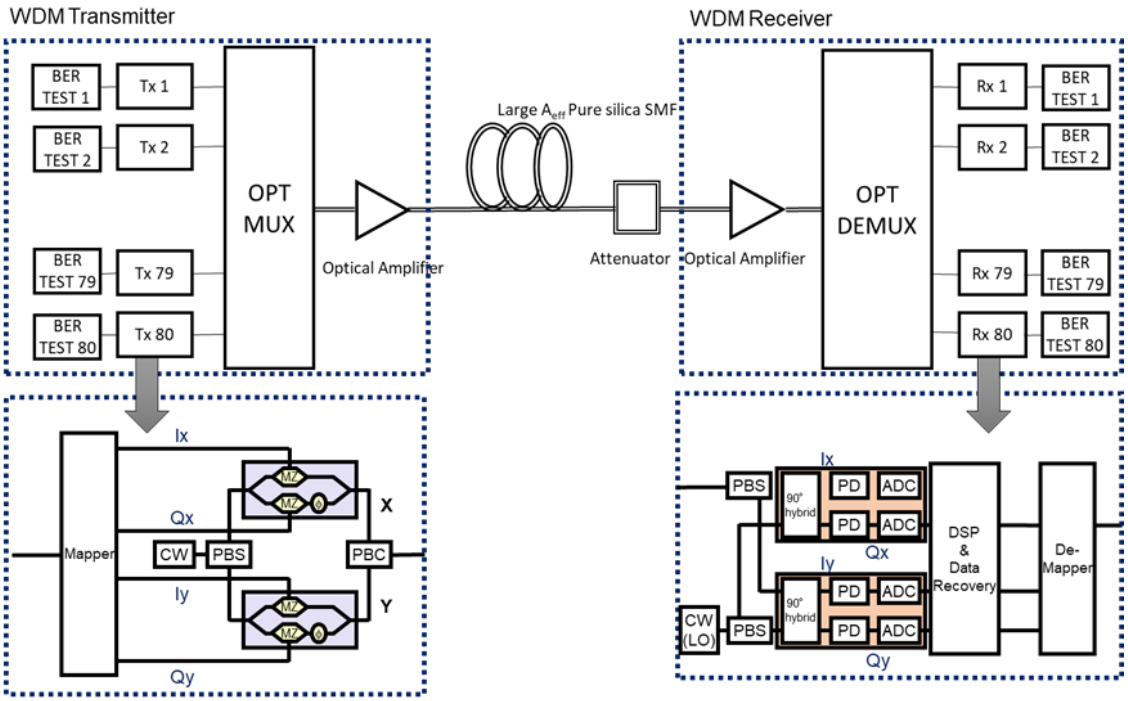

Figure 4.1 Non-repeatered system configuration for 120Gbps DP-QPSK, DP-16QAM and DP-64QAM formats. Tx is transmitter, OPT MUX is optical multiplexer, OPT DEMUX is optical demultiplexer, Rx is receiver, SMF is single mode fiber, CW is continuous wave laser source, PBS is polarization beam splitter, PBC is polarization beam combiner, LO is local oscillator, PD is photodiode, ADC is analog to digital converter, MZ is Mach-Zehnder Modulator and DSP is digital signal processor.

In the DSP of the receiver, the Digital Square and filter algorithm [12] is used for timing recovery scheme. Then, the adaptive equalizer by two-stage constant modulus algorithm-radius directed (CMA-RD) algorithm [13, 14] is used to compensate for residual chromatic dispersion, polarization mode dispersion (PMD) and to reduce inter- symbol interference. In the equalizer, the butterfly structure is applied for polarization demultiplex. After that, frequency offset estimation (FOE) and carrier phase offset

estimation (CPE), by the blind phase search (BPS) algorithm [15], are performed to regenerate the I/Q signal.

For numerical analyses, we have applied optical communication software simulation tool, OptiSystem ™ (Ver.14.1) from Optiwave Systems. This tool is adopted to adequately account for such system parameters as loss, dispersion, nonlinearity (Kerr effect) and polarization effects in optical fiber as well as coherent transmitter and receiver characteristics including optical ASE noise [16]. It should be worthy to note that, by adequate and careful parameters setting, general validity of system-level simulations by this kind of tools are checked in advance by comparing the simulation results with experimental results for long-distance transmission systems [4].

We have assumed the fiber loss constant and also have not taken into account the stimulated Raman scattering (SRS) effect, both of which will induce frequency-dependent WDM signal profile [17]. Separately-made test simulation considering the SRS has shown that the maximum Tx powers deviate approximately 0.4 dB_{p-p} for C-band, 50 GHz-spaced 80 channels (32 nm bandwidth). Therefore for extremely wideband system extended to C+L band, we need to consider the frequency-dependent effects to discuss the maximum transmitter powers and its distribution among WDM channels of non-repeatered systems.

In all the simulation described here, we have used pseudo random binary sequence (PRBS) of 2^{16} with a length of 65536. This data stream is bit-interleaved to configure two paths for X and Y polarizations. Then up to 1.5×10^{-5} BER can be calculated.

4.2.2 BER and constellation maps evolution for single-channel input

Firstly, we show in Fig. 4.2 examples of constellation map, i.e., received waveforms of DP-QPSK, DP-16QAM and DP-64QAM signals at several transmitter powers with single-channel transmission. Here, the transmission fiber length is set over 100km, fairly longer than the effective fiber length described, thus the results are applicable to any of long-length non-repeatered systems. In the following, one polarization component of X axis is shown since there was no noticeable difference between two polarization components. In case of the DP-QPSK signal, when the optical transmission power (Tx) exceeds +18 dBm (+15 dBm per polarization), the circular cloud of each symbol becomes an elongated ellipse in shape and its distribution is seen to further expand with the increase of Tx power.

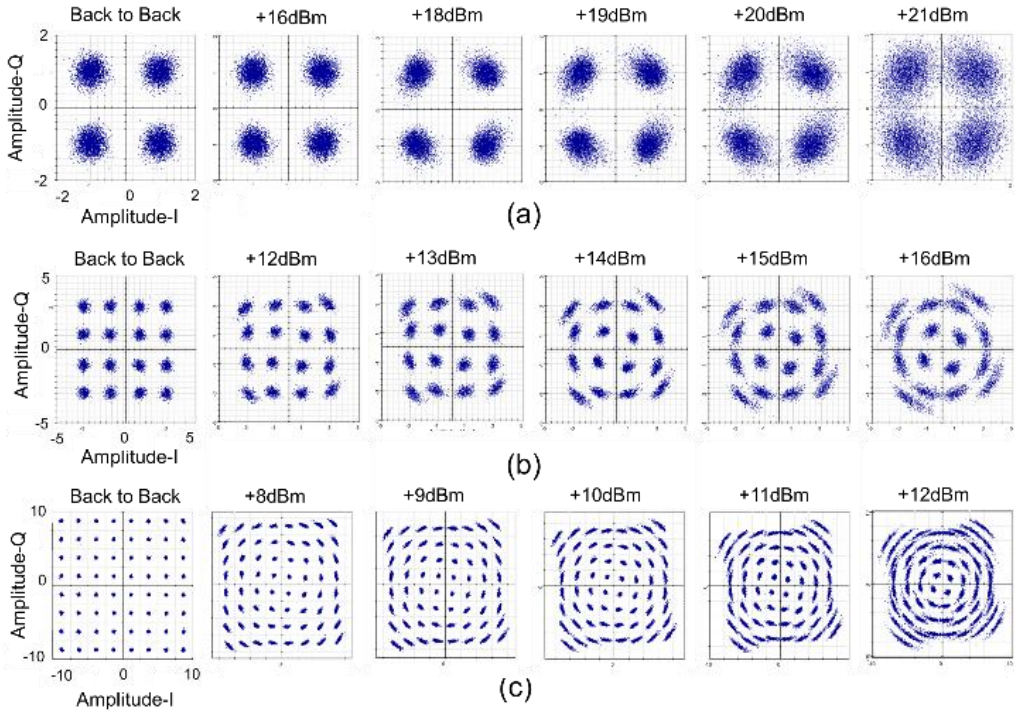

Figure 4.2 Evolution of constellation map (a.u.) with Tx power. (a) DP-QPSK, L=300 km transmission. (b) DP-16QAM, L=200 km transmission. (c) DP-64QAM, L=100 km transmission.

As will be shown in Fig.4.3, according to such a symbol distortion, the BER floor becomes significant, depending on the transmission power level. In case of DP-16QAM, the symbols begin to distort at Tx powers of +12 dBm (+9 dBm per polarization) or higher, then the distortion is further enhanced with the increase of Tx power. If we have a closer look at each of symbol distortion, the outer symbol is recognized to have more elongated elliptical shape because of its higher power, compared to inner symbol. Such a nonlinear behavior is more enhanced in case of DP-64QAM, as is clearly seen in Fig.4.2 (c): the symbol begins to distort at Tx Powers above +8 dBm (+5 dBm per polarization). Further, the more the symbol is located outside, the greater the distortion is. It is noted that even at Tx powers where the outer symbols are entirely distorted, the symbols near the center are still kept circular. If we roughly calculate the phase rotation (the rotation angle is defined as a spreading of a constellation point in the angular direction) of DP-64QAM from observed symbols at +12dBm, the phase rotations of the most inner four symbols are about 10 degrees, while those of the most outer four symbols at corners are read to be about 40-50 degrees. This is presumably due to enhancement of signal phase variance during transmission because of nonlinear phase noise [18].

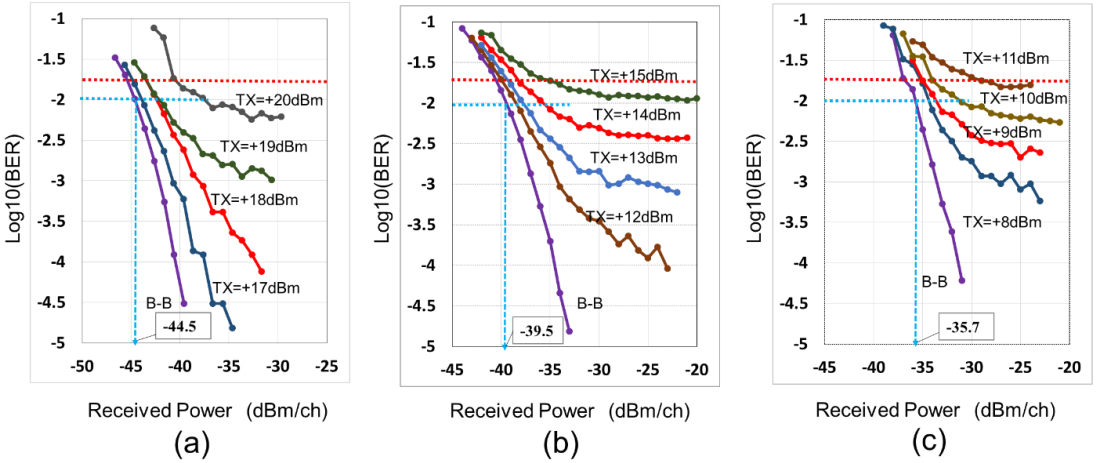

Figure 4.3 The BER characteristics for single channel DP-QPSK, DP-16QAM and DP-64QAM. (a) DP-QPSK-300km. (b) DP-16QAM-200km. (c) DP-64QAM-100km.

The above dependence on the modulation scheme will be attributable to the difference in symbol peak power. That is, QAM modulation applies both amplitude and phase modulation, while QPSK imposes only phase modulation. Then, in case of +16 dBm DP-QPSK, each symbol has +13 dBm power at the fiber input. On the other hand, in case of +16 dBm DP-16QAM, the symbols can be divided into three groups in terms of symbol powers. The most inner 4 symbols has a lowest power of +6.0 dBm and the most outer 4 symbols has a highest power of +15.6 dBm. Also, the rest of 8 symbols has a power of +13.0 dBm at the fiber input. Similarly, in case of +16 dBm DP-64QAM, the symbols can be divided in nine groups in terms of symbol powers, each of which are -0.2 dBm, +6.8 dBm, +9.3 dBm, +10.9 dBm, +12.1 dBm, +13.8 dBm, +14.4 dBm, +15.5 dBm and +16.7 dBm from the inner to outer symbols, respectively. Such a different amplitude and phase modulation would have resulted in the modulation dependence of the symbol distortion observed in Fig.4.2.

Figure 4.3 indicates the BER characteristics for 120 Gbps DP-QPSK, DP-16QAM and DP-64QAM with single-channel transmission. Here, the red dashed line shows FEC limit or detection limit with BER=1.8×10-2, achievable with 20% redundant bits [4]. Also, the blue dashed line gives back-to-back receiver sensitivity defined at BER=1.0 ×10-2. The calculated receiver sensitivities with 4th order Bessel filter with bandwidth of 0.75×0.5×symbol rate are -44.5dBm, -39.5dBm and -35.7dBm for DP-QPSK, DP-16QAM and DP-64QAM, respectively. On the other hand, shot noise limited sensitivities (signal power, Ps with dual polarizations) by a simple formula of Ps=SNR×4e×0.75B are -44.2dBm, -40.5dBm and -38.2dBm for DP-QPSK, DP-16QAM and DP-64QAM, respectively. Here, the SNR is baseband signal to noise ratio at BER = 1.0×10^{-2}, e is

electron charge, and B is symbol rate/2 (Electrical receiver bandwidth is assumed to 0.75B). The DP-QPSK sensitivity difference between the two is 0.3dB and this could happen due to possible approximation errors contained in application of the simple formula. On the other hand, the difference is increased to 1.0 dB and 2.5 dB for DP-16QAM and DP-64QAM, respectively, which is considered due to increase of inter-symbol interference in the coherent receiver.

It is clearly seen from the figures in Fig.4.3 that all three cases the BER deteriorates, pursuant to Tx powers and approaches to specific floor levels. In other words, achievable BER is dominantly determined by Tx power regardless of received signal level. If we define the maximum Tx power as the power at which BER floor levels are 1.0×10^{-2} at -25dBm received power or above, then those values are +20.4 dBm, +14.8 dBm and +10.6 dBm, for DP-QPSK, DP-16QAM and DP-64QAM, respectively. Here, linear extrapolation methodology is applied by using two curves close to 1.0×10^{-2} in Fig.4.4 for each modulation: For example, in case of DP-QPSK, the BER saturation level is 1.4×10^{-3} for 19dBm, while it is 5.7×10^{-3} for 20dBm, we get a value of +20.4 dBm by linear extrapolation of the above two points.

4.2.3 Maximum transmitter power dependence on the number of WDM channels

Next, we investigated high power DWDM transmission characteristics. Figure 4.4 gives 8WDM transmission performances for DP-16QAM, where constellation maps and BERs are shown. In this simulation, we did not consider SRS effect. Constellation map in Fig.4.5 (a) clearly indicates that there is no noticeable difference in nonlinear distortion among 8 channels. Here, the Tx power in this case is +18dBm/total or +9dBm/ch and the corresponding BER of each channel is around 3.0×10^{-4}. Fig.4.5 (b) further analyzes BER characteristics for 8 channels, ranging from +17dBm/total to +23dBm/total Tx powers. We see from this figure that BER distribution among 8 channels are very small. If we have a closer look at them, however, we also recognize that BER for center channel deteriorated slightly more as compared with that for outer channel. This is presumably due to the fact that the central channel is affected from its both sides by neighbor channels, while the edge channel is influenced only from one side of the channel.

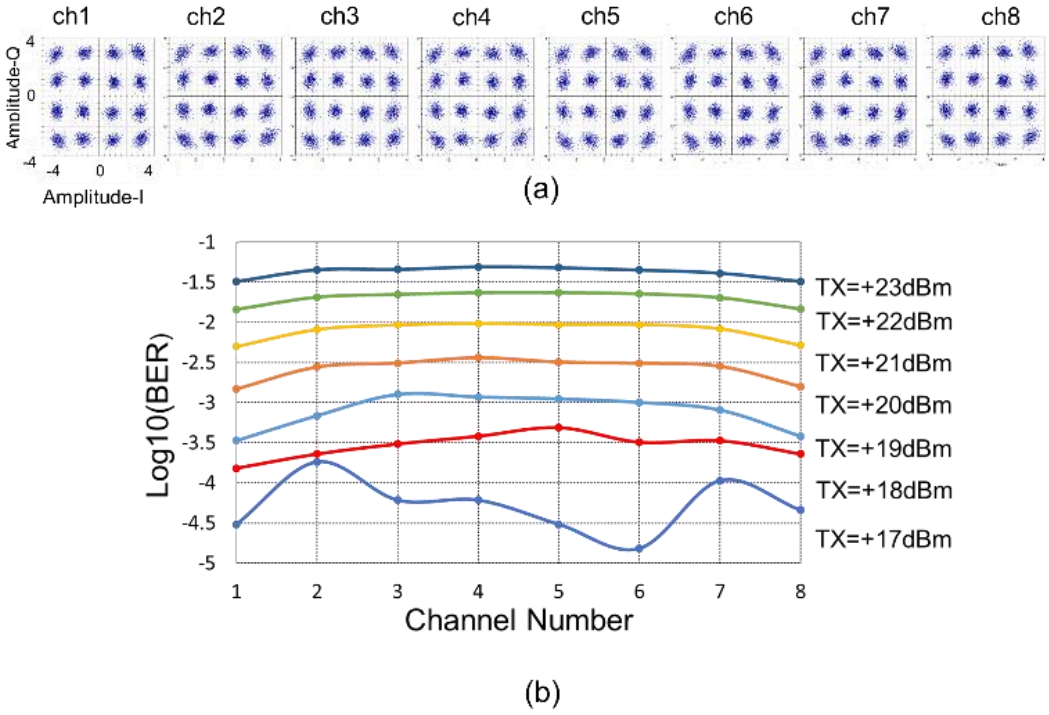

Figure 4.4 DP-16QAM 8WDM transmission characteristics. Fiber length is 100km. (a) Constellation map at +18dBm/total Tx power. (b) BER characteristics (received power is -25 dBm/ch).

Finally, Figure 4.5 shows the ensemble optical spectra for 120Gbps DP-16QAM 80WDM before and after 200 km transmission. Here, only in this case, the SRS is considered. The transmission channel power is +9dBm/ch where averaged BER for 80 channels is around 1.0×10^{-3}. In Fig.4.5 (a) of before transmission, we can confirm optical ASE noise level, which is generated by an optical amplifier in the transmitter. By contrast it is seen in Fig.4.5 (b) that new frequency components, slightly below ASE noise level, have developed outside the signal band. The new frequency components outside the signal band are presumably due to four-wave mixing and the same amount of the components should have imposed on each signal channel as well. We speculate that the new components are not dominant cause of the BER floors, but should develop further with the increase of transmitter power. It may be worthy to note that by taking the SRS effect into account, the WDM spectrum after transmission has tilted by 1.5dBp-p from shorter to longer wavelength. This in turn caused approximately 0.4dBp-p distribution in the maximum Tx power among 80 channels, while the average is kept unchanged.

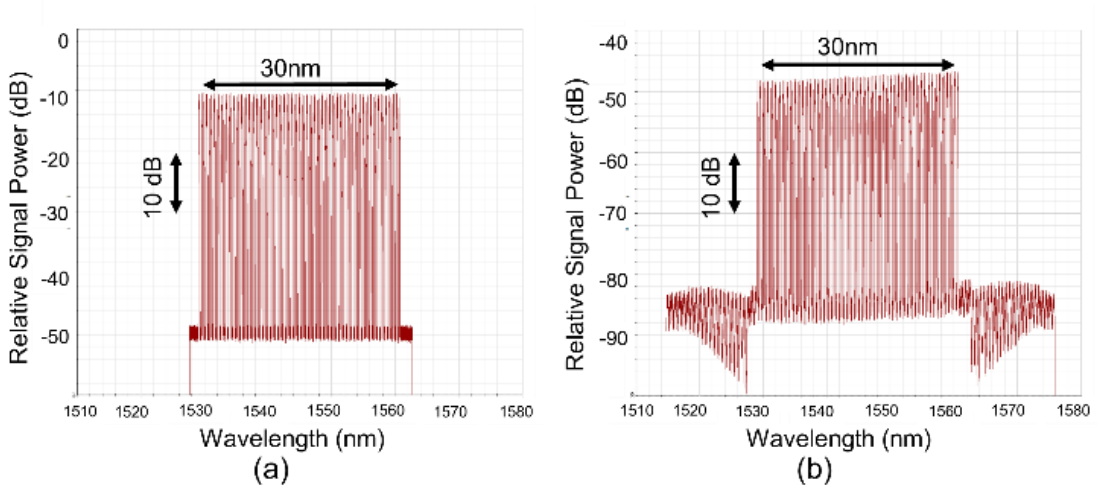

Figure 4.5 DP-16QAM 80WDM signal spectra at +9dBm/ch power. (a) Before 200km transmission. (b) After 200km transmission (with SRS effect). Resolution in optical spectrum is 0.001nm.

4.3 BER characteristic on symbol rate

4.3.1 System model and simulation method

We have tested three kinds of bit rates, that is, 120Gbps, 240Gbps and 360Gbps (Nyquist) Gray-coded DP-16 QAM (NRZ) with up to 80 WDM channels. The bit rate of 120Gbps corresponds to a net throughput of 100Gbps plus overhead/redundant bits for forward error correction (FEC), and so for other bit rates. This FEC scheme can correct bit errors by a few % and so we assume transmission limits at criteria of BER=$1x10^{-2}$ throughout this section.

Figure 4.6 shows optical spectra of DP-16QAM signals. The signal spectrum is seen to broaden with bit rate increase. Here, in the 360Gbps Nyquist case, raised cosine pulses are applied for Nyquist pulse shaping of both the I/Q channels before optical modulation so that we can get a rectangular spectrum.

The channel spacings are kept at 50GHz, and optical bandwidths are set 45GHz for both MUX and DEMUX. The transmission fiber assumed is a typical advanced silica SMF with a loss rare of 0.16 dB/km, effective core area of 130 um^2, chromatic dispersion of 20.5 ps/nm/km, and the nonlinear constant n^2 of 2.2×10^{-20} m/W. For theoretical analyses, we have applied commercial optical communication software simulation tool, OptiSystem ™ (Ver.14.2.1) from Optiwave Systems.

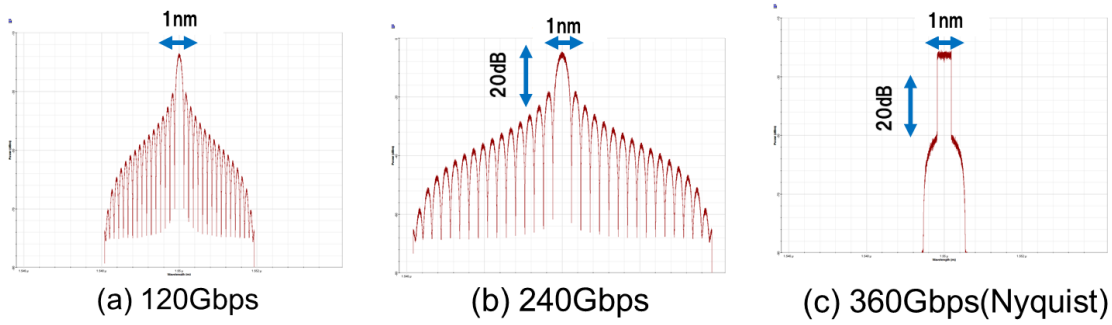

Figure 4.6 DP-16QAM signal spectrum for each bit rate.

4.3.2 Results and discussions

Figure 4.7 indicates the BER characteristics with several transmitter (Tx) powers for the three bit rates at single-channel operation. Here, the transmission fiber length is set 100km.

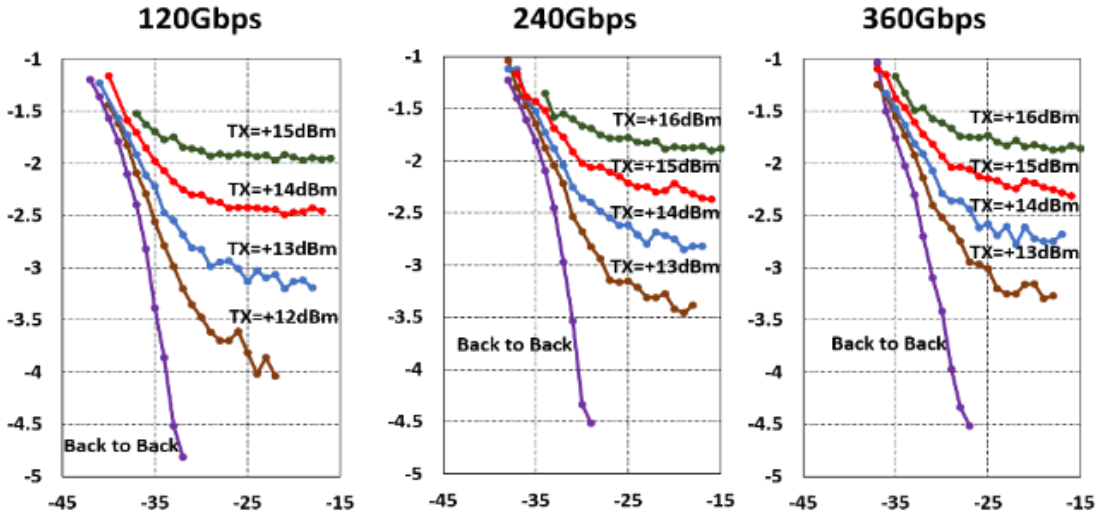

Figure 4.7 BER Characteristics for 120Gbps, 240Gbps and 360Gbps DP-16QAM for several Tx powers.

It is clearly seen from these figures that in all three cases the BER deteriorates, pursuant to Tx power and approaches to specific saturation levels. When the maximum input powers are defined as Tx powers at which BER saturates at $1x10^{-3}$ without FEC, those are approximately 13.3dBm, +13.5dBm and 13.9dBm, for 120Gbps, 240 Gbps and 360 Gbps, respectively..

On the other hand, back-to-back receiver sensitivities, defined at BER=$1x10^{-3}$ Rx powers, are approximately -35.5dBm, -32.5dBm and -31.5dBm, for 120Gbps, 240Gbps and 360 Gbps, respectively. Further, from the BER plots in Fig.4.7, the sensitivity changes

due to fiber transmission are found to be less than a few dB, when defined at BER=1x10^{-3}. Here, allowable span loss for non-repeated system can be interpreted by maximum Tx power minus Rx sensitivity. Figure 4.8 plots allowable span loss for DP-16QAM systems. The increase in maximum Tx power partly compensates for Rx sensitivity decrease due to bit rate increase. We believe this is a specific character for digital coherent systems with SMFs. The resultant allowable span losses are approximately 48.8dB, 46dB, and 45.4 dB for 120Gbps, 240Gbps and 360Gbps, respectively. These can be translated to the maximum transmission lengths of approximate 305 km, 290 km and 280 km for 0.16dB/km fiber.

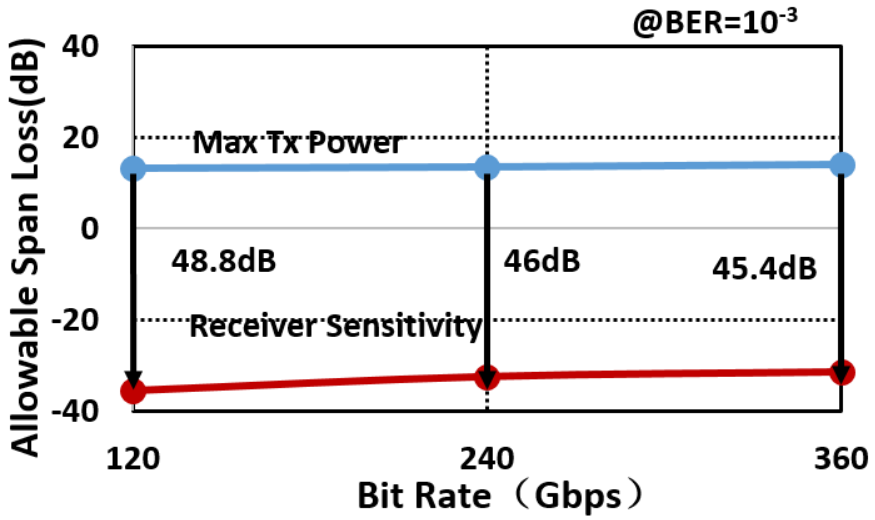

Figure 4.8 Allowable span loss for DP-16QAM systems.

Figure 4.9 shows the maximum Tx power dependence on the number of channels for 120Gbps and 360Gbps DP-16QAM cases. The maximum Tx powers are found to gradually decrease by a few dB, with the increase of the number of channels. So the allowable span loss and maximum transmission distance should be reduced accordingly, i.e., a few tens of km, compared with single-channel case.

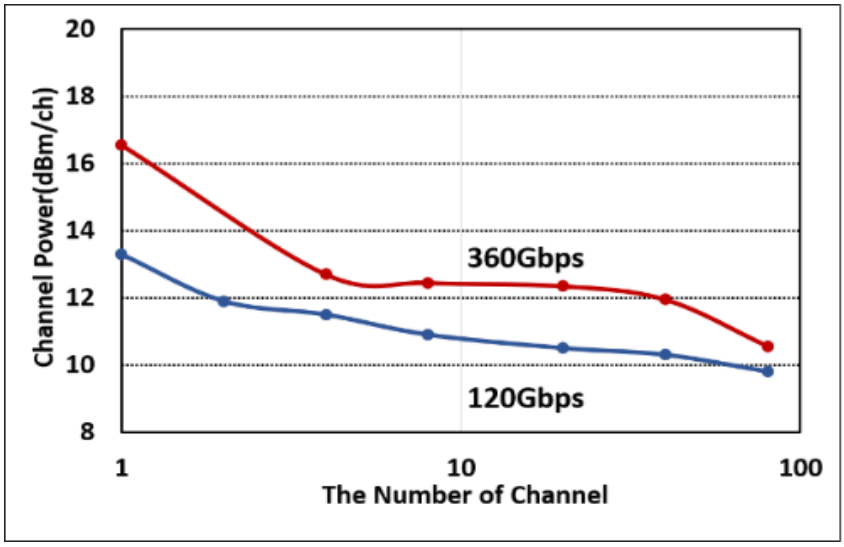

Figure 4.9 Maximum TX Power dependence on the number.

4.4 Concluding remarks

We have numerically evaluated very high power transmission property and BER performance of 120Gbps digital coherent signals. If the maximum transmitter powers are defined as the powers at which BER floor levels are 1.0×10^{-2} without error correction, those are found to be approximately +20.4 dBm, +14.8 dBm and +10.6 dBm, respectively, for single-channel 120Gbps DP-QPSK, DP-16QAM and DP-64QAM formats in large-core and low-loss single-mode silica fibers. In the simulations, we set fiber lengths over 100km, which is much longer than the effective fiber length, thus the results are applicable to any of long-length non-repeatered systems. We also show that the maximum transmitter powers gradually decrease in logarithmic feature with the increase of the number of DWDM channels. The channel number dependence is newly shown to be almost independent on the modulation format. In addition, the simulated results have been compared with the extended GN model with introducing adjustment parameters, not only to confirm the validity of the results but to show possible new analytical modeling for non-repeatered system.

We have theoretically evaluated very high power transmission property and BER performance of 120Gbps, 240Gbps and 360Gbps DP-16QAM digital coherent signals. The maximum reaches can be close to 300 km, which is almost independent on bit rate.

References

[1] Z. Xiang, and C. J. Xie, “Chapter 1 Introduction and references therein” in Enabling Technology for High-Efficiency Optical Communication Networks, ed. Z. Xiang and C. J. Xie, pp. 1-11, John Wiley & Sons, Inc., 2016.

[2] K. Kikuchi, “Fundamentals of Coherent Optical Fiber Communications,” Journal of Lightwave Technology, vol. 34, no. 1, pp. 157-179, 2016.

[3] M. Nakazawa, K. Kikuchi, and T. Miyazaki, ed., High Spectral Density Optical Communication Technologies, Springer, 2010.

[4] Y. Aoki, Y. Inada, T. Ogata, L. Xu, S. L. Zhang, F. Yaman, and E. Mateo, “Next-generation 100 Gb/s undersea optical communications,” IEEE Communications Magazine, vol. 50 , no. 2, pp. 50-57, 2012.

[5] “FASTER cable system ready for service,” http://www.capacitymedia.com/Article/3565973/FASTER-cable-system-ready-for-service. Jun. 2016.

[6] H. Fevrier, B. Clesca, P. Perrier, D. Chang, and W. S. Pelouch, “Chapter7 Unrepeatered Transmission and references therein” Undersea Fiber Com. Systems (2nd Ed.), ed. J. Chesnoy, pp. 261-300, Academic Press, 2016.

[7] V. Gainov, N. Gurkin, S. Lukinih, S. Makovejs, S. Akopov, S. Ten, O. Nanii, V. Treshchikov, and M. Sleptsov, “Record 500 km unrepeatered 1 Tbits/s (10×100G) transmission over an ultra-low loss fiber,” Optics Express, vol. 22, no. 19, pp. 22308-22313, 2014.

[8] H. Bissessur, C. Bastide, S. Dubost, and S. Etienne, “80 × 200 Gb/s 16-QAM unrepeatered transmission over 321 km with third order Raman amplification,” Optical Fiber Communication Conference 2015 (OFC2015), paper W4E.2, 2015.

[9] D. Chang, W. Pelouch, P. Perrier, H. Fevrier, S. Ten, C. Towery, and S. Makovejs, “150 × 120 Gb/s unrepeatered transmission over 409.6 km of large effective area fiber with commercial Raman DWDM system,” Optics Express, vol. 22, no. 25, pp. 31057-31062, 2014.

[10] D. Chang, P. Perrier, H. Fevrier, S. Makovejs, C. Towery, X. tie Jia, L. Deng, and B.zhong Li, “Ultra-long unrepeatered transmission over 607 km at 100G and 632 km at 10G,” Optics Express, vol. 23, no. 19, pp. 25028-25033, 2015.

[11] T. J. Xia, D. L. Peterson, G. A. Wellbrock, D. Chang, P. Perrier, H. Fevrier, S. Ten, C. Tower, and G. Mills, “557-km Unrepeatered 100G Transmission with Commercial Raman DWDM System, Enhanced ROPA, and Cabled Large Aeff Ultra-Low Loss Fiber

in OSP Environment," Optical Fiber Communication Conference 2014 (OFC2014), no. Th5A.7, 2014.
[12] M. Oerder, and H. Meyr, "Digital Filter and Square Timing Recovery", IEEE transactions on communications, vol. 36, no. 5, pp. 605-612, 1988.
[13] D. N. Godard, "Self-Recovering Equalization and Carrier Tracking in Two-Dimensional Data Communication Systems", IEEE Transactions on Communications, vol. COM-28, no. 11, pp. 1867-1875, 1980.
[14] W. A. Sethares, G. A. Rey, and C. R. Johnson, "Approaches to blind equalization of signals with multiple modulus," Proc. Int. Conf. Acoustics, Speech, Signal Process, vol. 2, pp. 972-975, 1989.
[15] T. Pfau, S. Hoffmann, and R. Noe, "Hardware-Efficient Coherent Digital Receiver Concept With Feed-forward Carrier Recovery for M-QAM Constellations", Journal of Lightwave Technology, vol. 27, no. 8, pp. 989-999, 2009.
[16] D. H. Richards, "Chapter 5 Commercial Optical Communication Software" in WDM Systems and Networks, Modeling, Simulation, Design and Engineering, ed. N. Antoniadeds, G. Ellinas and I. Roudas, pp. 189-235, Springer, 2012.
[17] D. Semrau, R. I. Killey, and P. Bayvel, "The Gaussian Noise Model in the Presence of Inter-Channel Stimulated Raman Scattering," Journal of Lightwave Technology, vol. 36, no. 14, pp. 3046-3055, July 15, 2018.
[18] G. P. Agrawal, ed., "Chapter10 Advanced Lightwave Systems" in Fiber-Optic Communication Systems, John Wiley & Sons, Inc. fourth edition, 2010.

Chapter 5 Extension of GN model and application to high power transmission

5.1 Introduction

The analytical model of the impact of nonlinear effects is very important for the performance evaluation of the system and networks. For effective design strategies can be explored for point to point systems without the help of lengthy computer simulation.

The well-known dual-polarization nonlinear Schrödinger equation (DP-NLSE, [1-3]) is a very successful analytical model. The numerical integration of DP-NLSE, or the related Manakov equation, is still one of the most powerful tools for studying and designing the nonlinear effects of optical systems. Some of the papers listed [4-14] in turn contain further extensive references. In the influential literatures [15, 16], there are also comprehensive bibliographies on non-linear modeling, although the main concerns of these literatures are different.

It should be stressed here that although long-length fiber transmission with dispersion-uncompensated SMF have already been clarified by the Gaussian-Noise (GN) model [17, 18] for long-haul repeatered system application, the results cannot be directly extended to the non-repeatered system, because it inevitably handles very high power transmission with localized nonlinearity (i.e., nonlinear interaction is less than the effective fiber length) while long-haul repeatered systems are configured with low signal powers, resulted in relatively mild nonlinearity over the entire system length. The establishment of high power transmission technology is particularly beneficial for non-repeatered application because it surely offers a greater power budget.

5.2 Getting to the GN model

The nonlinear Schrödinger equation (NLSE), where fiber dispersion, nonlinearities, and amplifier noise distort the signal is not the desired discrete-time model when designing the coding and modulation algorithms. The NLSE and fiber transmission is nonlinear in the general case, and often operated in a regime where the nonlinearity cannot be neglected. The coherent receiver should have negligible distortions, that is, operate in a regime where it linearly maps the optical field to the electrical domain for sampling and detection. Often these problems are neglected, which leads to the standard additive white Gaussian noise (AWGN) model for coherent links, where the signal is only distorted by additive amplifier spontaneous emission (ASE) noise [19, 20].

Thanks to the recent developments of the Gaussian noise (GN) model [21–23], the nonlinearity can be dealt with by a simple extension of the AWGN model. The GN model applies to links with strong dispersive broadening during propagation and electronic dispersion compensation in the receiver. Then, the impact of the nonlinearity can be accurately modeled as AWGN with a variance proportional to the average signal power cubed, which was first observed by Splett et al. in 1993 [24]. It was based on directly postulating that all non-linearity was produced by FWM acting among the WDM signal spectral components, assumed "incoherent." This latter assumption is equivalent to the signal-Gaussianity approximation. Though limited to single-polarization, ideal-distributed amplification and a rectangular overall WDM spectrum, the derived equations were essentially the same as those of the GN model for such idealized system scenario.

5.2.1 From model to system performance

Before we discuss NLI modeling, it is necessary to clarify how system performance is calculated and what the model needs to deliver to make it possible to calculate it. The system BER can be estimated by inserting the non-linear SNR of Equation into a suitable BER formula, which depends on the transmission format. For instance, for DP-QPSK, the BER formula is:

$$\mathrm{BER}_{\mathrm{DP-QPSK}} = \frac{1}{2}\,\mathrm{erfc}\sqrt{\frac{1}{2}SNR}$$

The BER formulas for the other main QAM formats are provided in Section 4.2.1.

5.2.2 Modeling approximations

Discussing the underlying approximation is key to the understanding of the various models because, in essence, it is the employed approximations that define them and characterize their behavior and effectiveness, viability, pros and cons.

The non-linear propagation models derived from the DP-NLSE typically exploit one or more of the following approximations [21-23]:

1. The Manakov equation approximation
2. The single-polarization approximation
3. The perturbation approximation
4. The signal Gaussianity approximation
5. The NLI additive-Gaussian-noise (AGN) approximation
6. The locally-white NLI noise approximation
7. The lossless fiber approximation

8. The incoherent NLI accumulation approximation
9. The noiseless propagation approximation
10. The frequency-domain XPM approximation.

5.2.3 GN model analytical derivation

Having introduced the GN model theoretical and bibliographical background, it would be in order to provide the model formulas and an outline of the model derivation analytical steps. The model formulas will be introduced in this section, whereas an outline of the main derivation steps is provided [17].

For single span, the power spectral density of NLI noise:

$G_{NLI}^{(1span)}(f)$

$$= \frac{16}{27}\gamma^2 L_{eff}^2 \iint_{-\infty}^{+\infty} \left| \frac{1 - e^{-2\alpha z} e^{j4\pi^2 \beta_2 (f_1 - f)(f_2 - f) z}}{1 - j2\pi^2 \beta_2 \alpha^{-1} (f_1 - f)(f_2 - f)} \right|^2 G_{WDM}(f_1) G_{WDM}(f_2) G_{WDM}(f_1 + f_2 - f) df_1 df_2$$

Fiber non-linearity coefficient. γ

Fiber effective length. L_{eff}

$$L_{eff} = \frac{1 - e^{-2\alpha L_s}}{2\alpha}$$

α loss coefficient. L_s span length.

Transmission spectrum $G_{WDM}(f)$

FWM efficiency among frequencies.

$$\rho_{FWM}(f_1, f_2, f) = \frac{1 - e^{-2\alpha z} e^{j4\pi^2 \beta_2 (f_1 - f)(f_2 - f) z}}{1 - j2\pi^2 \beta_2 \alpha^{-1} (f_1 - f)(f_2 - f)}$$

FWM efficiency shorthand: f_1 f_2. $f_3 = f_1 + f_2 - f$.

For multi-span, the power spectral density of NLI noise:

$$G_{\mathrm{NLI}}(0) = \frac{16}{27}\gamma^2 L_{eff}^2 \iint_{-\infty}^{+\infty} \left| \frac{1 - e^{-2\alpha z} e^{j4\pi^2 \beta_2 (f_1 - f)(f_2 - f) z}}{1 - j2\pi^2 \beta_2 \alpha^{-1} (f_1 - f)(f_2 - f)} \right|^2 \cdot \frac{sin^2(2N_s \pi^2 |\beta_2| L_s (f_1 - f)(f_2 - f))}{sin^2(2\pi^2 |\beta_2| L_s (f_1 - f)(f_2 - f))} G_{WDM}(f_1) G_{WDM}(f_2) G_{WDM}(f_1 + f_2 - f) df_1 df_2$$

"Phased array" factor

$$\chi(f_1, f_2, f) = \frac{sin^2(2N_s \pi^2 |\beta_2| L_s (f_1 - f)(f_2 - f))}{sin^2(2\pi^2 |\beta_2| L_s (f_1 - f)(f_2 - f))}$$

Assuming NL noise is Gaussian and additive, then system performance can be evaluated just by correcting the OSNR

OSNR dependence on launch power:

$$\mathrm{OSNR} = \frac{P_{ch}}{P_{ASE} + P_{NLI}}$$

$$P_{NLI} = \eta \cdot P_{ch}^3$$

$$\mathrm{OSNR} = \frac{P_{ch}}{P_{ASE} + \eta \cdot P_{ch}^3}$$

$$g_{WDM}(f) = G_{WDM}(f)/P_{ch}$$

$$\mathrm{G_{NLI}}(0) = P_{ch}^3 \frac{16}{27}\gamma^2 L_{eff}^2 \iint_{-\infty}^{+\infty} \rho_{FWM}(f_1, f_2, f) \cdot \chi(f_1, f_2, f) g_{WDM}(f_1) g_{WDM}(f_2) g_{WDM}(f_1 + f_2 - f) df_1 df_2$$

GNRF solution at the Nyquist limit:

$$\mathrm{G_{NLI}}(0) \approx \frac{8}{27}\frac{\gamma^2 \mathrm{G_{WDM}^3 L_{eff}^2}}{\pi|\beta_2|\mathrm{L_{eff,a}}} \mathrm{asinh}\left(\frac{\pi^2}{2}|\beta_2|\mathrm{L_{eff,a}} \mathrm{B_{WDM}^2}\right)$$

GNRF solution at the non-Nyquist limit:

$$\mathrm{G_{NLI}}(0) \approx \frac{8}{27}\frac{\gamma^2 \mathrm{G_{WDM}^3 L_{eff}^2}}{\pi|\beta_2|\mathrm{L_{eff,a}}} \mathrm{asinh}\left(\frac{\pi^2}{2}|\beta_2|\mathrm{L_{eff,a}} \mathrm{B_{ch}^2 N_{ch}^{2\frac{B_{ch}}{\Delta f}}}\right)$$

5.3 Extension to non-repeatered system GN nonlinear interference noise

Since, however, the non-repeatered systems with high transmitter powers apparently do not satisfy such assumptions of applying the GN model [21, 25] as the perturbation approximation (i.e., mild nonlinearity). Nevertheless we have tried to compare the results with the GN model by introducing adjustment parameters as described below. Note here that although some researchers have discussed recently modulation dependent terms to take into account non-Gaussian property (a fourth-order noise (FON) term [26]) of nonlinear noise, those discussions are limited to multi-repeatered systems. By contrast, the adjustment parameters tested here are to account for localized nonlinear interaction in a few tens of kilometers of the effective fiber length, which is specific to non-repeatered systems.

The objective of this section is not only to confirm the validity of our simulation but also to find out more practical and simple method based on analytical modeling, which may be useful for non-repeatered system application.

The shot noise limited sensitivity or the ultimate performance of optical coherent signal can be characterized by the signal-to-noise ratio (SNR), defined as

$$\mathrm{SNR} = \frac{\frac{\mathrm{Ps}}{2}}{0.75\mathrm{B}(2\mathrm{a}_1\mathrm{e} + 2\mathrm{a}_2\mathrm{R}\mathrm{G}_{\mathrm{NLI}}(0))}. \qquad (1)$$

where,

$$\mathrm{G}_{\mathrm{NLI}}(0) \approx \frac{8}{27}\frac{\gamma^2\mathrm{G}_{\mathrm{WDM}}^3\mathrm{L}_{\mathrm{eff}}^2}{\pi|\beta_2|\mathrm{L}_{\mathrm{eff,a}}}\mathrm{asinh}\left(\frac{\pi^2}{2}|\beta_2|\mathrm{L}_{\mathrm{eff,a}}\mathrm{B}_{\mathrm{ch}}^2\mathrm{N}_{\mathrm{ch}}^{2\frac{\mathrm{B}_{\mathrm{ch}}}{\Delta\mathrm{f}}}\right) \quad (2)$$

The derivation of GNLI is detailed in Ref. [21]. Note that GNLI is proportional to third power of GWDM because it has origin in third-order fiber nonlinearity such as self-phase modulation and cross-phase modulation. Here, the symbols are

1) Ps: total received signal power for dual polarization [W] (The received signal power for one polarization is given by Ps/2)

2) e: electron charge[C]

3) B: symbol rate/2 [Hz] (Electrical receiver bandwidth is assumed to 0.75B)

4) N_{ch}: the number of channel

5) a_1: linear adjustment parameter, which is introduced to fit the back to back receiver sensitivity in Fig.4.3

6) a_2: non-linear adjustment parameter, which is introduced to fit the BER curves and the maximum transmitter power in Fig.4.3

7) R: Ps/P_{Tx} where P_{Tx} is the total transmitted signal power

8) γ: the fiber non-linearity coefficient [W-1 ŀkm^{-1}]

9) G_{WDM}: the power spectrum density (PSD) of the WDM signal

10) L_{eff}: the effective length [km]. $L_{eff} = (1\text{-}e^{-2\alpha L}) / (2\alpha)$

11) Leff,a:1/ (2α) [km].α is the fiber loss coefficient [km^{-1}]

12) β_2: the dispersion coefficient [ps^2 ŀkm^{-1}]

13) asinh: the hyperbolic arcsin function

14) B_{ch}: the channel bandwidth [Hz]

15) Δf: the channel spacing [Hz].

Further, the BER for each modulation format is given by the following formula.

$$\mathrm{BER} = \mathrm{C}_1 \times \mathrm{erfc}\sqrt{\mathrm{C}_2 \times \mathrm{SNR}}, \qquad (3)$$

where C_1 and C_2 can be found in the following Table 5.1.

Table 5.1 C_1 and C_2 for different modulation formats.

Modulation Format	Symbol Rate	C_1	C_2
DP-QPSK	30	1/2	1/2

DP-16QAM	15	3/8	1/10
DP-64QAM	7.5	7/24	1/28

Table 5.2 the list of resultant a_1 and a_2 values used in Figs.5.1.

Modulation Format	a_1	a_2
DP-QPSK	1	1
DP-16QAM	1.27	1.25
DP-64QAM	1.8	3

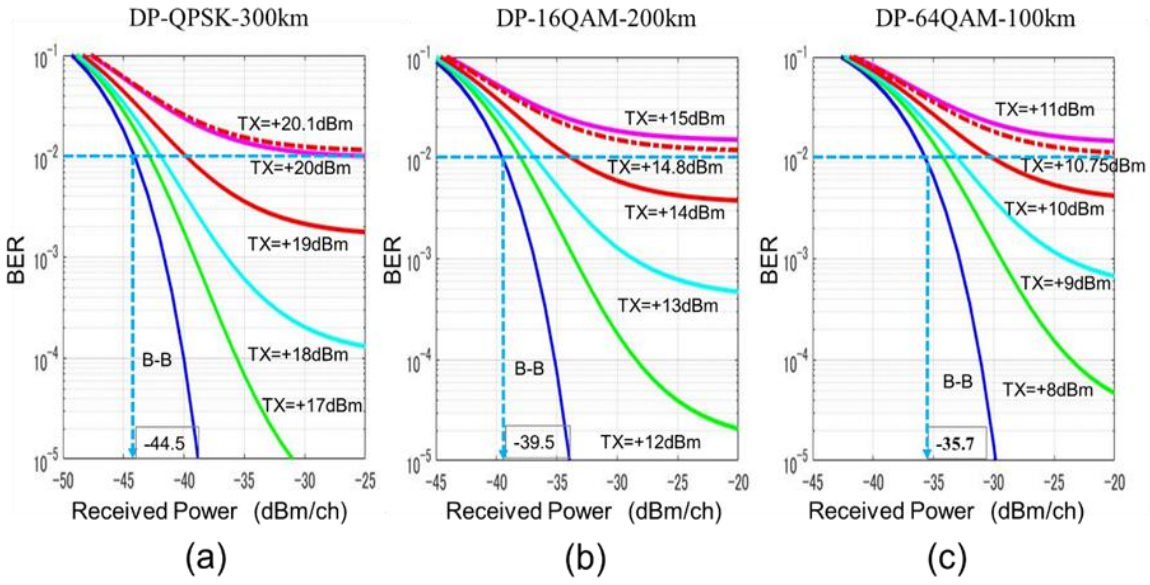

Figure 5.1 BER characteristics for DP-QPSK, DP-16QAM and DP-64QAM. (a) DP-QPSK-300km. (b) DP-16QAM-200km. (c) DP-64QAM-100km.

Figures 5.1 (a), (b) and (c) shows the calculated BER characteristics according to equations (1) through (3), corresponding to the Tx powers used in Fig.4.3. These are obtained by introducing linear and nonlinear adjustment parameters a_1 and a_2, respectively, on Table 5.2. It is very clear that the BER curves in Fig.4.3 are closely reproduced in Fig.5.1.

Here, the dash-dotted lines in Fig.5.1 are to obtain the maximum Tx powers. Then, the maximum Tx powers for DP-QPSK, DP-16QAM and DP-64QAM are found to be +20.1 dBm, +14.8 dBm and +10.8 dBm, respectively, which are very close to the values obtained from Fig.4.3. Further, the receiver sensitivities are -44.5 dBm, -39.5 dBm and -35.7 dBm for DP-QPSK, DP-16QAM and DP-64QAM, respectively, which are also in accordance with the simulation results in Fig.4.4.

Regarding to the values of a_1 and a_2, we found that BER curves in Fig.4.3 (a) for DP-QPSK case are reproduced in Fig.5.1 (a) with a_1=1 and a_2=1. This shows two approaches give almost identical performance. By contrast, the adjustment parameters becomes larger with higher order modulation. We think that the increase in a1 may be explained by inter-symbol interference in the coherent receiver as well as possible errors included in derivation of Eq. (3), due to shorter symbol distance. On the other hand, the increase in a2 will be partly attributable to power distribution among symbols. For example, if we assume the distance between symbols is 2A for 16QAM, then the powers of inner 4 symbols are $2A^2$ and those of corner 4 symbols are $18A^2$. Further the powers of the remaining 8 symbols are $10A^2$. Thus the averaged power for all 16 symbols are $10A^2$. On the other hand, nonlinear interference noise is proportional to the third power of each symbol power. If we hypothetically assume the waveform of the signal is kept unchanged along the fiber, the effective GNLI may be 0.008 ($=2^3/10^3$) for inner 4 symbols, 5.83($=18^3/10^3$) for corner 4 symbols, and 1.0 for remaining 8 symbols, which gives us 1.96 times increase on average. In actual, the signal envelope spreads along the SMF transmission, the a2 value may be in the range of 1 to 1.96, while we used a value of 1.25 to best fit the Fig.4.3 (b). With similar discussion we obtain that a_2 value for 64QAM may be in the range of 1 to 2.23, which value is smaller than the value of 3 we used. We are under study to explain this, including further confirmation on waveform evolution along the fiber.

Figure 5.2 shows the maximum Tx power dependence on the number of channels for DP-QPSK, DP-16QAM and DP-64QAM cases. Here, in this plot, the maximum powers are defined as input powers where averaged BER over DWDM channels is 1.0×10^{-2} at -25dBm receiver power as in the case of single channel. Also plotted by dotted lines are approximations following with the extended GN model with adjustment parameters on Table 5.2.

It is seen from this figure that the maximum Tx powers are found to gradually decrease in logarithmic feature with the increase of the number of channels. Also, the maximum Tx powers' dependence on the number of WDM channel is almost the same among three modulation schemes and for example, the maximum Tx power for 80 channel WDM is reduced by approx. 3.5dB compared with single-channel case. These results indicate that incremental degradation by WDM scheme is solely dependent on the number of the WDM channels. This property presumably has its origin in mutual interaction among many channels due to such effects as cross phase modulation. In other word, even in a single span, the amount of nonlinear noise due to cross phase modulation will be the same

among different modulations because of large walk-off effect brought by a large dispersion of 20.5 ps/nm/km.

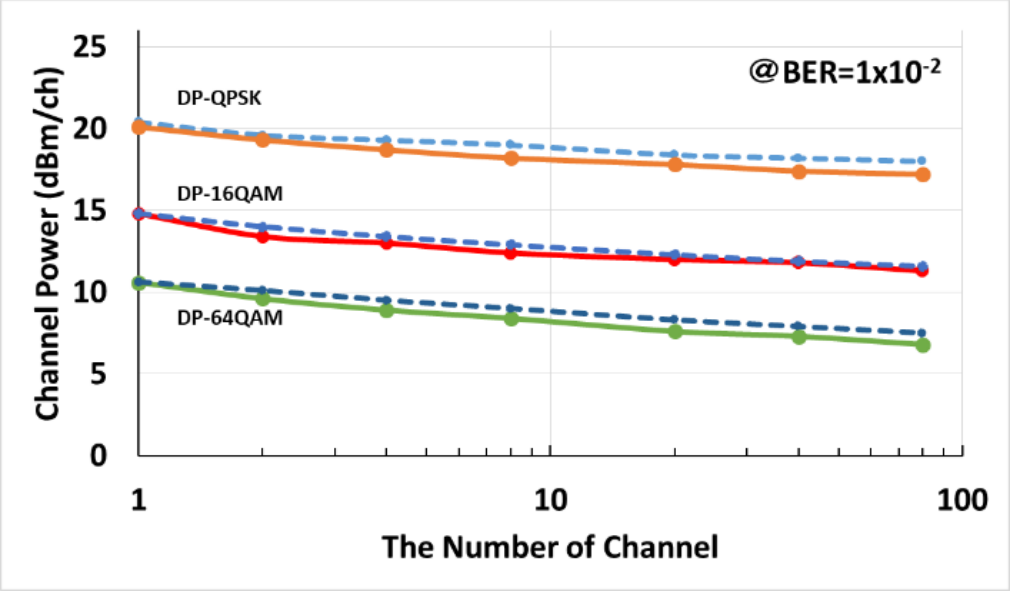

Fig. 5.2. Maximum Tx power dependence on the number of channels (BER=1×10-2). The solid lines are by numerical simulations while the dotted lines are by GN model with assumed adjustment parameters.

5.4 Concluding remarks

In all contexts, analytical models can be used for research purposes, to devise and theoretically test new and disruptive technologies. In this chapter we have introduced the GN model theoretical and bibliographical background, and introduced the model formulas, whereas an outline of the main derivation steps is provided.

And then we go directly to the topic of the accuracy tests on the GN model with adjustment parameters, since the observation of some of the GN model accuracy limitations was essential for motivating its evolution into the extended model.

The calculation results using extended Gaussian-Noise (GN) model with introducing adjustment parameters have been compared with the numerical simulation results, not only to confirm the validity of the results but to explore possible new analytical modeling for non-repeatered systems.

References

[1] C. R. Menyuk, “Nonlinear pulse propagation in birefringent optical fibers,” IEEE Journal of Quantum Electronics, vol. 23, no. 2, pp.174-176.1987.

[2] C. R. Menyuk, “Pulse propagation in an elliptically birefringent Kerr medium,” IEEE Journal of Quantum Electronics, vol. 25, no.12, pp. 2674-2682, 1989.
[3] G. P. Agrawal, Non-Linear Fiber Optics, 5th ed. Academic Press, New York, 2012.
[4] D. Marcuse, C. R. Menyuk, and P. K. A. Wai, “Application of the Manakov-PMD equation to studies of signal propagation in optical fibers with randomly varying birefringence,” Journal of Lightwave Technology, vol. 15, no. 9, pp. 1735-1746, 1997.
[5] A. Vannucci, P. Serena, and A. Bononi, “The RP method: a new tool for the iterative solution of the nonlinear Schrodinger equation,” Journal of Lightwave Technology, vol. 20, no.7, pp. 1102-1112, 2002.
[6] R. Holzlöhner, V. S. Grigoryan, C. R. Menyuk, and W. L. Kath, “Accurate calculation of eye diagrams and bit error rates in optical transmission systems using linearization,” Journal of Lightwave Technology, vol. 20, no. 3, pp. 389-400, 2002.
[7] J. Reis, and A. Teixeira, “Unveiling nonlinear effects in dense coherent optical WDM systems with Volterra series,” Optics Express, vol. 18, no. 8, pp. 8660-8670, 2010.
[8] A. D. Ellis, J. Zhao, and D. Cotter, “Approaching the non-linear Shannon limit,” Journal of Lightwave Technology, vol. 28, no.4, pp. 423-433, 2010.
[9] W. Shieh, and X. Chen, “Information spectral efficiency and launch power density limits due to fiber nonlinearity for coherent optical OFDM systems,” IEEE Photonics Journal, vol. 3, no. 2, pp. 158-173, 2011.
[10] S. Kilmurray, T. Fehenberger, P. Bayvel, and R. I. Killey, “Comparison of the nonlinear transmission performance of quasi-Nyquist WDM and reduced guard interval OFDM,” Optics Express, vol. 20, no. 4, pp. 4198-4205, 2012.
[11] A. Mecozzi, and R. J. Essiambre “Nonlinear Shannon limit in pseudolinear coherent systems,” Journal of Lightwave Technology, vol. 30, no. 12, pp. 2011-2024, 2012.
[12] P. Johannisson, and M. Karlsson, “Perturbation analysis of nonlinear propagation in a strongly dispersive optical communication system,” Journal of Lightwave Technology, vol. 31, no.8, pp. 1273-1282, 2013.
[13] P. Serena, and A. Bononi, “An alternative approach to the Gaussian noise model and its system implications,” Journal of Lightwave Technology, vol. 31, no. 22, pp. 3489-3499, 2013.
[14] M. Secondini, E. Forestieri, and G. Prati, “Achievable information rate in nonlinear WDM fiber-optic systems with arbitrary modulation formats and dispersion maps,” Journal of Lightwave Technology, vol. 31, no. 23, pp. 3839-3852, 2013.
[15] P. J. Winzer, and R. J. Essiambre, “Advanced modulation formats for high-capacity optical transport networks,” Journal of Lightwave Technology, vol. 24, no. 12, pp. 4711-4728, 2006.

[16] R. J. Essiambre, G. Kramer, P. J. Winzer, G. J. Foschini, and B. Goebel, "Capacity limits of optical fiber networks," Journal of Lightwave Technology, vol. 28, no.4, pp.662-701, 2011.
[17] P. Poggiolini, "The GN Model of Non-Linear Propagation in Uncompensated Coherent Optical Systems," Journal of Lightwave Technology, vol. 30, no. 24, pp. 3857-3879, 2012.
[18] D. Semrau, R. I. Killey, and P. Bayvel, "The Gaussian Noise Model in the Presence of Inter-Channel Stimulated Raman Scattering," Journal of Lightwave Technology, vol. 36, no. 14, pp. 3046-3055, 2018.
[19] I. Ezra, et al., "Coherent detection in optical fiber systems," Optics Express, vol. 16, pp. 753-791, 2008.
[20] K. Kikuchi, and S. Tsukamoto, "Evaluation of sensitivity of the digital coherent receiver," Journal of Lightwave Technology, vol. 26, no.13, pp.1817-1822, 2008.
[21] P. Poggiolini, "The GN model of non-linear propagation in uncompensated coherent optical systems," Journal of Lightwave Technology, vol. 30, no. 24, pp. 3857-3879, 2012.
[22] L. Beygi, E. Agrell, and M. Karlsson, "Optimization of 16-point ring constellations in the presence of nonlinear phase noise," Optical Fiber Communication Conference; paper OThO.4, 2011.
[22] L. Beygi, E. Agrell, and M. Karlsson, "Optimization of 16-point ring constellations in the presence of nonlinear phase noise," 2011 Optical Fiber Communication Conference and Exposition and the National Fiber Optic Engineers Conference, pp. 1-3, 2011.
[23] P. Johannisson and M. Karlsson, "Perturbation analysis of nonlinear propagation in a strongly dispersive optical communication system," Journal of Lightwave Technology, vol. 31, no. 8, pp. 1273-1282, 2013.
[24] A. Splett, C. Kurtzke and K. Petermann, "Ultimate transmission capacity of amplified optical fiber communication systems taking into account fiber nonlinearities," European Conference and Exhibition on Optical Communication, 1993.
[25] P. Poggiolini, G. Bosco, A. Carena, V. Curri, Y. Jiang, and F. Forghieri, "The GN-Model of Fiber Non-Linear Propagation and its Applications," J Journal of Lightwave Technology, vol. 32, no. 4, pp. 694-721, 2014.
[26] R. Dar, M. Feder, A. Mecozzi, and M. Shtaif, "Accumulation of nonlinear interference noise in fiber-optic systems," Optics Express, vol. 22, pp. 14199-14211, 2014.

Chapter 6 Mitigation of nonlinear limits in non-repeatered system

6.1 Introduction

The next generation wavelength-division-multiplexed (WDM) communication system are expected to operate at 400Gbps or 1Tbps rate. Meanwhile, transmission nonlinear impairments in optical fibers are the most significant factor limiting the capacity of the next generation WDM systems set by the nonlinear Shannon capacity [1-2].

Optical fiber impairments mitigation is a hot research topic for increasing the fiber capacity without loss in system performance. The transmission impairments can be divided into two categories: linear impairments, which include chromatic dispersion (CD), polarization mode dispersion (PMD), polarization dependent loss (PDL) and fiber loss; and nonlinear impairments, which include self-phase modulation (SPM), cross-phase modulation (XPM), cross-polarization modulation (XPolM), four wave mixing (FWM), stimulated Brillouin scattering (SBS) and stimulated Raman scattering (SRS). Until recently, compensation techniques for different impairments have been considered separately [3-12].

Digital back propagation (DBP) was proposed as a universal technique for jointly compensating linear and nonlinear impairments [3-4]. And special attention has been given to nonlinear compensation algorithms that are based on DBP, such as split-step BP [6-7], perturbation-based BP [8-9], or multi-stage BP [9-10]. The main drawbacks of BP are its excessive computational requirement and the PMD [11] and channel dependent frequency offsets [12] impairments may degrade the potential DBP gains. On the other hand, advancements in state of the art DSP, modulation formats, high speed electronics, transmission fibers, and broadband amplification have resulted in recent experimental single mode fiber (SMF) capacity improvements [13-15].

It is worth mentioning that there is no detailed NLC approaches applied in nonrepeatered systems, because it inevitably handles very input high power with localized nonlinearity (i.e., nonlinear interaction is less than the effective fiber length) while long-haul repeatered systems are configured with low signal powers, resulted in relatively mild nonlinearity over the entire system length[16].

In this work we evaluate the performance of digital coherent non-repeatered systems by utilizing higher-order modulation based on 120Gbps DP-16QAM, nonlinearity compensation by digital back propagation (DBP), larger effective area ultra-low loss

fibers, and broaden bandwidth EDFAs. We have achieved a large nonlinear compensation benefit of 2dB for single channel by using DBP technique.

This chapter is organized as follows. In Section 6.2, we present a brief overview of nonlinear impairments in the optical link. And then we focus on the DBP technique. We introduced a computationally simpler algorithm for solving the NLSE based on a non-iterative asymmetric split-step Fourier method (SSFM). In Section 6.3, we introduce the system configuration, simulation method and DSP algorithms. After analyzing the bit error rate (BER) characteristic of both single channel and 8/20 WDM non-repeatered systems, we show that DBP has more effective influence on self-phase modulation and get the maximum input power for single channel with DBP. Finally in Section 6.6, we make a conclusion in this work.

6.2 Digital backward propagation (DBP)

6.2.1 How DBP works

Nonlinear in-band interference can be fully compensated by means of digital back propagation (DBP). This technique can be implemented either at the transmitter, as in [5], or at the receiver side [17], or a perturbation based approach in the time domain [18-19], or in the frequency domain [20]. DBP is based on the split-step Fourier method (SSFM) [21], which represents an efficient and widely used technique to solve the Manakov equation (nonlinear Schrödinger equation (NLSE)).

In the receiver of coherent optical communication system, the received photocurrent is linearly mapped to the optical field, making the optical amplitude and phase available to the digital processor of the receiver. The received signals can be transmitted digitally through the inverse fiber mode to compensate for the dispersion and fiber nonlinearity. Different ways of DBP implementation have been proposed depending on the implementation order of the linear and nonlinear parts [17, 22]. Digital back propagation requires the inverse NLSE to be solved for the parameters of the optical link. For a single polarization and with spatial domain negated, the NLSE is given by:

$$\frac{\partial \mathrm{E}}{\partial(-z)} = (\mathrm{D} + \mathrm{N})\,\mathrm{E} \qquad (1)$$

where E is the complex field of the received signal, D is the differential operator accounting for linear effects (CD and attenuation) and N is the nonlinear operator, which are given by:

$$\mathrm{D} = \frac{j}{2} \cdot \beta_2 \cdot \frac{\partial^2}{\partial t^2} - \frac{\alpha}{2} \qquad (2)$$

$$N = j\gamma|E|^2 \quad (3)$$

where α is the attenuation factor, β2 is the group velocity dispersion parameter and γ is the nonlinearity parameter.

The split-step Fourier method (SSFM) is used [23-24] to solve the Eq. (1). The optical fiber is regarded as a series of linear segments (considering only D) and dispersion nonlinear segments (considering only N). More steps lead to more accurate results, but increase the computation time. The linear part of DBP is the same as that used for CD compensation. The nonlinear part of DBP is the same as the nonlinear part used in the single-step nonlinear compensator. The phase shift of each sample is:

$$\theta_{NL}(t) = k\gamma L_{eff}|E|^2 \quad (4)$$

where k is a compensation factor which is optimized and L_{eff} is the effective length of each step. If each BP step only compensates for a fraction of a span, L_{eff} is

$$L_{eff} = \frac{1-\exp(-aL_{step})}{\alpha} \quad (5)$$

The interplay between dispersion and nonlinearity manifests after the first dispersion and nonlinearity computation pair. At the end of the fiber, the signal will be different from the transmitted signal. If the received signal is detected coherently, preserving both the amplitude and phase, it can be sent into a virtual fiber in the digital domain whose dispersion and nonlinearity are exactly opposite to those of the real transmission fiber. The dispersion and nonlinear effects in the real fiber are then piecewise canceled by the virtual fiber as shown in Figure 6.1. At the end of propagation in the virtual fiber, the signal will be the same as the transmitted signal except with a delay. Since propagation in a fiber with opposite dispersion and nonlinearity is the same as propagating backwards in the real fiber this digital nonlinear compensation method is called DBP. Even though physical fiber with negative nonlinearity does not exist, the beauty of digital signal processing is that the virtual fiber can assume any dispersion and nonlinearity.

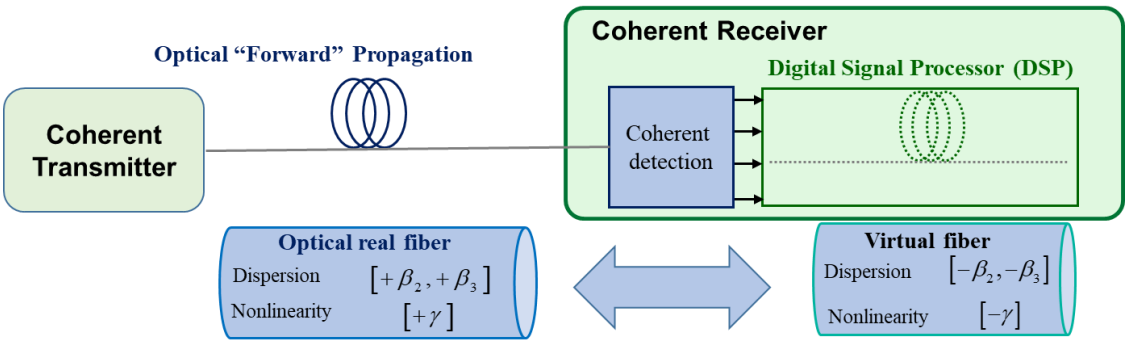

Figure 6.1 Schematic of the SSM for simulating forward propagation in real fiber and DBP in virtual fiber.

6.2.2 Computational complexity of DBP

Once the feasibility of DBP is demonstrated experimentally, the number of operations, which translates to power consumption, required for DBP becomes the critical issue for practical applications. The number of operations for a given optical link depends on the number of steps (ns), and hence, on the step size. The SSFM accuracy depends fundamentally on the mutual influence of dispersion and nonlinearity within the step length. Due to the nature of the dispersion and nonlinearity operators, the step size has to be chosen such that (i) the nonlinear phase shift is small enough to preserve the accuracy of the dispersion operation and (ii) the optical power fluctuations due to dispersion effects are small enough to preserve the accuracy of the nonlinear operation.

6.3 Simulation demonstration of DBP

6.3.1 System configuration and simulation method

We have investigated 120 Gbps DP-16QAM (Gray coded, NRZ) with up to 20 channels, which equivalent to 100 Gbps of net throughput plus 20% forward error correction (FEC).

In all the simulations described in this section, 2^{16} pseudo random bit stream (PRBS) sequences with a bit length of 65536 bits are used to compute up to 1.5×10^{-5} bit error rate (BER). The laser linewidth is assumed to be 100 kHz (FWHM, Gauss). For DP-16QAM, the optical bandwidth of OPT MUX and OPT DEMUX is assumed to be 30 GHz with the 5th Bessel filter and the channel spacing is 50 GHz. A typical advanced silica single-mode fiber with loss coefficient of 0.16 dB/km, effective core area of 130 um^2, dispersion of +20.5 ps/nm/km and nonlinear refractive index of 2.2×10^{-20} m^2/W is used. The PMD is assumed 0.05 $ps/km^{1/2}$. Table 6.1 summarizes the link parameters used for simulation.

The receiver fourth order Bessel filter with a bandwidth of $0.75 \times 0.5 \times$ symbol rate is applied. Each coherent receiver is set to receive -10 dBm/ch signal power via an optical preamplifier with a noise figure of 4 dB, and the local oscillator power in the receiver is set to + 10 dBm, thus realizing the receiver sensitivity limited by shot noise. It is assumed that the frequency response of the circuit is perfectly flat in Tx and Rx. And the nonlinear compensation is performed using the digital back propagation method. For numerical analyses, we have applied optical communication software simulation tool, OptiSystem™ (Ver.15.2) from Optiwave Systems.

Table 6.1 System Parameters

Parameter Description	Value
Channel symbol rate	30 GBd
Channel spacing	50 GHz
Length	100km
Dispersion	20.5 ps/nm/km
Nonlinear refractive index	2.2×10^{-20} m^2/W
Effective area	130 μm^2
PMD	0.05 $ps/km^{1/2}$
Loss coefficient	0.16 dB/km
Amplification type	EDFA
KK dependence (in Eq.(4))	0.5
Nonlinear ratio dependence (**)	0.5
Nonlinear step size dependence (in DBP)	2km

****nonlinear ratio dependence: defines the points, for each nonlinear step, where the nonlinear mixing is modeled. For example when set to 0.5, the nonlinear section is located at the half way point of the DBP step.**

6.3.2 Results and discussion

First we show in Figure 6.2 examples of constellation map, i.e., received waveforms of DP-16QAM singles with and without (w/o) nonlinear compensation (DBP) at several transmitter powers with single channel transmission. When the optical transmitter power (TX) exceeds +13dBm, the circular cloud of each symbol becomes an elongated ellipse in shape and its distribution is seen to further expand with the increase of Tx power. This is presumably due to enhancement of signal phase variance during transmission because of nonlinear phase noise.

In case that with nonlinear compensation, if we have a closer look at each of symbol distortion, there is less elongated elliptical shape compared to that without nonlinear compensation at the same transmitter power. For example, in case of tx power 15dBm the error vector magnitude (EVM) is about 19.63 and log10 of BER (bit error rate) is -1.74 without nonlinear compensation, and with nonlinear compensation EVM value becomes 14.45, and the BER value is -2.92 which concludes that using nonlinear compensation has effective influence on the transmission performance development.

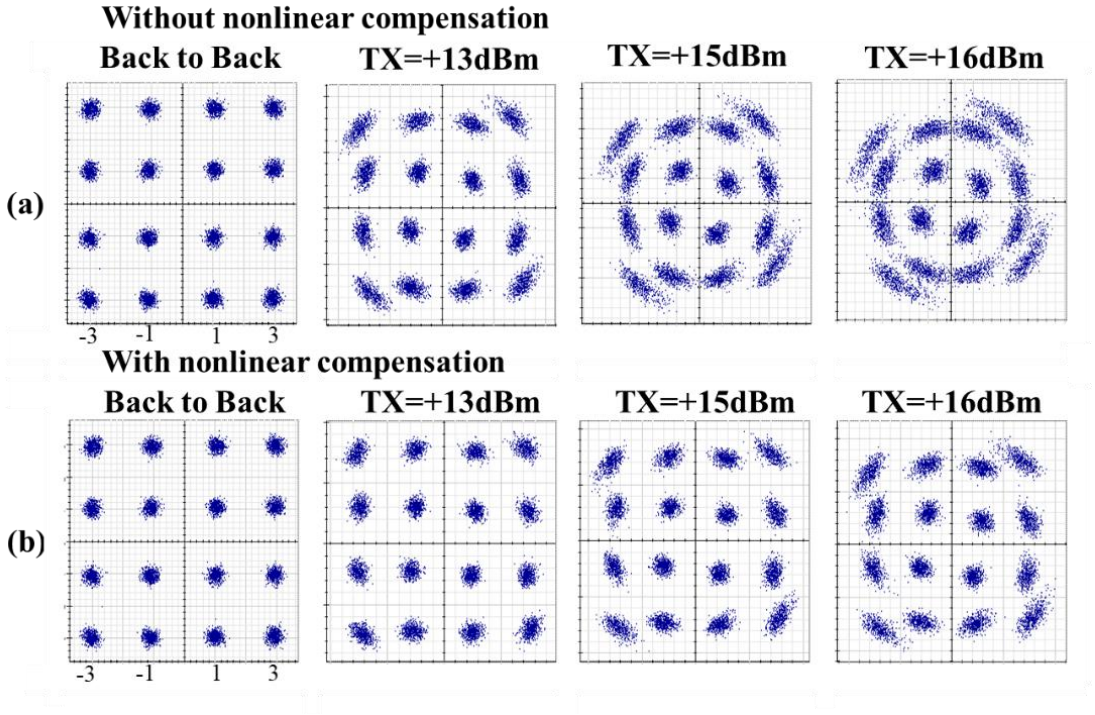

Figure 6.2 Evolution of constellation map for DP-16QAM with Tx power. L=100k (a) without nonlinear compensation. (b) With nonlinear compensation.

Figure 6.3 indicates the BER characteristic for 120Gbps DP-16QAM with single channel transmission depending on the transmission power w/o nonlinear compensation. It is clearly seen from the figures in Fig.6.3 that all two case the BER deteriorates, pursuant to Tx powers and approaches to specific saturation levels. In other words, achievable BER is dominantly determined by Tx power regardless of received signal level. If we define the maximum Tx power as the power at which BER saturated to 1.0×10^{-2} at -25dBm received power or above. Then the values are 15.2dBm and 17.2dBm for DP-16QAM w/o nonlinear compensation, respectively.

Next, we investigated DWDM transmission characteristics. Fig. 6.4 shows 8 and 20 channels WDM BER characteristics w/o nonlinear compensation. In case of 8WDM, the log10 of BER was improved from -1.6 to -2.0 at Tx power +22dBm. In order to estimate effective factor of nonlinear compensation, we increase the Tx power to the value where the BER performance with nonlinear compensation are approached to the BER curve without nonlinear compensation. Then we have found that the effective factor is about 0.6dB. We did the same for 20 DWDM and we have got the same value of 0.6dB. This implies that the 0.6dB improvement will be kept even if the number of DWDM channels increases. This is due to disturbance from neighboring DWDM channels.

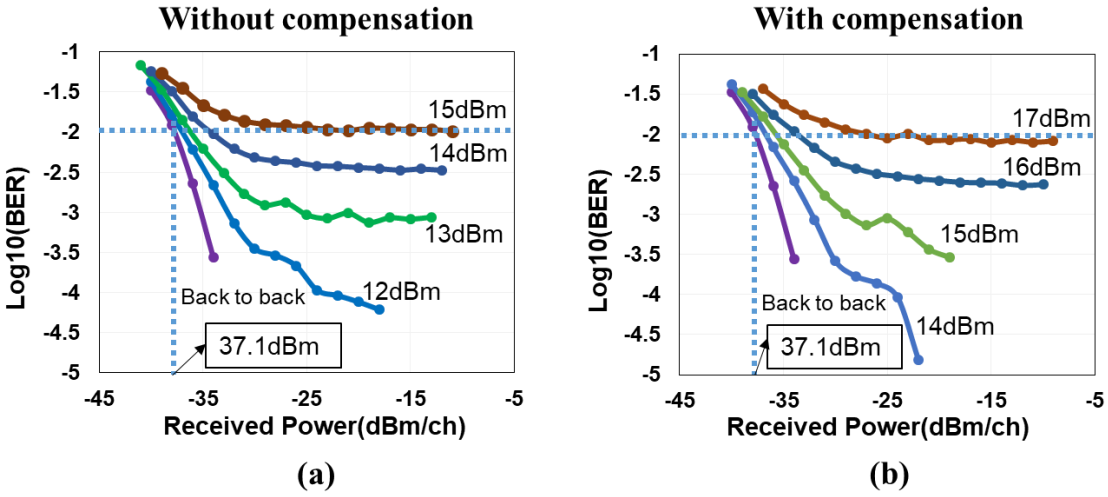

Figure 6.3 BER characteristic for DP-16QAM. Left: without compensation. Right: with compensation.

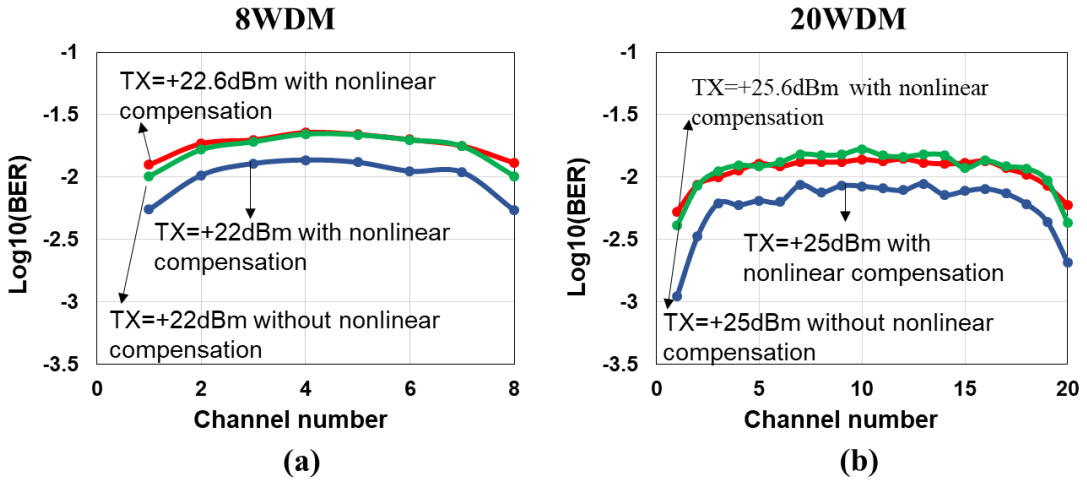

Figure 6.4 DP-16QAM 8WDM and 20WDM transmission characteristic. Fiber length is 100km. Left: 8WDM. Right: 20WDM.

And also, comparing the same Tx power 22dBm and 25dBm with compensation the BER values decrease and the central channels has less decrease than the side channels. It concludes that DBP has more effective influence on self-phase modulation (SPM) than cross-phase modulation (XPM) and four wave mixing (FWM).

Interestingly, from Fig.6.5, it is evidently that if we add a 5km single mode fiber with a dispersion of -20.5 ps/nm/km in Tx side before the transmitter amplifier for 120Gbps DP-16QAM single channel non-repeatered system, then the BER performance have slightly developed, which corresponded to the total through input power would increase by 0.2dB. In fact Self-phase modulation causes a frequency shift, known as frequency

chirping, which interacts with the dispersion in the optical fiber and results in spectral broadening of the optical pulse. The pulse broadening increases in transmission systems with high input power because the chirping effect is proportional to the injected power. As a result, the negative dispersion which change the optical pulse has a positive influence on the transmission performance.

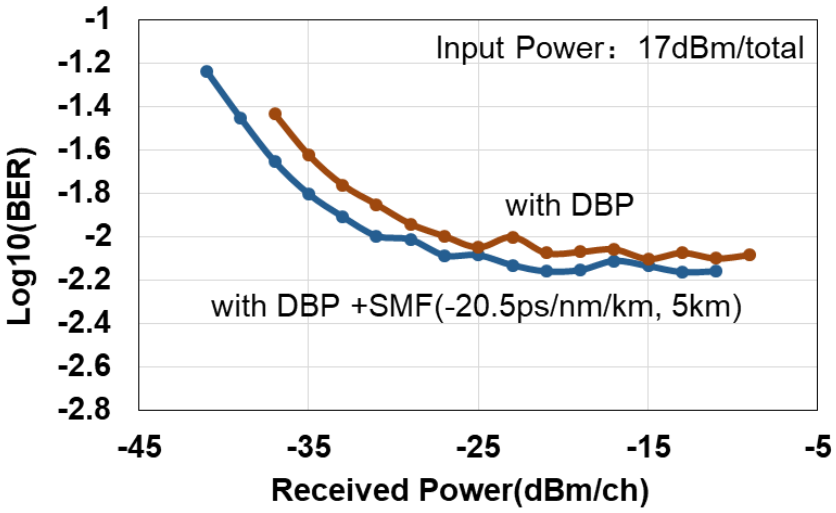

Figure 6.5 120Gbps DP-16QAM BER characteristic dependence on receiver power w/o 5km SMF (D= -20.5 ps/nm/km) in Tx side of 100km non-repeatered systems using digital back propagation.

6.4 Constellation Shaping

Constellation shaping has been proposed to improve the power efficiency of modulation formats over conventional QAM modulation and reduces the performance gap with respect to the linear Shannon limit. There are two approaches for constellation shaping: geometric shaping (GS) and probabilistic shaping (PS). GS has been implemented using circular based constellations such as amplitude-phase-shift-keying (APSK). This is achieved without introducing any redundancy. PS on the other hand does require redundancy but has attracted more attention due to its capability to approach Shannon lime closer.PS requires a transformation of equally distributed input bits into constellation symbols with non-uniform distribution. Such transformations have been implemented using prefix codes, many-to-one mapping combined with a turbo code, distribution matching or cut-and-paste method.

Shaping gain is the difference in achievable information rate between shaped and unshaped formats at the same spectral efficiency. In general, PS can outperform circular based GS by up to a few tenths of a dB in shaping gain for the same number of

constellation points. Still, both GS and PS significantly outperform conventional QAM formats thanks to their superior power efficiency.

6.5 Concluding remarks

The degree to which fiber impairments are compensated determines the transmission capacity of fiber-optic transmission systems. Compensation of nonlinear impairments in fiber has become the next logical step in increasing the capacity of WDM systems. In this chapter, with nonlinear compensation by using digital back propagation (DBP) approach, we have comprehensively evaluated by numerical simulation very high power transmission property and bit error rate (BER) performance of 120Gbps DP-16QAM modulation formats in large effective area and low loss SMFs in non-repeatered system. We started with a brief description of the optical link nonlinear impairments. Following this overview of nonlinear impairments induced by Kerr effect, nonlinear compensation by DBP technique was presented.

Using DBP approach, based on the BER characteristics, we have quantitatively discussed the maximum transmitter powers set by fiber nonlinearity. If the maximum transmitter powers are defined as the powers at which BER floor levels are 1.0×10-2 without error correction, the maximum transmitter power is +17.2 dBm for single-channel 120Gbps DP-16QAM formats in large-core and low-loss single-mode silica fibers. There is 2 dB development compared without using DBP approach. However, the performance is affected by nonlinear interference in DWDM non-repeatered systems, the improvement has been reduced to 0.6dB due to disturbance from neighboring DWDM channels. And DBP has more effective influence on SPM than XPM and FWM. Furthermore the negative dispersion which change the optical pulse in transmitter side increase the maximum input power by 0.2dB in single channel.

References

[1] R. Essiambre, G. Kramer, P. J. Winzer, G. J. Foschini, and B. Goebel, “Capacity Limits of Optical Fiber Networks,” Journal of Lightwave Technology, vol. 28, no. 4, pp. 662-701, 2010.

[2] A. Carena, V. Curri, G. Bosco, P. Poggiolini, and F. Forghieri, “Modeling of the Impact of Nonlinear Propagation Effects in Uncompensated Optical Coherent Transmission Links,” Journal of Lightwave Technology, vol. 30, pp. 1524-1539, 2012.

[3] X. Li, X. Chen, G. Goldfarb, E. Mateo, I. Kim, F. Yaman, and G. Li, “Electronic post-compensation of WDM transmission impairments using coherent detection and digital signal processing,” Optics Express, vol.16, no. 2, pp. 881–888, 2008.

[4] W. Shieh, H. Bao, and Y. Tang, “Coherent optical OFDM: Theory and design,” Optics Express, vol. 16, no. 2, pp. 841–859, 2008.
[5] R. J. Essiambre, and P. J. Winzer, “Fibre nonlinearities in electronically pre-distorted transmission,” European Conference on Optical Communications ECOC 2005, paper Tu.3.2.2, 2005.
[6] E. Ip, and J. M. Kahn, “Compensation of dispersion and nonlinear impairments using digital backpropagation,” Journal of Lightwave Technology, vol. 26, pp. 3416–3425, 2008.
[7] Z. Tao, L. Dou, W. Yan, L. Li, T. Hoshida, and J. C. Rasmussen, “Multiplier-free intrachannel nonlinearity compensating algorithm operating at symbol rate,” Journal of Lightwave Technology, vol. 29, pp. 2570–2576, 2011.
[8] A. Ghazisaeidi, and R. J. Essiambre, “Calculation of coefficients of perturbative nonlinear pre-compensation for Nyquis pulses,” European Conference on Optical Communication ECOC 2014, paper WE.1.3.3, 2014.
[9] M. Secondini, D. Marsella, and E. Forestieri, “Enhanced split-step Fourier method for digital backpropagation,” European Conference on Optical Communications ECOC 2014, paper We.3.3.5, 2014.
[10] X. Liang, and S. Kumar, “Multi-stage perturbation theory for compensating intra-channel nonlinear impairments in fiber-optic links,” Optics Express, vol. 22, pp. 29733-29745, 2014.
[11] G. Gao, X. Chen, and W. Shieh, “Influence of PMD on fiber nonlinearity compensation using digital back propagation,” Optics Express, vol. 20, pp. 14406-14418, 2012.
[12] E. Temprana, E. Myslivets, B. P. Kuo, L. Liu, V. Ataie, N. Alic, and S. Radic, “Overcoming Kerr-induced capacity limit in optical fiber transmission,” Science, vol. 348, pp. 1445-1448, 2015.
[13] A. Ghazisaeidi, I. F. de Jauregui Ruiz, R. Rios-Muller, L. Schmalen, P. Tran, P. Brindel, A. C. Meseguer, Q. Hu, F. Buchali, G. Charlet, and J. Renaudier, “65Tb/s transoceanic transmission using probabilistically-shaped PDM-64QAM,” European Conf. on Optical Communication (ECOC), paper Th.3.C.4, 2016
[14] D. G. Foursa, et al., “44.1 Tb/s Transmission over 9,100 km Using Coded Modulation Based on 16QAM Signals at 4.9 bits/s/Hz Spectral Efficiency,” Proc. ECOC’13, PD3.E.1, 2013.
[15] J. X. Cai, Y. Sun, H. Batshon, M. Mazurczyk, H. Zhang, Foursa D, et al. “54 Tb/s transmission over 9,150 km with optimized hybrid Raman-EDFA Amplification and coded modulation,” ECOC’2014, PD3.3, 2014.

[16] J. X. Cai, H. G. Batshon, M. V. Mazurczyk, O. V. Sinkin, D. Wang, M. Paskov, W. W. Patterson, C. R. Davidson, P. C. Corbett, G. M. Wolter, T. E. Hammon, M. A. Bolshtyansky, D. G. Foursa, and A. N. Pilipetskii, "70.46 Tb/s Over 7,600 km and 71.65 Tb/s Over 6,970 km Transmission in C+L Band Using Coded Modulation With Hybrid Constellation Shaping and Nonlinearity Compensation," Journal of Lightwave Technology, vol. 36, pp.114-121, 2018.
[17] E. Ip and J. M. Kahn, "Compensation of dispersion and nonlinear impairments using digital back propagation," Journal of Lightwave Technology, vol. 26, no. 20, pp. 3416-3425, 2008.
[18] W. Yan, Z. Tao, L. Dou, L. Li, S. Oda, T. Tanimura, T. Hoshida, and J.C. Rasmussen, "Low complexity digital perturbation back-propagation," European Conference on Optical Communication (ECOC), paper Tu-3, 2011.
[19] A. Ghazisaeidi and R. J. Essiambre, "Calculation of coefficients of perturbative nonlinear pre-compensation for Nyquist pulses," European Conference on Optical Communication (ECOC), paper WE.1.3.3, 2014.
[20] F. P. Guiomar, J. D. Reis, A. L. Teixeira, and A. N. Pinto, "Calculation of coefficients of perturbative nonlinear pre-compensation for Nyquist pulses," Optics Express, vol. 20, pp. 1360-1369, 2012.
[21] O. V. Sinkin, R. Holzlohner, J. Zweck, and C. R. Menyuk, "Optimization of the split-step fourier method in modeling optical-fiber communications systems," Journal of Lightwave Technology, vol. 21, no. 1, pp. 61-68, 2003.
[22] D. Rafique, M. Mussolin, M. Forzati, J. Martensson, M. N. Chugtai, and A. D. Ellis, "Compensation of intra-channel nonlinear fibre impairments using simplified digital back-propagation algorithm," OSA Optics Express, vol. 19, no. 10, pp. 9453-9460, 2011.
[23] K. Kikuchi, M. Fukase, and S. Y. Kim, "Electronic post-compensation for nonlinear phase noise in a 1000-km20-Gbit/s optical QPSK transmission system using the homodyne receiver with digital signal processing," Optical Fiber Communication Conference, OTuA2, 2007.
[24] A. J. Lowery, "Fiber nonlinearity mitigation in optical links that use OFDM for dispersion compensation," Photonics Technology Letters, vol. 19, pp. 1556-1558, 2007.

Chapter 7 Raman Amplified Non-repeatered System

7.1 Raman Amplification

7.1.1 Theory of Raman amplifier

Fiber loss is one limitation to the optical fiber transmission distance. In order to overcome the limitations, a means of optical amplification was sought. Two competing technologies emerged: erbium-doped fiber amplifiers (EDFA) [1, 2] and the Raman amplification [3-6]. With the improvement of pump laser technology Raman amplification is now an important way of expanding span transmission and capacity.

Raman amplification occurs due to an inelastic scattering of optical radiation with molecular vibrations in a material. The scattered “Stokes” waves are at a lower energy, or longer wavelength, than the incident optical radiation. The driving optical field is typically called the “pump” and the scattered light, the “signal”. An incoming light at the signal wavelength stimulates the fiber molecules, excited by the pump light, to emit light in phase and at the same wavelength as the signal wavelength, resulting in the optical amplification process. The Raman gain coefficient of this process is related to the scattering cross section which is material dependent. Raman scattering is a nonlinear effect [7]. For high enough pump powers, the scattered light can grow rapidly with most of the pump energy converted into scattered light. This process is called SRS, and it is the gain mechanism in Raman amplification.

There are two advantages of Raman amplification in the transmission system are considered. The first is how to use it to improve the noise figure of the system; the second is how to obtain a flat gain profile. The performance of modern Raman amplifiers is affected by many factors such as spontaneous Raman scattering, double Rayleigh backscattering, pump noise transfer, and polarization mode dispersion.

A schematic of an optical communication system with Raman amplification is shown in Figure 7.1, the signal propagates from the transmitter (Tx) to the receiver (Rx). The pump travelling in the same direction as the signal is called the forward pump, the pump traveling in the opposite direction of the signal is called the backward pump.When the pumped fiber is the actual transmission span connecting the two points, this setup is called a distributed Raman amplifier. If the amplifier is included in a box at the transmitter or

receiver side of the system, it is called a discrete Raman amplifier. Another distinguishing feature between distributed Raman amplifiers and discrete Raman amplifiers is the length of the fiber used. A typical distributed Raman amplifier has a length greater than 40 kilometers, while a discrete Raman amplifier has a length of approximately 5 kilometers.

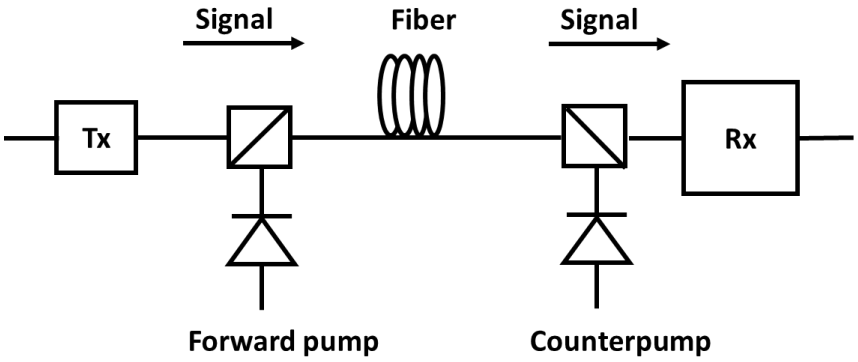

Figure 7.1 Schematic of Raman amplification optical communication system.

There are a number of different configurations in which Raman can be utilized on a fiber span. The Raman pumps may be counter-propagating with respect to the signal and/or co-propagating with the signal and, additionally, residual pump power from Raman can power a remotely optically pumped amplifier. Figure 7.2 shows different signal power profiles for different amplification schemes. The baseline comparison case is a fiber span with an EDFA at the end with its gain set to the preceding span loss.

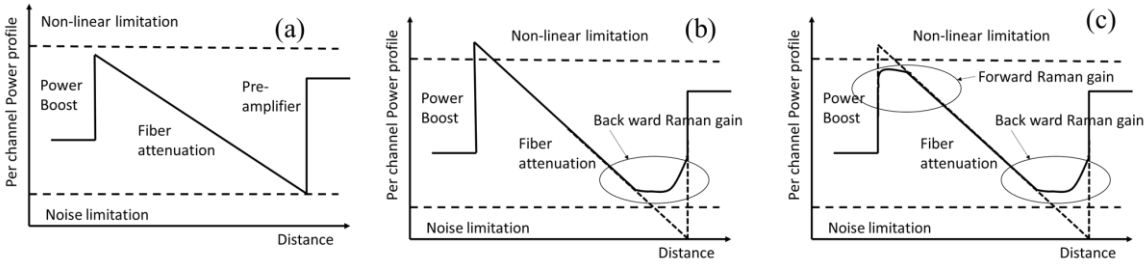

Figure 7.2 Perchannle power profile as a function of the transmission distance in an unrepeatered system: (a) With discrete amplifiers only (b) with backward distributed Raman gain (c) with forward and backward distributed Raman gain.

7.1.2 Raman gain spectrum

The most important parameter characterizing Raman amplifiers is the Raman gain coefficient g_R, which is related to the cross section of spontaneous Raman scattering [8]. It describes how the Stokes power grows as pump power is transferred to it through SRS. On a more fundamental level, g_R is related to the imaginary part of the third-order

nonlinear susceptibility [9]. In a simple approach, valid under the CW or quasi-CW conditions, the initial growth of a weak optical signal is governed by

$$\frac{dI_s}{dz} = \gamma_R(\Omega) I_p I_s \qquad (7.1)$$

where $\gamma_R(\Omega)$ is related to g_R, $\Omega = \omega_p - \omega_s$ represents the Raman shift, and ω_p and ω_s are the optical frequencies associated with the pump and signal fields having intensities I_p and I_s, respectively.

The most significant feature of the Raman gain spectrum for silica fibers is that the gain exists over a large frequency range (up to 40THz) with a broad peak located near 13.2 THz. This behavior is due to the noncrystalline nature of silica glasses. In amorphous materials such as fused silica, molecular vibrational frequencies spread out into bands that overlap and create a continuum. As a result, in contrast to most molecular media, for which the Raman gain occurs at specific well-defines frequencies, it extends continuously over a broad range in silica fibers. Optical fibers can act as broadband Raman amplifiers because of this feature.

Another important feature of Figure 7.x is the polarization dependence of the Raman gain. The gain nearly vanishes when pump and signal are orthogonally polarized. As discussed in section 2.3, the polarization-dependence of the Raman gain affects the performance of Raman amplifiers in several different ways.

7.1.3 Single-pump Raman amplification

Consider the simplest situation in which a signal CW pump beam is launched into an optical fiber used to amplify a CW signal. And fiber losses should be included. Moreover, the pump power does not remain constant along the fiber. When these effects are included, the Raman-amplification process is governed by the following set of two couple equations,

$$\frac{dP_s}{dz} = g_R P_p P_s - a_s P_s, \qquad (7.2)$$

$$\pm\frac{dP_p}{dz} = -\frac{\omega_p}{\omega_s} g_R P_p P_s - a_p P_p, \qquad (7.3)$$

where a_s and a_p account for fiber loss at the Stockes and pump wavelengths, respectively.

Equations 7.2 and 7.3 can be derived rigorously from Maxwell equations. They can also be written phenomenologically by considering the process through which photos appear in or disappear from each beam. The frequency ratio ω_p/ω_s appears in equation because the pump and signal photons have different energies.

Equations 7.2 and 7.3, are not easy to solve analytically because of their nonlinear nature. In many practical situations, pump power is so large compared with the signal power that pump depletion can be neglected by setting g_R=0 in 7.3, which is then easily solved.

In the forward-pumping case， $P_p(z) = P_0\exp(-\alpha_p z)$, where P0 is the input pump power at z=0. If we substitute this solution in Eq. (7.2), we obtain

$$\frac{dP_s}{dz} = g_R P_0 \exp(-\alpha_p z) P_s - a_s P_s. \qquad (7.4)$$

This equation can be easily integrated to obtain

$$P_s(L) = P_s \exp\left(g_R P_0 L_{eff} - \alpha_s L\right) = G(L) P_s(0), \quad (7.5)$$

where G(L) is the net signal gain, L is the amplifier length, and L_{eff} is an effective length defines as

$$L_{eff} = \left[1 - \exp\left(-\alpha_p L\right)\right]/a_p. \qquad (7.6)$$

The solution shows that, because of pump absorption, the effective amplification length is reduced from L to L_{eff}.

Forward pumping is superior from the noise viewpoint. However, for a long-haul system limited by fiber nonlinearities, backward pumping may offer better performance because the signal power is the smallest throughout the link length in this case.

7.1.4 High order Raman amplification

In higher order pumping schemes, one or more pumps that are two or more Stokes shifts away from the signal are used to primarily amplify the first-order pumps, which in turn amplify the signal [10-14]. When the pump is two Stocks shifts away from the signal it is referred to as second-order Raman amplification and so forth for higher order pumping schemes. Higher order pumping reduces the NF of amplifier by more evenly distributing the gain across the length of the fiber.

7.2 Simulation demonstration of Raman amplification

7.2.1 System configurations

Figure 7.3 shows the system configuration in the simulation. We have investigated 120 Gbps DP-16QAM (Gray coded, NRZ), in all the simulations described in this section, 216 pseudo random bit stream (PRBS) sequences with a bit length of 65536 bits are used to compute up to 1.5 $\times 10^{-5}$ bit error rate (BER). The laser linewidth is assumed to be 100 kHz (FWHM, Gauss). A typical advanced silica single-mode fiber with loss coefficient

of 0.16 dB/km, effective core area of 130 um^2, dispersion of +20.5 ps/nm/km and nonlinear refractive index of 2.2 $\times 10^{-20}$ m^2/W is used. The PMD is assumed 0.05 $ps/km^{1/2}$.

In this scheme, forward first-order, second-order and third-order pump were used. The higher-order pump amplified the lower-order pump at the signal input. The noise transfer was reduced compared to first-order pumping since the second-order pump only provided a small amount of direct gain to the signal and was forward propagating to the first-order pump.

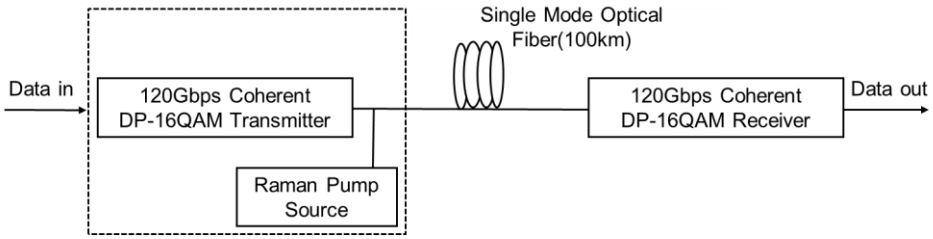

n-order Raman	Pump Power
first-order	1450nm : variable
second-order	1360nm : variable 1450nm:10mW
third-order	1280nm : variable 1360nm : 10mW.1450nm:10mW

Figure 7.3 System configuration.

7.2.2 Results and discussion

As shown in Figure 7.4, the effect of Raman amplification on the evolution of the signal power in distributed Raman amplifier, with first-order Raman, second-order Raman and third-order Raman. The signal power is large at the receiver in the span containing Raman amplification. The power at the final pump wavelength (1450 nm) is seen to reach its maximum value ~ 20 km from the receiving terminal.

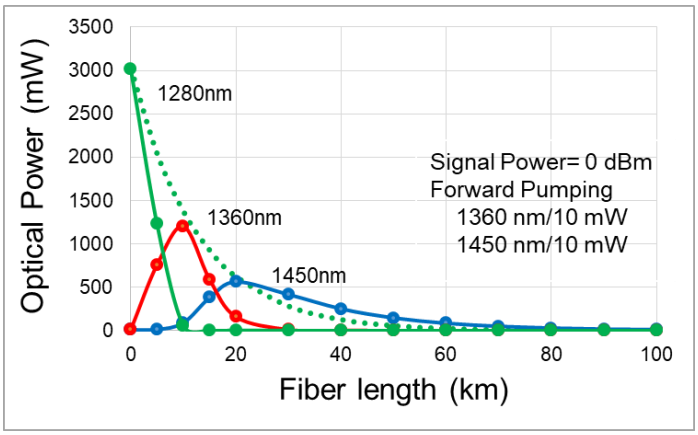

Figure 7.4 Raman pump and signal power along the span

Table 7.1 shows the Equivalent TX power for different Raman amplifier. Transmitter signal power is 0dBm, equivalent TX power of each case is about +15dBm 18dBm, 22.8dBm, and 24dBm. With Raman amplifier, signal power through the fiber is relatively small, which can reduce the influence of nonlinear effects.

Table 7.1 Equivalent TX power of n-order Raman.

with and w/o Raman	w/o Raman	1st Raman	2rd Raman	3rd Raman
Equivalent TX power	+15dBm	+18.0dBm	+22.8dBm	+24.0dBm

In Figure 7.5, from this three figure, we can see that with the increasing pump power, Raman Gain increase. For the same pump power, signal which has a higher signal power has a lower gain, because of interaction between signals and pump powers.

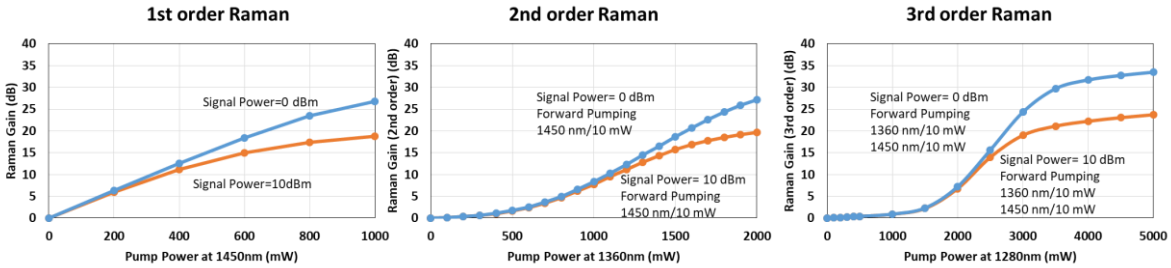

Figure 7.5 Raman Gain for DP-16QAM with first order Raman amplifier, second order Raman amplifier and third order Raman amplifier.

In Figure 7.6, this four figures shows without Raman amplifier, with the first Raman, second order Raman and Third order Raman characteristics for different pump power. For third Raman the equivalent tx power is 24 dBm, about 8dB increase compare that without Raman Amplifier. As a result, 50km transmission distance increase.

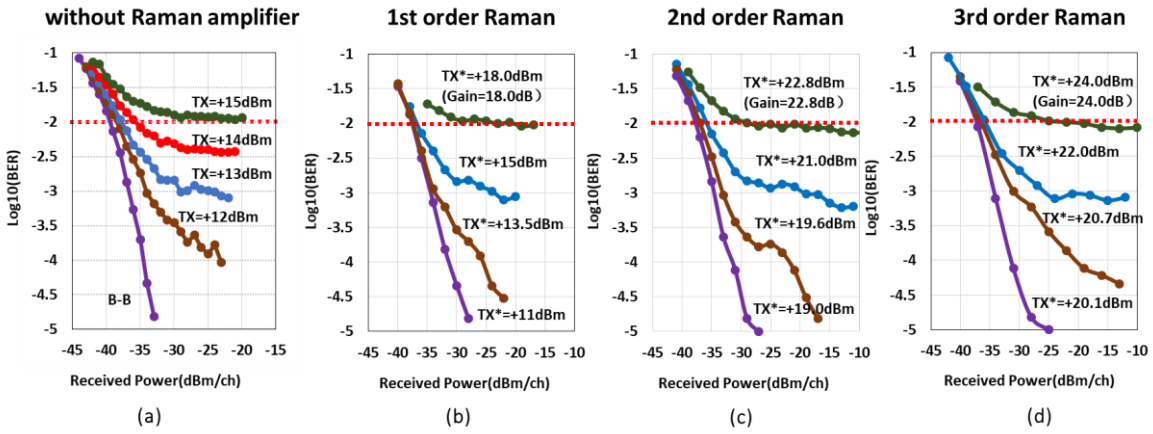

Figure 7.6 BER characteristics for DP-16QAM without Raman amplifier (a) and with first order Raman amplifier (b). With second order Raman amplifier (c). With third order Raman amplifier (d).

7.3 Concluding remarks

In this chapter, Raman amplifier is studied to improve the maximum transmitter power in non-repeatered systems. We investigated the implementation of up to third-order Raman amplification as well as conventional (first order) Raman amplification. Then, a comparison of the resulting performances are made for first-order through third-order pumpings. For third-order Raman amplification, the equivalent Tx power is enhanced +24.0dBm, about 8dB increase compared with that without Raman Amplifier.

References

[1] E. Desurvire, Erbium-Doped Fiber Amplifiers, Wiley, 1994.

[2] P. C. Becker, N. A. Olsson, and J. R. Simpson, Erbium-Doped Fiber Amplifiers Fundamentals and Technology, Academic Press, 1999.

[3] R. H. Stolen, E. P. Ippen, and A. R. Tynes, "Raman Oscillation in Glass Optical Waveguide" Applied Physics Letters, vol. 20, no. 2, pp. 62-64, 1972.

[4] R. H. Stolen and E. P. Ippen, "Raman gain in glass optical waveguides" Applied Physics Letters, vol. 22, no. 2, pp. 276-278, 1973.

[5] L. Eskildsen, P. B. Hansen, S.G. Grubb, A. J. Stentz, T.A. Strasser, J. Judkins, J. J. DeMarco, R. Pedrazzani, and D. J. DiGiovanni, "Capacity upgrade oftransmission systems by Raman amplification," Optical Amplifiers and Their Applications, Paper ThB4, 1996.

[6] P. B. Hansen, L. Eskildsen, S.G. Grubb, A. J. Stentz, T.A. Strasser, J. Judkins, J. J. DeMarco, R. Pedrazzani, and D. J. DiGiovanni, “Capacity upgrades transmission systems by Raman amplification,” IEEE Photonics Technology Letters, vol. 9, no. 2, pp. 262-264, 1997.
[7] G. P. Agrawal, Chapter 8 in Nonlinear Fiber Optics, Academic Press, 1995.
[8] Y. R. Shen, The Principles of Nonlinear Optics (Wiley, New York, 1984),
Chap. 10.
[9] R.W. Boyd, Nonlinear Optics, 2nd ed. (Academic Press, San Diego, 2003),
Chap. 9
[10] J. C. Bouteiller, K. Brar, and C. Headley, “Quasi-constant signal power transmission”, ECOC 2002 Paper, S3.04, 2002.
[11] S. Kodo, Y. Emori, S. Namiki, N. Tsukiji, J. Yoshida, and T. Kimura, “Broadband flat-noise Raman amplifier using low noise bi-directionally pumping sources”, ECOC, Paper PD.F.1.8, 2001.
[12] L. Labrunie, F. Boubal, E. Brandon, L. Buet, N. Darbois, D. Dufournet, V. Havard, P. La Roux, M. Mesic, L. Piriou, A. Tran, and J. P. Blondel, “1.6Terabit/s (160×10.66 Gbit/s) unrepeated transmission over 321 km using second order pumping distributed Raman amplification” (Optical Amplifers and Their Applications), Paper PD3,2001.
[13] S. B. Papernyi, V. I. Karpov, and W. R. L. Clements, “Third-Order Cascaded Raman Amplification”, Optical Fiber Communication Conference, Paper FB4, 2002.
[14] C. Martinelli, D. Mongardien, J. C. Antona, C. Simonneau, and D. Bayart, “Analysis of bidirectional and second-order pumping in long-haul systems with distributed Raman amplification” European Conference on Optical Communication, Paper P3.30, 2002.

Chapter 8 Summary and conclusions

8.1 Summary

With the increase of bandwidth consuming applications, worldwide communication capacity demand has increased rapidly over the past a few decades. While fiber optic communication systems have already being served as infrastructures for such global and core networks, much efforts are continuously being paid to develop higher capacity and longer systems by adopting the state-of-the-art technologies. Because optical signal is transmitted through optical fiber, transmission performance impairments caused by optical fibers nonlinearity are one of the most important factors that limit the capacity of the next generation Wavelength Division Multiplexing (WDM) systems. In this paper, the nonlinear transmission property of optical signal in optical fiber for next generation optical communication systems is studied.

The thesis consists of 8 chapters. The second chapter is devoted to the modulation formats and detection schemes. The coherent detection technology based on Digital Signal Processing (DSP) technology combined with advanced modulation formats, can significantly improve the transmission capacity of the system, and simplify the complexity of the system if the polarization multiplexing technology is recombined. Polarization multiplexing (PM) can double the spectral efficiency of the system. In this chapter, we summarize the modulation format and Forward Error Correction (FEC) of optical coherent link, and describe some important aspects of DSP and coherence detection.

Chapter 3 focuses on fiber dispersion and nonlinearity, which are extremely important to consider for the high-capacity systems. Starting with introducing the fundamental nonlinear Schrodinger equation, such as attenuation, chromatic dispersion, polarization model dispersion (PMD), nonlinear interference noise. Then, we have comprehensively investigated transmission property of single-channel 10 Gbps signal in dispersion shifted fiber (DSF). Quite different feature of signal degradation in positive and negative dispersion regimes is clarified in terms of signal operation wavelength as well as transmission distance. Intrinsic nonlinear degradation near zero dispersion is found to be symmetric in terms of wavelength despite that modulation instability gain should vanish in normal dispersion with deviation from zero dispersion.

Chapter 4 investigates the non-repeatered systems performance using numerical method for 100Gbps and beyond 100Gbps systems. We have numerically evaluated very high power transmission property and BER performance of 120Gbps digital coherent

signals. If the maximum transmitter powers are defined as the powers at which BER floor levels are 1.0×10^{-2} without error correction, those are found to be approximately +20.4 dBm, +14.8 dBm and +10.6 dBm, respectively, for single-channel 120Gbps DP-QPSK, DP-16QAM and DP-64QAM formats in large-core and low-loss single-mode silica fibers. We also show that the maximum transmitter powers gradually decrease in logarithmic feature with the increase of the number of DWDM channels. The channel number dependence is newly shown to be almost independent on the modulation format.

Chapter 5 investigated that the modified GN-model with adjustment parameters, can be an accurate way to describe the nonlinearity impairments in non-repeatered transmission system. In this chapter we have introduced theoretically the GN model and bibliographical background, and introduced the model formulas, also the main derivation steps are given. Then we directly discuss the subject of GN model accuracy with adjustment parameters. The calculation results using extended Gaussian-Noise (GN) model with adjustment parameters have been compared with the numerical simulation results, not only to confirm the validity of the results but to explore possible new analytical modeling for non-repeatered systems.

Chapter 6 is devoted to nonlinear mitigation techniques, digital back propagation to compensate nonlinearity impairments in non-repeatered systems. With nonlinear compensation by using digital back propagation (DBP) at receiver side, we have found that 2 dB improvement is achievable compared with the performance without DBP. However, the performance is affected by nonlinear channel interference in DWDM non-repeatered systems, the improvement has been reduced to 0.6dB due to disturbance from neighboring DWDM channels. Furthermore we newly confirmed that the negative dispersion which change the optical pulse waveform at transmitter side increase the maximum input power by 0.2dB in single channel.

In chapter 7, Raman amplifier is studied to improve the maximum transmitter power in non-repeatered systems. We investigated the implementation of up to third-order Raman amplification as well as conventional (first order) Raman amplification. Then, a comparison of the resulting performances are made for first-order through third-order pumpings. For third-order Raman amplification, the equivalent Tx power is enhanced +24.0dBm, about 8dB increase compared with that without Raman Amplifier.

Finally, chapter 8 gives a conclusion of this paper.

8.2 Future work

The analysis model of non-repeatered transmission system based on GN model needs to be improved in accuracy. In addition, for other high-order modulation systems, updated adjustment parameters need to be validated.

Although DBP and other techniques have a good effect in optical fiber nonlinear compensation. There are still many problems to be solved. The two main reasons are computational load and reliability. In the dispersive unmanaged transmission system, the amount of computation required by DBP is too large. In terms of reliability, DBP is not accurate enough with large PMD systems. Such problems should be solved in the future.

List of publications

Paper:

1. Xin Zhang, Yasuhiro Aoki, "Nonlinear Propagation Characteristics of 10 Gbps Optical Signal at and near Zero Dispersion of Dispersion-Shifted Optical Fiber", IEICE communications Express, Vol.7, No.4, pp. 120-124, 2018.
2. Xin Zhang, Yasuhiro Aoki, "Maximum Transmitter Power set by Fiber Nonlinearity-Induced Bit Error Rate Floors in Non-Repeatered Coherent DWDM Systems", Accepted for publication and scheduled to appear in IEICE Transaction on Communication, Vol.E102-B, No.6, and June 2019.

International Conference:

1. X. Zhang, Y. Aoki, "On the Impact of Digital Back Propagation Nonlinearity Compensation in Non-Repeatered Transmission WDM Systems", Inter Photonics 2018, Antalya, Turkey, Oct.10, 2018. Poster session ID-232.
2. Y. Aoki, X. Zhang and Q. Tong, "Nonlinear Transmission Characteristics of DWDM Coherent Optical Signal through Multiple Dispersion-Shifted Fiber Spans", The 23rd OptoElectronics and Communications Conference (OECC 2018) Technical Digest P1-28.
3. Y. Aoki, A. Algamidi and X. Zhang, "Mitigation of Optical Nonlinear Degradation by Optical Spread Spectrum in Coherent Optical Fibre Transmission Systems", OECT2017 (2017 International Conference on Optics, Electronics and Communication Technology) (Beijing, China 2017).ISBN: 978-1-60595-496-7.
4. Y. Aoki, X. Zhang and A. Algamidi, "Maximum Input Power of Large-Core and Low-Loss SMF for Non-Repeatered Coherent DWDM Systems", Nonlinear Optics2017 (Hawaii, USA 2017) paper NW4A.12.
5. X. Zhang and Y. Aoki, "Nonlinear Propagation Characteristics of 10 Gbps Optical Signal at and near Zero Dispersion of Dispersion-Shifted Optical Fiber", Nonlinear Optics2017 (Hawaii, USA 2017), paper NW4A.13.

Domestic conference:

1. Xin Zhang, Yasuhiro Aoki, "Mitigation of Nonlinear Impairment by Using Digital Back Propagation in Digital Coherent Optical Non-Repeatered Transmission System", the 79th JSAP Autumn Meeting 2018, Nagoya, Japan, Sept.20, 2018, E 20a-211B-4.
2. 張 鑫、青木 恭弘、「非線形補償を用いたデジタルコヒーレント無中継光伝

送システムの検討」第 16 回埼玉工業大学若手研究フォーラム（2018 年）、pp.66-67.

3. 張 鑫、アルガミディ　アハメド、青木 恭弘、「数百 Gbps DWDM ディジタルコヒーレント無中継伝送システムの最大伝送距離の検討」、2017 年 電子情報通信学会ソサイエティ大会 B-10-44.
4. アルガミディ　アハメド、張 鑫、青木 恭弘、「DP-16QAM, 300 Gbps ナイキスト DWDM 信号の大洋横断超長距離光ファイバ伝送特性の検討」、2017 年電子情報通信学会ソサイエティ大会 B-10-45.
5. 張 鑫、青木 恭弘、「低損失・大口径ＳＭＦを用いたディジタルコヒーレント無中継光ファイバシステムの検討」、第 15 回埼玉工業大学若手研究フォーラム（2017 年）、pp.116-117.
6. アルガミディ アハメド、張 鑫、青木　恭弘、「数 100Gbps DP-16QAM ナイキスト WDM 信号の大洋横断超長距離光ファイバ伝送特性の検討」、第 15 回埼玉工業大学若手研究フォーラム（2017 年）、pp.114-115.
7. 張 鑫、青木 恭弘、「ＤＳＦ零分散波長域での 10 Gbps 信号の非線形伝送特性の数値解析」、2016 年 電子情報通信学会ソサイエティ大会 B-10-17.
8. 張 鑫、アルガミディ　アハメド、青木 恭弘、「低損失・大口径ＳＭＦにおけるデジタルコヒーレント信号光の高光パワー伝送特性の検討」2017 年電子情報通信学会 総合大会、B-10-15.
9. アルガミディ アハメド、張 鑫、青木　恭弘、「光スペクトル拡散による光ファイバ非線形抑制効果を用いた大容量光ファイバ伝送方式の基礎検討」、2017 年電子情報通信学会 総合大会、B-10-27.
10. 張 鑫、青木 恭弘、「分散シフト光ファイバにおける長距離光伝送特性の理論的検討」、第 14 回埼玉工業大学若手研究フォーラム（2016 年）、pp.106-107.

Appendix

A. MATLAB program on the BER characteristic dependent on received power.

```
Non-repeatered system BER V.S.P    QPSK
clear all, close all
%BERvsP DP-QPSK non-repeatered system
% parameter setting
Rx_power= -55: 1: 0;        % dBm, power.
Nch=1;                       %channel number.
Tx_power0=-20;
Tx_power1=17;
Tx_power2=18;
Tx_power3=19;
Tx_power4=20;
Tx_power5=20.1;
Tx_power0W=10^-3*10^ (Tx_power0/10);
Tx_power1W=10^-3*10^ (Tx_power1/10);
Tx_power2W=10^-3*10^ (Tx_power2/10);
Tx_power3W=10^-3*10^ (Tx_power3/10);
Tx_power4W=10^-3*10^ (Tx_power4/10);
Tx_power5W=10^-3*10^ (Tx_power5/10);

a = 0.16;                    %Fiber Loss [dB/km]
L = 300;                     %km
e = 1.6 * 10. ^ (-19);       %MKS electron charge
hv = 1.28 * 10.^(-19);       %MKS one photon energy
OF = 30 * 10.^(9);           %MKS optical signal bandwidth/DP16QAM/=symbol rate
gamma = 0.8;                 %W-1,km-1 nonlinear coefficient
alpha = log(10.^(a/10))/2;   %km-1 Fiber Loss in MKS unit
                              % nsp= 1.255943;
                              %excess noise factor    4[dB]
a1=1;                        %linear adjustment parameter
a2=1;                        %nonlinear adjustment parameter
CH = 50*10^9;                %channel spacing    50[GHz]
D = 20.5;                    %ps/nm/km fiber group velocity dispersion
```

```
Beta2 = 1.2746*D;                %ps^2/km phase velocity dispersion
L_effa = 1 / (2*alpha);          %km ultimate effective fiber length
RB = 15 * 10.^(9);               %Receiver electrical bandwidth(=symbol rate/2)
B_wdm = Nch*CH;                  %total WDM optical bandwidth (=5000[GHz])
L_eff = (1-exp(-2*alpha*L))/(2*alpha);%km    effective fiber length

for i = 1 : length((Rx_power)-min(Rx_power)+1)
Rx_power0(i)=10^-3*10^(Rx_power(i)/10);
Ratio0(i)=Rx_power0(i)/Tx_power0W;
G_wdm = Tx_power0W/2/OF;
G_nli0 =gamma^2 *G_wdm^3 *L_eff^2 *(2/3)^3*...
(asinh(1/2*pi^2* Beta2 *10^-24 *L_effa *OF^2*Nch^(2*OF/CH))/(pi *Beta2*10^-24
*L_effa));
SNR0(i) =Rx_power0(i)/2/(RB*0.75*(a1*2*e+Ratio0(i)*a2*2*G_nli0));
Pe0(i)=(1/2)*erfc(sqrt(SNR0(i)/2));
end

for i = 1 : length((Rx_power)-min(Rx_power)+1)
Rx_power1(i)=10^-3*10^(Rx_power(i)/10);
Ratio1(i)=Rx_power1(i)/Tx_power1W;
G_wdm = Tx_power1W/2/OF;
G_nli0 =0.75*gamma^2 *G_wdm^3 *L_eff^2 *(2/3)^3*...
(asinh(1/2*pi^2* Beta2 *10^-24 *L_effa *OF^2*Nch^(2*OF/CH))/(pi *Beta2*10^-24
*L_effa));
SNR1(i) =Rx_power1(i)/2/(RB*0.75*(a1*2*e+Ratio1(i)*a2*2*G_nli0));
Pe1(i)=(1/2)*erfc(sqrt(SNR1(i)/2));
end

for i = 1 : length((Rx_power)-min(Rx_power)+1)
Rx_power2(i)=10^-3*10^(Rx_power(i)/10);
Ratio2(i)=Rx_power2(i)/Tx_power2W;
G_wdm = Tx_power2W/2/OF;
G_nli0 =0.75*gamma^2 *G_wdm^3 *L_eff^2 *(2/3)^3*...
(asinh(1/2*pi^2* Beta2 *10^-24 *L_effa *OF^2*Nch^(2*OF/CH))/(pi *Beta2*10^-24
*L_effa)); SNR2(i) =Rx_power2(i)/2/(RB*0.75*(a1*2*e+Ratio2(i)*a2*2*G_nli0));
Pe2(i)=(1/2)*erfc(sqrt(SNR2(i)/2));
```

```
end

for i = 1 : length((Rx_power)-min(Rx_power)+1)
Rx_power3(i)=10^-3*10^(Rx_power(i)/10);
Ratio3(i)=Rx_power3(i)/Tx_power3W;
G_wdm = Tx_power3W/2/OF;
G_nli0 =0.75*gamma^2 *G_wdm^3 *L_eff^2 *(2/3)^3*...
(asinh(1/2*pi^2* Beta2 *10^-24 *L_effa *OF^2*Nch^(2*OF/CH))/(pi *Beta2*10^-24
*L_effa));
SNR3(i) =Rx_power3(i)/2/(RB*0.75*(a1*2*e+Ratio3(i)*a2*2*G_nli0));
Pe3(i)=(1/2)*erfc(sqrt(SNR3(i)/2));
end

for i = 1 : length((Rx_power)-min(Rx_power)+1)
Rx_power4(i)=10^-3*10^(Rx_power(i)/10);
Ratio4(i)=Rx_power4(i)/Tx_power4W;
G_wdm = Tx_power4W/2/OF;
G_nli0 =0.75*gamma^2 *G_wdm^3 *L_eff^2 *(2/3)^3*...
(asinh(1/2*pi^2* Beta2 *10^-24 *L_effa *OF^2*Nch^(2*OF/CH))/(pi *Beta2*10^-24
*L_effa));
SNR4(i) =Rx_power4(i)/2/(RB*0.75*(a1*2*e+Ratio4(i)*a2*2*G_nli0));
Pe4(i)=(1/2)*erfc(sqrt(SNR4(i)/2));
end

for i = 1 : length((Rx_power)-min(Rx_power)+1)
Rx_power5(i)=10^-3*10^(Rx_power(i)/10);
Ratio5(i)=Rx_power5(i)/Tx_power5W;
G_wdm = Tx_power5W/2/OF;
G_nli0 =0.75*gamma^2 *G_wdm^3 *L_eff^2 *(2/3)^3*...
(asinh(1/2*pi^2* Beta2 *10^-24 *L_effa *OF^2*Nch^(2*OF/CH))/(pi *Beta2*10^-24
*L_effa)); SNR5(i) =Rx_power5(i)/2/(RB*0.75*(a1*2*e+Ratio5(i)*a2*2*G_nli0));
Pe5(i)=(1/2)*erfc(sqrt(SNR5(i)/2));
end
semilogy( Rx_power, Pe0 ,'b-', Rx_power, Pe1 ,'g-',  Rx_power, Pe2 ,'c-',  Rx_power,
Pe3 ,'r-',  Rx_power, Pe4 ,'m-', Rx_power, Pe5 ,'-.r', 'LineWidth', 3)
xlabel(' dBm ', 'FontSize', 18)
```

```
ylabel(' SNR ', 'FontSize', 18)
set(gca,'FontSize',15);
ylim([1*10^-5 1*10^-1])
xlim([-50 -25])
grid on
```

B. MATLAB program on relationship between BER and SNR

```
clear all, close all
%BERvsSNR for BPSK, QPSK, 8QAM,16QAM, 64QAM & 256QAM
% parameter setting
start_snr=0;
stop_snr=30;
step_snr=0.1;
snr=start_snr:step_snr:stop_snr;
% calculation process
for i=1:length(snr),snr_liner0=10^(snr(i)/10);
      Pe0(i)=(1/2)*erfc(sqrt(snr_liner0));                  %BPSK
end;

for i=1:length(snr),snr_liner=10^(snr(i)/10);
      Pe(i)=(1/2)*erfc(sqrt((snr_liner)/2));                %QPSK
end;

for i=1:length(snr),snr_liner2=10^(snr(i)/10);
      Pe2(i)=(2/3)*erfc(sqrt(3/14*snr_liner2));             %8QAM
end;

for i=1:length(snr),snr_liner3=10^(snr(i)/10);
      Pe3(i)=(3/8)*erfc(sqrt(1/10*snr_liner3));             %16QAM
end;

for i=1:length(snr),snr_liner4=10^(snr(i)/10);
      Pe4(i)=(7/24)*erfc(sqrt(1/28*snr_liner4));            %64QAM
end;

for i=1:length(snr),snr_liner5=10^(snr(i)/10);
    Pe5(i)=(/)*erfc(sqrt((/)*(snr_liner5)));                %128QAM
end;

for i=1:length(snr),snr_liner6=10^(snr(i)/10);
       Pe6(i)=(15/64)*erfc(sqrt((1/85)*(snr_liner6)));  %256QAM
```

```
end;
% -------------------------------------------------
semilogy(snr,Pe0, 'b-',snr,Pe, 'c-',snr,Pe2,'g-',snr,Pe3,'y-',snr,Pe4,'r-',snr,Pe6,'m-','LineWidth', 3)
legend({'BPSK', 'QPSK', '8QAM', '16QAM', '64QAM', '256QAM'},'Location','southwest', 'FontSize', 11)
ylim([1*10^-6 0.1])
title('', 'FontSize', 20)
xlabel(' SNR    [dB]', 'FontSize', 18)
ylabel(' BER ', 'FontSize', 18)
set(gca,'FontSize',16);
grid
```